Numerical Modelling of Aeolian Sediment Transport, Vegetation Growth and Blowout Formation in Coastal Dunes

L. M. Meijer

TU Delft Deltares

Numerical Modelling of Aeolian Sediment Transport. Vegetation Growth and Blowout Formation in Coastal Dunes

by

L.M. Meijer

to obtain the degree of

Master of Science
in Civil Engineering

at the Delft University of Technology,
to be defended publicly on Tuesday September 29, 2020 at 14:30.

Student number:	4379861	
Project duration:	November 2019 – September 2020	
Thesis committee:	Dr. ir. S. de Vries	TU Delft
	Prof. dr. ir. A.J.H.M. Reniers	TU Delft
	MSc C. van IJzendoorn	TU Delft
	Ir. B. van Westen	Deltares

An electronic version of this thesis is available at http://repository.tudelft.nl/.

Cover photo: Blowout features at Meijendel ©Dunea Duin en Water

TU Delft Delft University of Technology

Deltares

Preface

This thesis finalises my MSc study in Hydraulic Engineering at Delft University of Technology with a specialization in Coastal Engineering. This research on numerical modelling of blowout formation in coastal dunes forms only a small part of a larger development and application plan for the fairly new numerical model AeoLiS. While most work on this research was carried out at my very own dining table due to the COVID-19 crisis, the topic is a cooperation between the TU Delft and the research institute Deltares. Their cooperation is hereby gratefully acknowledged. Despite these somewhat strange circumstances I am more than proud of the process and final results. Before you start reading this work, I would like to use the opportunity to express my gratitude to everyone who contributed to this thesis, in real life and online.

I would like to thank all members of my graduation committee, Sierd de Vries, Ad Reniers, Christa van IJzendoorn and Bart van Westen, for their supervision, interest and guidance during this project. The defence of this thesis will be the first time we are all together in the same room. I am looking forward to this moment where I don't have to watch you through my computer screen.

I wish to express my appreciation to Sierd, chair of the committee, for your expertise and enthusiasm related to this topic, which you were more than happy to share with me (from the other side of the world). Even though we spoke mostly online, I think that our meetings were very interesting and progressive with respect to the field of work. Ad and Christa, thank you for your constructive feedback and critical questions during the progress meetings. Your insights from a different perspective really helped me along the process of this project. And Bart, I owe you a big thank you for your insights, help and support these last ten months. Your unfailing enthusiasm for dunes is very catching. I really enjoyed working with you on this project.

Special thanks to Harrie van der Hagen and Gijs ten Napel from Dunea Duin en Water. Harrie, thank you for showing me around in the dune area of Meijendel. This (very windy) day in the field really gave me some practical insight on aspects that I was only trying to write in code before. Gijs, thank you for providing me with the data on blowout features at Meijendel.

Furthermore, I want to give a shout-out to the group of friends I met at the introduction weekend of Civil Engineering. I cannot believe it is already six years ago that we sat in lecture hall A for analyse and structural mechanics. Many thanks for all the good times together, working on assignments, drinking beers in psor and for the nice trips we made.

Last but not least, I would like to thank my family and friends from back home. Middelburg will always be a home to me because of you. By now, many of you will probably be tired of me talking about dunes and sand, but at least you all now what I am talking about just a little. Zeeland, with dunes just around the corner, was the perfect environment to grow up. Mum, dad and Jesse, I would not have made it to Delft if it wasn't for you. Thank you for your unconditional faith and support. Finally, I like to thank Joey for everything, but especially for coping with me and my mood swings during the last six months that I was working from home. This accomplishment and everything that comes next will not mean the same without you.

In front of you is the final product of my master thesis on numerical modelling of blowout formation in coastal dunes. I really enjoyed working on this topic and will never look the same to dunes again. I have had a great time the past six years as student at the TU Delft, including an extraordinary internship period in Vietnam. It is now time to enter the next phase of my life in the Hydraulic Engineering world, to which I am really looking forward. Enjoy reading.

L.M. Meijer
Delft, September 2020

Abstract

Coastal dunes are dominant features along much of the world's sandy coastlines serving as the first line of protection against coastal flooding. Besides this primary purpose, the coastal dunes also provide a variety of other functions such as the supply of drinking water, nature conservation and recreational areas. With the secondary functions in mind, the Dutch coastal management strategy changed in 1990 from erosion control and stabilization of the coastline (reactive) to a policy of dynamic preservation (pro-active) with the introduction of a law called ''Dynamic preservation of the Dutch coast'' (Koster and Hillen, 1995). This new dynamic strategy naturally induced irregularities in dunes that were completely stabilized before (Arens et al., 2020). One of these irregularities is the formation of a blowout, a small depression or hollow in the foredunes formed by wind erosion or wave impact that may grow in time as sediment from the beach and foredunes is transported into the back dunes (Hesp, 2002). In several Dutch cases such a blowout features were artificially initiated to increase the exchange of sediment from the coastal system into the back dunes which enhances the biodiversity significantly.

Due to the high importance of the coastal dune performance as flood protection, good understanding and prediction of the (dynamic) coastal dune system is desired. Lately, general interest in this topic increased even more due to new societal challenges, such as decisions on coastal development for longer time scales, more complex management settings and sustainability.

Coastal dunes and blowouts are shaped by wind induced sediment transport (aeolian sediment transport), biological - and hydrodynamic processes. To better understand and increase the predictability of dynamic systems, this study focusses on simulating the development of artificially initiated blowout features by including the combination of these relevant processes in the numerical model AeoLiS (Hoonhout, 2015). This process-based model was originally developed to simulate aeolian sediment transport in supply-limited conditions, such as coastal areas.

Some significant improvements were made to the model, such that it is now applicable for (stable) simulations that include directionally varying wind fields, multi-fraction sediment transport in combination with a spatial varying saltation velocity and the competition between aeolian sediment transport and stabilization by vegetation. Also, the model allows for long term simulations with an increased time step by using a steady state solution.

Towards performing simulations of blowout features with the numerical model, two more simple cases of academic dune development are considered: barchan and parabolic dunes. These academic cases are used to validate the applicability of individual processes related to aeolian sediment transport and vegetation stabilization. A third academic case considers all processes in the formation of an artificially initiated blowout in a coastal system. Finally, a practical case is considered where numerical model results are compared to field data by van der Hagen et al. (2017) on the development of multiple artificially blowout features in the Dutch coast at Meijendel.

Simulation results on the barchan dunes show that the model is reasonably capable of performing this type of dune development where aeolian sediment transport is the governing process. Results regarding sediment fluxes and morphological relations are quantitatively comparable with typical behaviour of barchan dunes as described in literature.

The second academic case simulations show that the interaction in the model between aeolian sediment transport and stabilization by vegetation is able to represent the transformation of a barchan dune into a parabolic dune. The vegetation characteristics in these simulations are based on the conceptual idea of forming such a parabolic dune and are therefore not related to quantitative reality. For now, the results are only qualitatively comparable with literature on the formation of this dune type.

Numerical results on the academic blowout formation show that the model is capable of combining the processes that are governing for blowout formation. Where the initiation phase of the blowout formation is included in the model set-up of this academic case, the conceptual ideas of blowout development and closure are performed well by the simulations. The development is again based on the

interaction between aeolian sediment transport and stabilization by vegetation, while the closure phase is governed by a dominant vegetation growth.

Simulations of a small domain including two blowout features of the field case at Meijendel show that the overall erosion patterns and the order of magnitude of the bed level change are to some extent qualitatively comparable with the field measurements over a period of two years. However, the deposition patterns are abrupt compared to the measured data, which is most likely linked to a too large influence of the vegetation on the sediment transport further into the back dunes.

Regarding simulations of practical blowout features, especially the lack of quantitative validation on the vegetation characteristics limits the applicability of the model. A more process based description of the moisture content, vegetation characteristics and angle of repose is expected to positively influence the model results and practical applicability.

Concluding, the numerical model AeoLiS can be used to perform simulations that include all the relevant processes for blowout formation in coastal dunes, but is not yet suitable as tool to predict the development of blowouts that can be validated quantitatively.

The combination of processes that confirms the conceptual ideas on the development of different academic landforms in this study, is only validated in a qualitative matter. The practical application of the model on blowout features at Meijendel shows that further development is required regarding the processes that are especially important in coastal areas, before it can produce quantitatively comparable results for cases that include practical blowout formation.

Contents

List of symbols

Symbol	Description	Unit
α	Real-world grid cell orientation w.r.t. the North	deg
Γ	Roughness factor for the shear stress reduction by vegetation	-
γ	Maximum wave height over depth ratio	-
γ_{veg}	Constant on influence of sediment burial	-
$\Delta z_{b,opt}$	Sediment burial for optimal growth	m/y
Θ	Fixation index	-
Θ_{dyn}	Dynamic angle of repose	deg
Θ_{stat}	Static angle of repose	deg
κ	Von Kármán constant	-
ξ	Surf similarity parameter	-
ρ_a	Density of air	kg/m^3
ρ_g	Density of grains	kg/m^3
ρ_v	Vegetation cover	-
ρ_w	Density of water	kg/m^3
σ_{veg}	Standard deviation in Gaussian distribution of vegetation filter	m
σ_w	Standard deviation in Gaussian distribution of wind direction	deg
τ	Shear stress	kg/m^3
c	Instantaneous sediment concentration	kg/m^2
c_b	Slope of separation bubble	-
c_u	Equilibrium sediment concentration	kg/m^2
d	Grain size	m
f	Factor for relative sediment flux at boundaries	-
g	Gravitational constant	m/s^2
H_s	Significant wave height	m
h_{veg}	Height of vegetation	m
H_{veg}	Maximum height of vegetation	m
l	Inner layer height in perturbation	m
L	Typical length scale of dune feature	m
n	Sediment porosity	-
$n_{fractions}$	Number of sediment fractions	-
n_{layers}	Number of bed layers	-
$p_{germinate}$	Possibility of vegetation germination per year	$1/y$
$p_{lateral}$	Possibility of lateral vegetation expansion per year	$1/y$

Symbol	Description	Unit
p_g	Geotechnical mass content	-
p_v	Volumetric water content	-
Q	Instantaneous sediment transport flux	$kg/m/s$
Q_0	Undisturbed sediment transport flux over a flat bed	$kg/m/s$
R	Wave run-up	m
t_{avg}	Time period over which the bed level change is averaged	s
T	Adaptation time scale for saltation process	s
T_{swash}	Adaptation time scale for salinisation	s
u	Mean horizontal saltation velocity	m/s
u_*	Shear velocity	m/s
u_f	Settling velocity of the grains	m/s
u_{th}	Threshold velocity	m/s
u_w	Wind velocity at height z	m/s
v	Air viscosity	m^2/s
V_{lat}	Lateral vegetation growth rate	m/y
V_{ver}	Vertical vegetation growth rate	m/y
z	Measurement height of wind velocity	m
z_0	Roughness length of the bed layer	m
z_1	Reference height in saltation layer	m
z_b	Characteristic height of saltation layer	m
z_s	Water level	m
z_{sep}	Surface of the separation bubble	m

1

Introduction

1.1. Coastal dunes and blowouts

Coastal dunes are dominant features along much of the world's sandy coastlines serving as the first line of protection against coastal flooding. Besides this primary purpose, coastal dunes also provide a variety of secondary services, such as the supply of drinking water, nature conservation and recreational areas. Coastal dunes are shaped by wind induced sediment transport (aeolian sediment transport), and biological and hydrodynamic processes. While desert dunes, shaped by only aeolian sediment transport, are very dynamic and mobile, coastal dunes are mostly stabilized due to the presence of vegetation. Also, hydrodynamics in the intertidal zone influence the development of coastal dunes as the amount of sediment that is available for transport is limited. The complex interaction between these processes makes the development of coastal dunes a difficult system to understand.

Figure 1.1: Blowouts in foredune at Noordsvaarder, Terschelling the Netherlands from (Arens, 2010).

One possible result of the complex interaction between aeolian sediment transport, vegetation growth and hydrodynamics in the dune system is the formation of a blowout. A naturally formed blowout is a depression or hollow in the foredunes formed by wind erosion or wave impact (Hesp, 2002). Foredunes refer to the dune row closest to the shoreline. Onshore wind that creates the blowout transports sediment from the beach and foredunes into the back dunes. This interaction between the beach and (back)dunes increases the dynamic behaviour of the system and enhances the biodiversity significantly.

As the consequences of dynamic behaviour are considered beneficial for the secondary services of the coastal system, blowout features were artificially initiated at several locations along the Dutch coast . Here, the positive feedback between wind induced erosion and growth of the blowout is stimulated by manually creating a depression in the dune.

Once a blowout is initiated, naturally or artificially, it will develop further under the influence of both environmental and ecological processes. The interaction between these processes causes a highly variable morphology of the blowout feature. Vegetation present in and around the blowout is affected by the wind induced erosion, causing the blowout feature to grow where the vegetation is not longer able to hold the sediment captive. The highly variable morphology of a blowout depends, among others, on wind regime, initial bed profile, vegetation characteristics and human interference (Hesp and Walker, 2013). Usually, a deflation basin, connected depositional lobe and erosional walls can be distinguished. Cooper (1967) defined two primary blowout types, namely saucer and trough blowouts which are illustrated in figure 1.2. Although a wide range of blowout types can be distinguished, from relatively simple cup, bowl, and slots shapes to more complex and mixed shapes, many of the blowouts can be classified into one of these two primary types.

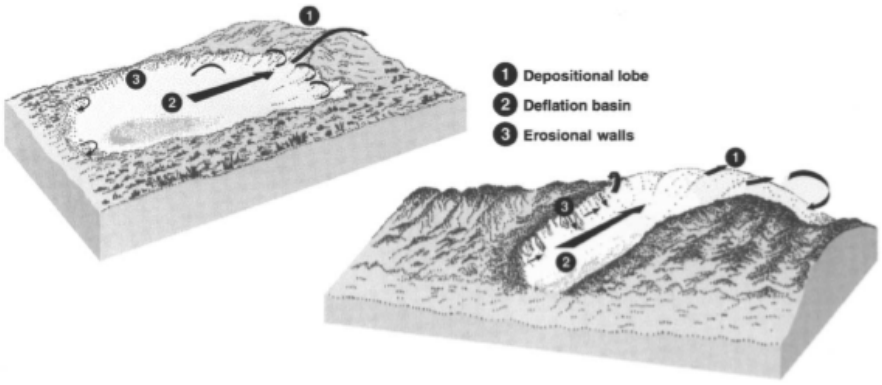

Figure 1.2: Schematic diagrams of a saucer (left) and trough blowout (right) with typical wind flow patterns indicated by Hesp (2002).

1.2. Relevance of modelling coastal dune development

The Dutch coast is about 350 kilometres long and 75% of this length consists of sandy beaches and dunes. Due to the high importance of the coastal dune performance as flood protection, good understanding and prediction of these sandy coastal dune systems, including possible blowout formation, is desired.

Besides interest related to the current safety of dunes, general interest in this topic increased due to new societal challenges. For example, decisions on coastal development for longer time scales (Bochev-van der Burgh, 2012), more complex management settings and sustainability. Within these (societal) challenges, uncertainties in the prediction of coastal dune development are raised as a consequence of (i) dynamic coastal management strategies, (ii) climate change and (iii) application of new nature-based engineering solutions.

1.2.1. Dynamic preservation of the Dutch coast

The Dutch coastal system is characterized by an erosive trend since the construction of the Afsluitdijk in 1932. To prevent the retreating coastline from threatening the coastal dunes, marram grass was planted to strengthen the foredunes and guarantee the safety of the hinterland. The dense vegetation on the static dunes worked as a barrier for sediment transport in inward direction, resulting in a decrease of the biodiversity and in prevention of the back dune to grow in height (de Vries et al., 2012). As a result, the typical Dutch coastal landscape changed from a biodiverse, unique and dynamic system into a static forest-like area, reducing both ecological and recreational values.

Due to more awareness of the consequences of these static dunes on the secondary services, people became more interested in the behaviour of dynamic dunes. In 1990, a new approach to protect the coast from erosion was implemented in the Dutch national law. With ”Dynamic preservation of the

Dutch coast" the coastal management strategy changed from reactive to pro-active. From then on the entire Dutch coastline were to be maintained at the 1990 position, meaning that artificial sand nourishments were required to deal with the coastal erosion (Koster and Hillen, 1995).

Since the strategy for maintaining the coast has changed from erosion control and stabilizing the coastline to a policy of dynamic preservation, both aeolian sediment transport and habitat development of the dune vegetation have been influenced positively. At specific locations planting of marram grass was no longer necessary and the dynamic character of the coastal system was allowed to return (Arens et al., 2020). This dynamic character stimulates the formation of blowouts as an uncontrolled interaction between aeolian sediment transport and vegetation growth allows development of irregularities in the dunes.

Although dynamic coastal management is only applied at locations where the safety is guaranteed, it is not clear what the effects are on other functions of the coastal system, such as drinking water facilities and recreation. In order to determine these effects, and to expand the range of potential locations for dynamic coastal management, an increase in the prediction and quantification of coastal dune development, including knowledge on blowout formation, is required.

1.2.2. Climate change

Climate change impacts the development of coastal dunes on different aspects. The most obvious impact is due to sea level rise (SLR). The sediment budget of coastal systems is reduced by higher water levels as the shoreline retreats land inwards. Eventually, this process results in erosion of the dunes and a new dune profile (Ranasinghe et al., 2012). Figure 1.3 illustrates the response of the coastal dune profile to SLR.

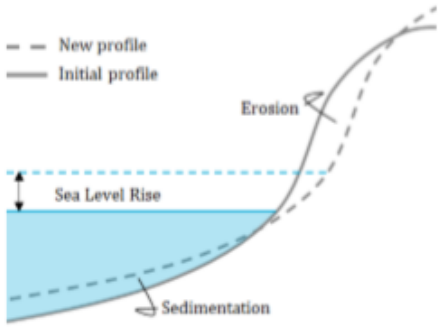

Figure 1.3: Response of coastal dune profile to SLR after van Westen (2018).

Besides the impact due to SLR, changes in wind and waves climate may also result in an erosive trend of coastal dunes. For the Netherlands it is predicted that the winter storms will become stronger and more North-West orientated than usual, leading to an increase in frequency and severity of storm surges that impact the Dutch coast (van den Hurk et al., 2014). The wave attack related to this storm surges will increase erosion of foredunes.

Also, due to a higher frequency of storms the time scale of calm conditions, in which dune recovery takes place, is influenced. The coastal system might not be able to return towards an equilibrium profile before the next storm impacts the dunes. This induces erosion of the dunes even further.

The specific effects of climate change induced SLR and increased erosion rates on the formation and development of blowouts in coastal dunes is unknown at the moment. However, it is expected that in some cases the occurrence and formation of blowouts in foredunes may increase the back dune resilience towards sea level rise, as the vertical accretion of these back dunes is enhanced by the sediment transported from the blowout.

Also, changing climate conditions itself are expected to play a role. Hesp (2002) states that in the past climate changes have contributed to blowout formation via more windy periods in a yearly wind regime and via weakened vegetation covers due to dry or arid periods.

1.2.3. Nature-based sandy solutions

The new dynamic management strategy induced new engineering approaches, like beach and foreshore nourishments, artificial initiation of blowouts and placement of mega-nourishments.

At first, sand nourishments were executed on the beach to maintain the 1990 Dutch coastline. However, the dredged sediment from the North Sea contained a different sediment distribution than the distribution of natural deposited sediment, resulting in an unnatural redistribution of the sediment in the coastal system. To avoid this unnatural sediment distributions, the sand nourishment were later executed on the foreshore at a depth of approximately -5 meter NAP. The sediment supply to the beach from this type of nourishment is way more similar to a natural distribution due to the interaction with waves and currents. The 'natural sorted' sediment supplied to the beach is transported by the wind further in the coastal system.

An example of a project where blowout formation was artificially initiated, can be found at the coastline of Meijendel. This 6 kilometer long Dutch coastline between Scheveningen and the Wassenaarse Slag, is used as study location for dynamic dune processes. In 2015, the formation of blowouts was initiated at five segments of 50 to 70 meters wide. The artificial initiation was executed by removing the vegetation cover of the segments together with excavating a maximum of 1.5 meters of the top bed layer. The activities were extended from the dune towards the beach and therefore also included the excavation of recently formed foredunes.

Other projects on artificial initiated blowouts that did not include this excavation of the top layer directly linked to the beach, such as somewhat North of Meijendel at Berkeheide, have largely failed or required additional work to ensure an increase of the dynamics in the system.

Directly after execution of the project, a high resolution altitude model of the coastal system was produced with the use of drone pictures. In 2017 and 2019 new data was gathered to estimate bed level changes in the costal system with a particular interest in the evolution of blowouts. A first conclusion is drawn and shows an increase of the dynamics in the coastal system. All five artificial initiated blowouts features have been growing for the last four years and show a net sediment transport into the back dunes (van der Hagen et al., 2017).

Figure 1.4: Picture of the coastal system of Meijendel in 2020, five years after the artificially initiation of blowouts at five segments in the dunes. Retrieved from Google Earth.

The placement of a mega-nourishment follows the Building with Nature philosophy (EcoShape, 2019), by using the natural power of wind, waves and the tide to spread the sediment of the nourishment along the adjacent coast. This more sustainable form of a nourishment mitigates the negative effects of multiple smaller nourishments.

In 2011, such a mega-nourishment was placed time along the Dutch coast for the first. The project called the Sand Engine (Stive et al., 2013), consisted of a nourishment with a volume of 21 Mm^3, that was designed to protect the Delfland coast for approximately 20 years. The elevation of the nourishment was relatively high, resulting in a considerable portion of surface area above the waterline where aeolian sediment transport of significant importance takes place (Luijendijk et al., 2019). However, the study by Hoonhout and de Vries (2017) shows that more than half of all aeolian sediment deposits in the domain are supplied by the low-lying beaches that are affected by both aeolian and marine processes, despite that this area is periodically flooded and smaller than the upper dry beach area. After the construction of the mega nourishment., sediment supply from the higher beaches diminished after half a year, resulting in a smaller contribution to the total sediment deposits. This is likely due to formation of a beach armour layer. Therefore, dune development conditions and governing process at a mega nourishment differ from natural beaches.

The understanding and predicting of coastal dune development becomes even more important when dealing with these new engineering approaches, as little is known on the effects of this new type of interventions.

1.3. Aeolian modelling

To deal with rising uncertainties due to climate change, dynamic management strategies and implemented nature-based solutions on coastal dune development, predictions and quantification of the consequences are necessary. This is especially the case for blowout formation in the coastal dunes as little is known of the consequences of these landforms on the performance of dunes as flood protection.

Trying to fill this knowledge gap, multiple numerical models are developed concerning aeolian sediment transport. Models typically make use of a simplification of reality which helps to better understand a complex phenomena A numerical model uses mathematical equations to describe the behaviour of real-life complex system. Often the equations are solved for a spatial grid and over multiple time steps.

As a first step towards better understanding and predictability of consequences on blowout formation in coastal dunes the existing numerical model AeoLiS will be used (Hoonhout, 2015). AeoLiS is a process-based numerical model that is developed for the simulation of aeolian sediment transport in supply-limited conditions, such as coastal areas. This model is favourable compared with other aeolian sediment transport related models as AeoLiS simulates bed surface properties and sediment availability, while other models only parametrizes them. The influence of bed surface properties and sediment availability on aeolian sediment transport appear to be very important in coastal environments following De Vries (2013). Therefore, it is assumed that these are also of importance for the prediction of dune development and blowout formation.

1.4. Research objective

This thesis focusses on improving the numerical model AeoLiS in order to simulate blowout formation in coastal dunes. This includes the implementation of governing processes of blowout development and adjustments on the numerical part of the model. Improving applicability of numerical simulations on blowout formation is part of a broader research in which AeoLiS is developed to serve as a engineering tool for aeolian sediment transport and dune modelling for both coastal engineering and (dynamic) management purposes.

The following research question is proposed to meet the objective of simulating blowout formation:

To what extend can the numerical model AeoLiS be used as a tool to predict the development of artificially initiated blowout features in coastal dunes?

The sub-questions related to the research question are:

- What are the relevant processes in the development of blowout features and how could these be described by a numerical model?
- How can the combination of these processes be used to model the development of several academic cases relevant for blowout formation?
- How do numerical model results compare to a field case with artificially initiated blowout formations?

1.5. Thesis outline

The first phase of this research, which consists of a literature study on governing processes of coastal dune development, blowout formation and academic land formations, is presented in chapter 2. Chapter 3 describes the method that is followed to derive results of blowout simulations. The method includes a brief model description and basic model set-up, after which four different numerical simulation types are described, concerning the academic development of barchan and parabolic dunes, an academic case of blowout formation and a practical case of blowout features at the Dutch Coast. The results of the numerical modelling are presented in chapter 4. Chapter 5 discusses the significance and limitations of the model development, shortcoming in results and validation, and the significance of this study overall. The main conclusions and recommendations are summarised in chapter 6.

2

Literature review

This chapter presents a literature review concerning the processes in coastal dune development and background information on blowout formation plus two academic landforms which are considered as more simple dune development cases.

The aim of this literature review is to answer part of the research question related to relevant processes in blowout formation and to determine the (knowledge) gaps in the process of simulating blowout formation that this study can potentially fill.

2.1. Processes of coastal dune development

Development of coastal dunes is the result of a complex interaction between physical and biological processes as showed in figure 2.1. The two main processes that drive development of the coastal dunes are sediment transport by wind and the interaction of the sediment with vegetation. This section elaborates on all the different processes.

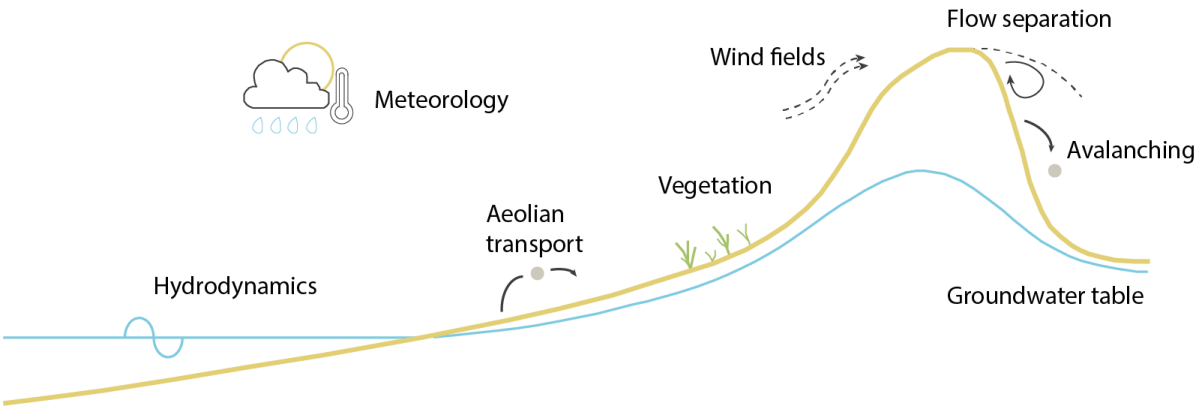

Figure 2.1: Complex physical and biological processes

2.1.1. Aeolian sediment transport

The key process in driving dune development is the transportation of sediment by the wind: Aeolian sediment transport. Bagnold (1937) was the first to systematically study this and he developed a first expression for the sediment flux as function of the wind velocity, based on physics and laboratory experiments.

Using Prandtl-Von Kármán's Law of the Wall, the wind velocity u_z [m/s] at any height z [m] can be described as a function of the shear velocity u_* [m/s] according to:

$$u_z = \frac{u_*}{\kappa} ln(\frac{z}{z_0}) \tag{2.1}$$

where:

u_z	[m/s]	Wind velocity
u_*	[m/s]	Shear velocity
κ	[-]	Von Kármán's constant ($\kappa = 0.4$)
z_0	[m]	Roughness length

For sandy beds, individual grains start to move when the shear stress exceeds a certain threshold value. The velocity threshold u_{th} [m/s]is described by Bagnold (1941) as:

$$u_{th} = A \sqrt{\frac{\rho_s - \rho_a}{\rho_a} g d_n} \tag{2.2}$$

where:

A	[-]	Empirical coefficient (A≈0.1)
ρ_s	$[kg/m^3]$	Density of sediment
ρ_a	$[kg/m^3]$	Density of air
g	$[m/s^2]$	Gravitational acceleration

The critical shear velocity describes a dynamic threshold. If the wind velocity exceeds this threshold, initial movement of sand grains on the surface occurs and the process of sand transport down-wind will continue due to new flying grains.

Bagnold defined the equilibrium or saturated sediment flux S_{eq*} [kg/s/m] as a function of the wind shear velocity and threshold velocity to the third power as:

$$S_{eq*} = \alpha C \frac{\rho_a}{g} \sqrt{\frac{d_n}{D_N}} (u_* - u_{th})^3 \tag{2.3}$$

where:

α	[-]	Conversion constant
C	[-]	Empirical coefficient related to the grain size distribution (C=1.5 - 1.8)
D_n	[m]	Reference grain size (D_n=250 μm)

Typical values for C were assigned for different type of sediments, ranging from 1.5 for nearly uniform sand, 1.8 for dune sands, to 2.8 for sands with a wide range in grain size. The conversion constant α accounts for the conversion of measured wind velocity to the near-bed shear velocity and follows from equation 2.1 while assuming a logarithmic velocity profile:

$$\alpha = \left(\frac{\kappa}{ln(z/z_0)} \right)^3 \tag{2.4}$$

Following the definition of Bagnold itself, the shear velocity is the only factor that limits the aeolian transport rate. Therefore, this type of approach is called transport limited. Transport limited situations persist in wide open areas, where sediment availability is no constraint and no other factors influence the process, such as the desert.

For coastal areas a transport limited approach is not valid, as the aeolian transport rate does not seem te be constant along the beach width (Delgado-Fernandez, 2010). The shoreline increases the moisture content of the sandy surface and limits the transport rate as moist sediment is harder to pick up. Close to the shoreline the sediment transport rate will thus be less than in onshore direction. The length of the surface area over which the wind is able to pick up sediment, is the limiting factor in this transport situation. This length is called the fetch area. Bauer and Davidson-Arnott (2003) defined an approach to include the effect of fetch-limited sediment transport in a model. For the maximum transport rate, the transport-limited formulation of Bagnold was included.

One other type of transport approach is defined by De Vries et al. (2014b) for a more process-based representation of the shoreline influence. Due to the in time varying water level elevation, the velocity threshold becomes variable in time with correspondence to, among other things, the tide. This approach is called supply-limited transport. As this transport rate describes limiting factors on a process-based

approach, other spatio-temporal limiting factors can be included as well. For example, effects of meteorology on the surface moisture content, the emergence of non-erodible roughness elements and beach armouring (sheltering of fine grains behind coarser ones).

2.1.2. Saltation

Key to the aeolian transport processes is saltation, the wind driven lift-off, hopping and splashing of sand-sized particles. After the first expression for the aeolian sediment flux as a function of wind velocity by Bagnold, more refined expressions for the saltation process have been proposed.

In general it is agreed that the saltation process is driven by both wind drag on airborne particles and ejection of soil particles by impacting saltators ('splashing'). The main difference between the expressions lies in the definition of particle trajectories.

Saltation is in steady state when its primary characteristics, such as the horizontal mass flux and the concentration of saltating particles, are approximately constant in space and time (Martin and Kok, 2017). Saltation will thus be highly intermittent for wind regimes with substantial (turbulent) fluctuations. However, from field measurements and numerical model results it appears that the saltation flux reacts to changes in wind speed with a characteristic time scale of one second. Therefore it is assumed that saltation is close to steady state in most conditions Kok et al. (2012). For transport limited saltation, where the amount of saltating sediment is limited by the availability of wind momentum to transport the sand, steady state saltation means that there is exactly one particle leaving the bed layer for each particle impacting it.

Based on the classic formulation of Bagnold (1937), the saltation model by Kawamura (1951) presumes that the initial lift-off speeds of saltator trajectories is effected by both splash and fluid lifting. Therefore, the saltation hop heights and mean particle speeds scale with the wind stress. However, more recent models by Sauermann et al. (2001) and Kok et al. (2012) argue that particle entrainment under steady state saltation, is predominantly driven by splashing. Due to the presence of airborne particles, near-surface wind speeds are reduced significantly and as a result, the contribution of fluid lifting to particle entrainment becomes much less important. To maintain the steady state in this splash dominated case, the mean saltator lift-off and impact speeds do not change with the wind shear stress.

In terms of the definition of the aeolian sediment flux for steady state saltation, the two approaches differ in scaling of the shear stress τ $[Pa]$ to the sediment flux Q [kg/m/s]. The classics models, with fluid lifting contributing to the net entrainment, produce non-linear 3/2 stress-flux scaling (Q $\sim \tau^{3/2}$), while more recent models, with splash dominated entrainment, produce linear or nearly-linear stress-flux scaling (Q $\sim \tau$). The definitions of the sediment flux for the various saltation models are summarized in table 2.1. Figure 2.2 illustrates the significant difference between these definitions under the same conditions. The mass flux is displayed as a function of the bed roughness z_0, which is related to the shear velocity u_* via equation 2.1.

Table 2.1: List of saltation mass flux relations

Study	Mass flux relation	Constant coefficient
Bagnold (1941)	$Q_{bagnold} = C_b\sqrt{\frac{d}{D_n}}\frac{\rho_a}{g}(u_* - u_{th})^3$	$C_b = 1.5 - 1.8$
Kawamura (1951)	$Q_{kawamura} = C_k\frac{\rho_a}{g}(u_* - u_{th})^2(u_* - u_{th})$	$C_k = 2.78$
Lettau and Lettau (1978)	$Q_{lettau} = C_l\sqrt{\frac{d}{D_n}}\frac{\rho_a}{g}u_*^2(u_* - u_{th})$	$C_l = 6.7$
Kok et all. (2012)	$Q_{dk} = C_{dk}\frac{\rho_a}{g}u_{th}(u_*^2 - u_{th}^2)$	$C_{dk} \approx 5$

The difference in scaling of these models originates from the approach to determine the mean horizontal particle speed (short the saltation velocity) u [m/s], as the mass flux is the product of sediment concentration, which scales with the shear velocity squared, and this saltation velocity: $Q = Cu$ $[kg/m/s]$.

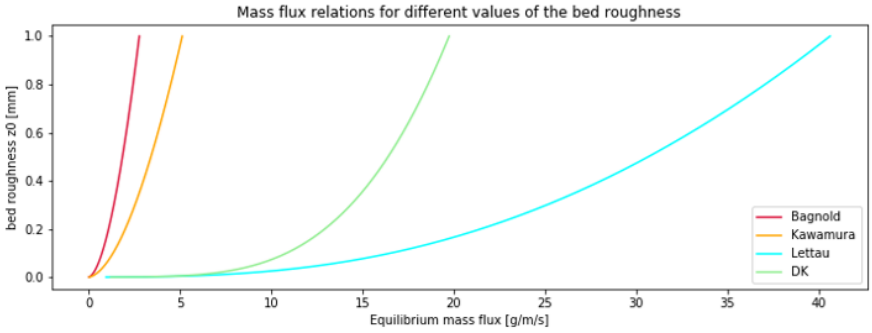

Figure 2.2: Mass flux relations

Saltation velocity

The mean speed of the particles high in the saltation layer can be expected to increase with the wind speed and thus with the shear velocity u_* induced by the wind only. Assuming that the mean horizontal particle speed near the surface of a flat bed is independent of this shear velocity, the particle speed must converge towards a common value near the surface. In Kok et al. (2012) recent wind tunnel tests, field measurements and numerical saltation models are combined to confirm this convergence, see figure 2.3.

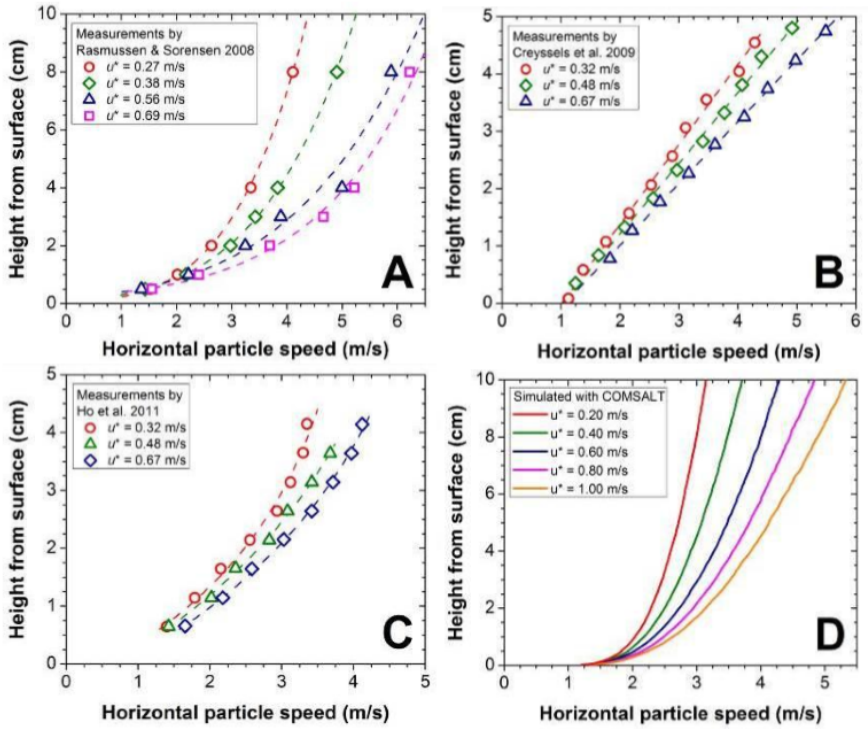

Figure 2.3: Vertical profiles of the horizontal particle speed in steady state saltation from wind tunnel experiments (a,b and c) show that the particle speed converges to a common value near the surface. This is reproduced by numerical saltation models (d). From Kok et al. (2012)

However, when shear stresses induced by the interaction between wind field and morphology (with vegetation) are taken into account, the saltation velocity at the surface will no longer be independent of the net shear velocity. In this case, the saltation velocity is to be determined from the momentum balance between the drag force acting on the grains, the momentum loss by the splashing of grains onto the bed and the gravity term (Sauermann et al., 2001).

2.1.3. Wind field

Spatial variations in shear stresses, which are induced by the interaction between wind fields and morphology, result in spatial variations for the sediment transport in the coastal system and cause an erosion and deposition pattern. This pattern, due to the spatial variations in the wind fields, enables the spatial development of dunes. To illustrate the interaction between wind and morphology, an example of a sandy hill with fictitious wind-streamlines is presented in figure 2.4.

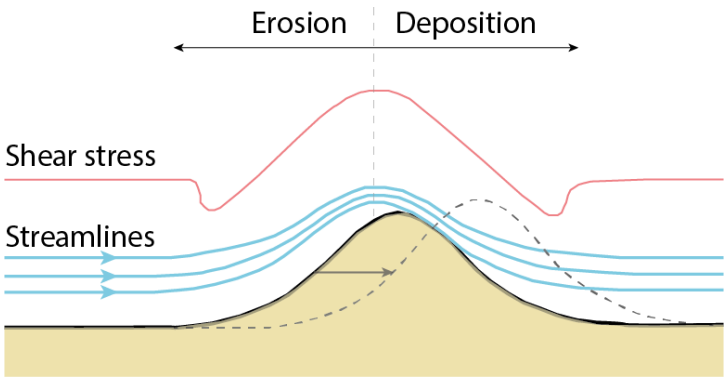

Figure 2.4: Streamlines of wind flow over a smooth sandy hill, after van Westen (2018).

Streamlines that encounter the smooth, sandy hill, convergence towards the top and diverge at the lee side again. Converging streamlines lead to an acceleration of the wind speed and thus an increased shear stress, while diverging streamlines lead to deceleration of the wind speed and a decreased shear stress. An increasing shear stress on the erodible sand layer results in an increase of the aeolian sediment transport and vice versa.

If the shear stress within a domain is uniform, the sediment flux that is coming in, is equal to the flux that is going out. At the uphill side of the example the wind is accelerating and the sediment flux going out of the domain is larger than the incoming flux, resulting in an erosive trend. At the downhill slope the opposite is the case and decelerating wind speeds cause sedimentation due to a lager incoming sediment flux. So, the sandy hill is migrating in windward direction.

The wind field over the dune profile has a laminar, symmetric part which is dominant over the turbulent, asymmetric part (Kroy et al., 2002). The small turbulent contribution to the wind flow induces a phase lag between the shear stress- and dune profile. The maximum shear stress is slightly upwind of the crest of the dune due to this phase lag and it is called saturation length (L_{sat}). The height of the dune is influenced by this, as deposition of sediment starts in front of the crest.

The analytical perturbation theory by Weng et al. (1991) for turbulent boundary layer flow over smooth hills is widely used to include the turbulent part of the wind field in models. As it is an analytical solution, it is suitable for the modelling of large-scale systems. Detailed solving for turbulent flows over a hill would increase the computational time significantly and is therefore considered unsuited. However, the perturbation theory is only valid for smooth hills and at the top of dunes this forms a problem, as sharp edges and steep slopes can occur, inducing secondary flow patterns. This problem occurs because the analytical model does not account for non-linear effects like flow separation. In order to make it possible to model turbulent flows over dunes, Sauermann et al. (2001) suggested to implement a separation bubble, defined as the surface that limits the region of recirculating flow behind the brink resulting from the separation of flow. The flow velocity within the separation bubble is low compared to the velocity threshold, it is therefore assumed by Kroy et al. (2002) that the flow velocity is zero.

Parteli et al. (2014) discussed two extra secondary flow effects in the separation bubble, (i) reversed flow due to peaks where the turbulent flow does exceed the threshold, and (ii) spiral flow along the crest of a dune due to oblique incoming winds.

2.1.4. Hydrodynamics

Hydrodynamic processes directly influence the sediment budget by inducing erosion and accretion in the nearshore region. The aeolian sediment transport is usually an order of magnitude smaller than sediment transport induced by hydrodynamic processes as waves and tide. Beach profiles are therefore mainly dominated by hydrodynamics and it is valid to assume that bed level changes induced by aeolian transport will be smoothened. So, during calm conditions sediment supply by hydrodynamics compensates for the aeolian transport in the intertidal area.

The interaction between hydrodynamic and aeolian processes occurs at the intertidal zone. Here, the aeolian sediment transport rate is reduced locally by swash induced moisture, salt intrusion and the alteration of the groundwater table as function of the tide (De Vries et al., 2014b). The threshold of motion for aeolian transport of this temporary moist sand is higher than for dry sand, because of cohesive effects. Also, it seems that the transition of momentum from grains in saltation to grains on bed is less effective for a higher moisture content (Hoonhout et al., 2013).

De Vries et al. (2014a) found a correlation between the aeolian sediment transport rate and the tidal elevation. Figure 2.5 shows that the measured aeolian sediment transport varies on the tide time-scale, while measured winds are fairly constant. Around 90% of the total aeolian transport occurred during low tide, when the moisture content of the intertidal beach is lowest. This implies that the influence of the soil moisture content on the aeolian sediment transport rate is significant.

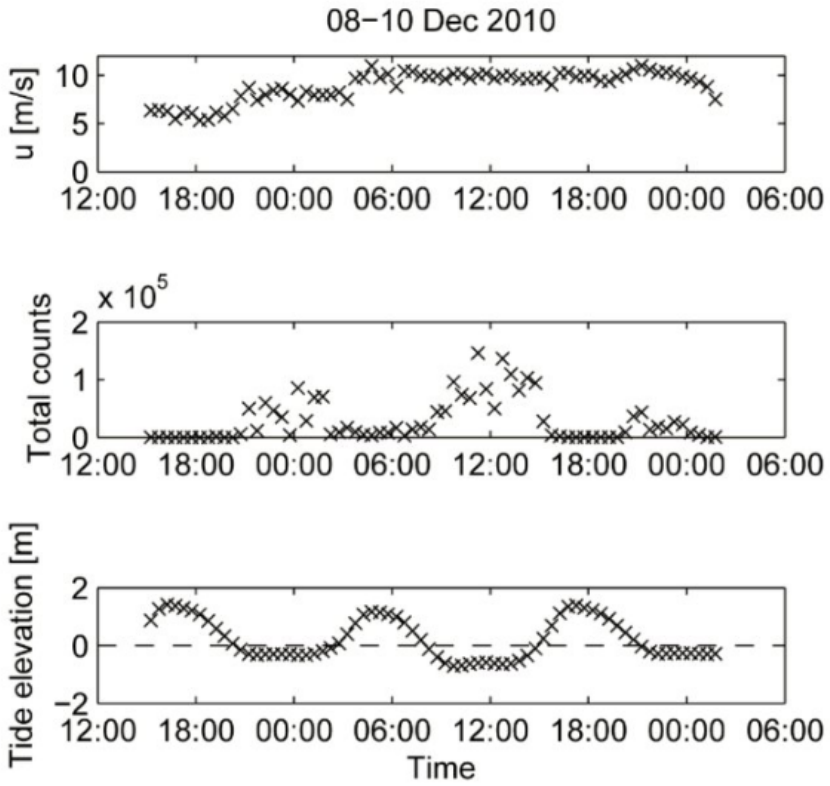

Figure 2.5: Measured wind speed, aeolian sediment transport and tidal elevation from De Vries et al. (2014a)

Besides limiting the sediment transport rate, hydrodynamics can also enhance the sediment supply as waves and the tide induce mixing of the soil top layer. This mixing of the top layer reduces the supply limiting effect of an armour layer (Hoonhout, 2015).

Hydrodynamic processes are typically linked with dune erosion, but new insights by Cohn et al. (2018) suggest that the processes are not unconditionally destructive and can cause dunes to accrete. From the analysis of morphologic change data sets of a dissipative beach, it is estimated that hydrodynamic processes can directly contribute to the annual dune growth.

2.1.5. Non-erodible elements

A non-erodible element cannot be eroded by aeolian sediment transport. Such non-erodible elements can either be objects or layers. Examples of non-erodible elements are natural rock, clay and saturated sediment layers or man-made objects such as concrete slabs, fences and (beach)buildings. Since the non-erodible elements do not take part in the dynamics of the coastal system, complex flow patterns around the objects result in three dimensional flow separation. The non-erodible layers cause a difference in the sediment supply for aeolian transport along the coastal system.

2.1.6. Vegetation

The presence of vegetation in coastal systems has a stabilizing effect on the dune development and allows the dunes to grow in height. The vegetation species that are found in coastal areas have unique characteristics that allow them to grow in dynamic regions with high salinity concentrations. The growth of these dune species and the influence of the vegetation on coastal dune development is summarized by four processes according to figure 2.6:

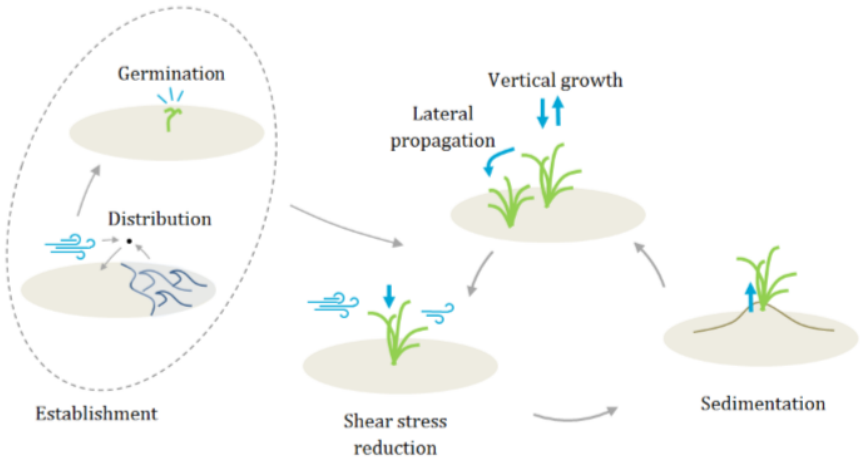

Figure 2.6: Vegetation processes by van Westen (2018)

Vegetation establishment consists of two elements: the distribution and germination of seeds. Distribution of seeds occurs under the influence of aeolian or hydrodynamic processes, or by intervention by humans. The establishment of vegetation happens often near existing vegetation as the distance over which the seeds have to be distributed is small. The germination of a seed depends on various conditions. Biotic factors that are suggested to be the most important limiting factors for establishment of dune grasses such as Marram grass *(Ammophila arenaria)* are: nutrient deficiency, lack of moisture, extreme sand accretion, high wind stresses, soil salinity and spray (Maun, 1994). Besides the vegetation establishment through distribution and germination of seeds, a plot can also be vegetated by lateral propagation via the rhizomes of already existing plants. Goldstein et al. (2017) found that the relative speed with which the vegetation cover expands in lateral direction compared to the local change of the vegetation cover, influences the shape of coastal dunes. A small lateral propagation speed leads to dunes with a relative steep hill as the sediment is trapped at single plots of vegetation. A large lateral propagation speed results in wider and lower dunes as the sediment is trapped over a larger range of vegetated plots.

Once established, vegetation act as a roughness element in the coastal system. It locally reduces the wind shear velocity, causing deposition of the aeolian transported sediment. A relation for the shear stress reduction by the vegetation was proposed by Raupach et al. (1993). The trapping of sediment by vegetation causes the dune to grow, which result in (partial) burial of the vegetation.

Dune species are known for their unique characteristic of burial tolerance, which is a result of a relative high growing velocity. Also, during the burial of vegetation the micro-environmental properties of the soil change, potentially driving the growth of typical dune species. So, besides the burial tolerance, dune species growth is often stimulated by sedimentation (Maun, 2009).

Present vegetation plots in the coastal system are affected by hydrodynamics during extreme events due to erosion of the profile and increased salinity concentrations. Mechanical erosion of vegetation at such an extreme event depends on the water level elevation, wave height and wave strength. The implementation of this process is described as a static, user defined cross-shore distance between the shoreline and first vegetation plots in available numerical models (Durán and Moorde, 2013). However, the dying of vegetation due to hydrodynamics could be described more realistic by using a dynamic limit, directly based on the hydrodynamics (van Puijenbroek et al., 2017).

2.1.7. Avalanching

Avalanching is the process where the surface slope becomes to steep and resets under the influence of gravity to the angle of repose. This is the maximum gradient under which the surface slope is stable. The angle of repose differs per sediment type and depends also on external conditions such as moisture content and vegetation characteristics. Avalanching of a coastal dune can be the result of erosion by hydrodynamic processes, a change in stabilization by vegetation or an increased sediment deposition.

2.2. Blowout formation

Now that all the processes involved in dune development are known, the formation of a blowout feature in relation to this processes is researched. Blowouts are typical dynamic features in coastal dune systems, which cause alongshore spatial variability in the cross-shore coastal dune profile.

A blowout is defined as a depression in the ground where the topsoil or sand has been carried away by the wind. Blowouts in coastal dunes form naturally when onshore winds are strong enough to erode a gap in the foredune or in a series of beach ridges. As the newly created gap grows, the wind transports sand from both the beach and the dune into the back dunes.

Both environmental and ecological processes play an important role in the evolution of blowouts. The feedback between the processes seems to be critical for different stages of the blowout evolution. Three successional phases, depending on the relative importance of environmental and ecological processes, are linked to the morphological development of blowouts (Hesp, 2002, Schwarz et al., 2018):

1. blowout initiation, governed by environmental processes like aeolian sediment transport
2. blowout development, governed by the interaction between sediment transport and vegetation processes
3. blowout closure, mainly governed by vegetation re-colonization

2.2.1. Initiation

Coastal blowouts form commonly in the foredunes, as this location is subject to wind and wave erosion. However, they may form on any dune type. The initiation depends on processes disturbing the dune surface. Two situations are normally observed: (i) the blowout develops at a location where the stabilizing vegetation cover has been damaged or destroyed (by natural causes or by human interference), or (ii) the blowout develops where an un-vegetated cliff or loose sand is present due to wave action on the foredune. The first type is of particular interest concerning dynamic dune management strategies.

As blowout formation is governed by aeolian sediment transport, the wind strength is of major importance. Therefore, natural blowouts are particularly initiated during strong wind seasons. Regardless of the initiation by men or nature, two type of responses have been observed: (i) in absence of a predominant wind direction erosion and deposition occur radially in multiple locations and directions, resulting in a more complex initial shape, and (ii) if a dominant wind direction is present, erosion and deposition tends to occur primarily in response to this wind direction, resulting in enlargement and extension in that direction and a more elongated shape (Schwarz et al., 2018).

In this study, artificially initiated blowouts are considered for the model simulations as natural initiation is a (too) complex process to include and the actual event that triggers the initiation of a blowout is largely unknown. Besides that, man-made blowout formation is a recent topic of the Dutch coastal dune management strategy.

2.2.2. Development

The morphology of a blowout is highly variable, however most blowouts, regardless of type, have three topographic features or units: a erosional deflation basin or flats, a depositional lobe, and marginal erosional walls, see figure 2.7. The topography of a blowout becomes more pronounced during its evolution with as characteristic feature sand being eroded from the deflation basin, transported inward and depositioned at the deposition lobe or further in the back dunes. There are two blowout shapes that appear most common: saucer and trough blowouts.

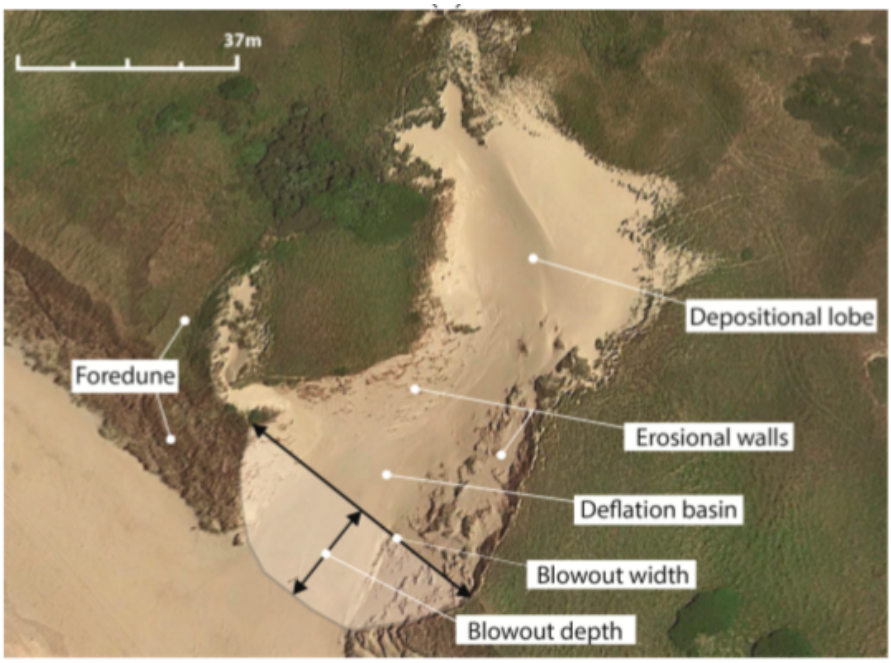

Figure 2.7: Schematic overview of a trough blowout, Zuid-Kennemerland from Schwarz et al. (2018).

Saucers blowouts

Saucer shaped blowouts have saucer-shaped hollows or depression and are shallow, concave and circular or elliptical. As both wind flow acceleration and deceleration have been measured over the deflation basin, erosion is probably driven mainly by the availability of sand. This erosion occurs typically at the deflation basin and at the windward located blowout edge. The depositional lobe is thus formed at the downwind edge, and the saucer blowout grows against the prevailing wind direction.

Trough blowouts

Trough shaped blowouts are generally more elongate, deeper and have narrower deflation floors and basins, with steeper, longer erosional walls or slopes. The sediment transport is governed by the dominating wind direction, which is mostly onshore. The steering and accelerating of wind by the blowout topography often results in jet flow. This jet flow induces a positive feedback between the blowout topography evolution and the wind field. Erosion of the defaltion basin is stimulated and erodes continuously until a base level is reached. The base level is often related to the groundwater table or an immobile layer. As the basin deepens, the blowout widens through undercutting and slumping of the side-walls.

2.2.3. Closure

All types of blowouts may eventually evolve into parabolic dunes distinguished by the development of trailing ridges. However, many do not reach this form as the dunes gradually stabilize by vegetation colonization or sediment infilling. The stabilization occurs when the blowout reaches a critical size, for which sediment transport along the deflation basin can no longer be supported by the morphometry. Stabilization processes typically involve (Hesp and Walker, 2013):

- Vegetated slump blocks falling on the blowout walls
- Relative high moisture levels at the base level of the deflation basin that reduce erosion and facilitate the colonization by vegetation
- Pioneer species growing on the outside margins of the depositional lobe, up and into the blowout
- Forming of incipient foredunes across the entrance of the blowout, which induces a barrier for sediment transport from the beach into the blowout

Maintenance or reactivation of blowouts need disturbances such as overwash and high wind events, to counteract the stabilization processes van Boxel et al. (1997). Coastal dunes are constantly adjusting to previous events and are therefore lagging behind on the continuously changing climate, meaning that the morphological adaption of the dunes is typically out of sync with the present climate. This lag time also affects closure and reactivation dynamics of blowouts and are influenced by vegetation characteristics (Barchyn and Hugenholtz, 2012).

2.3. Academic landforms

Simulating the formation of blowouts in coastal systems is not directly possible with the current capabilities of numerical models. Therefore, two more simple academic cases of a typical dune development landform are introduced to start with.

In general, two type of dunes are distinguished based on the influencing dune development processes; desert and coastal dunes. Desert dune development depends mainly on aeolian sediment transport, and these landforms are therefore highly mobile. Coastal dunes on the other hand, develop under the influence of aeolian sediment transport, hydrodynamics and ecological processes.

The first academic case considers a typical desert dune: a barchan dune. The development of this dune is thus governed by aeolian sediment transport and occurs at a rather short time scale of months to years. The second academic case considers the development of a parabolic dune, which can be found in coastal system. Despite the presence of this dune type in coastal systems, hydrodynamics are not of great importance in the formation of this dune type, which makes it a more simple case than the blowout. The development of a parabolic dune is governed by aeolian sediment transport and stabilization by vegetation, which increases the time scale (in the order of multiple years) compared to the development of a barchan dune. Both dune types are described in the sections below.

2.3.1. Barchan dunes

Barchan dunes are formed under the influence of aeolian sediment transport processes only. This landform is shaped under limited sediment availability and a unidirectional wind. A barchan dune represents a crescentic shape with two horns pointing in downwind direction. The dune is divided into two areas by the sharp edge on top: the windward side and the slip face.

The development of a barchan dune is described based on an initial situation with an isolated pile of sand following Hersen (2004), see figure 2.8.

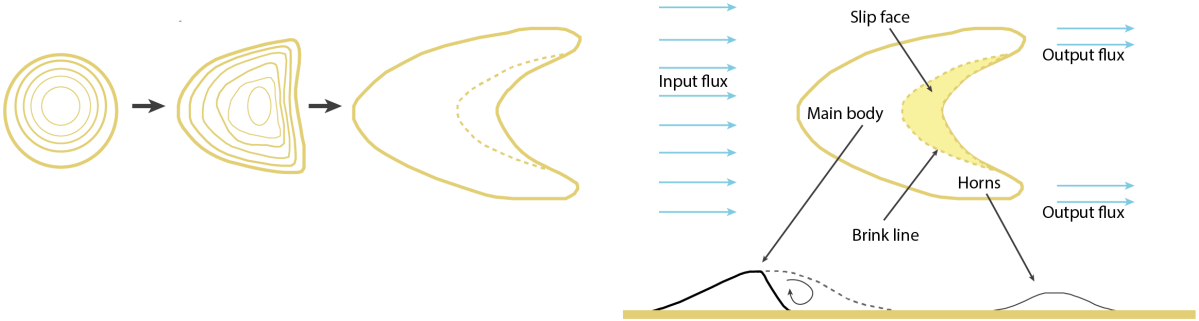

Figure 2.8: Barchan dune properties, after van Westen (2018) and Hersen (2004)

Approaching wind starts to accelerate over the isolated sand pile, inducing an erosive trend at the windward side. Due to flow separation along the top sharp edge, a large eddy develops at the downwind side. Wind speeds decrease drastically in this eddy and sand is deposited. Consequently, the pile of sand starts migrating. The migration speed is larger for smaller pile heights, therefore the sides of the sand pile move faster in windward direction than the main body. The characteristic horns start to grow. At the slip face of the main body a steep slope occurs due to the reversed flow of the separation bubble. When the slope of the slip face becomes too steep, avalanching will occur.

Sauermann et al. (2000) measured several barchan dunes in Southern Morocco and determined scaling characteristics for different parts of the barchan dune from gathered data. Also, a simple model for dune shapes was determined by using the data to determine model parameters. The data and simple model for barchan dune shapes from this study form a simple, but adequate validation case.

2.3.2. Parabolic dunes

Parabolic dunes are typically U- and V-shaped dunes, formed by the interaction between aeolian sediment transport and stabilization by vegetation. Figure 2.9 shows the development of a parabolic dune from a barchan dune due to vegetation stabilization. Vegetation growth is related to sediment burial: it is not likely to grow in areas that are prone to high erosion or sedimentation. In areas with small bed level changes, like at the horns and the brinkline of barchan dunes, vegetation is able to grow and capture sedimentation.

The windward side of a barchan dune is subject to an erosive trend, resulting in no vegetation grow at this side. At the slip face of the dune, sediment is deposited, so no vegetation will grow there either. However, the horns of the barchan dune do advance in vegetation growth as the bed level changes are small. The horns get stabilized due to the vegetation and form two marginal trailing ridges, while the main body advances downwind.

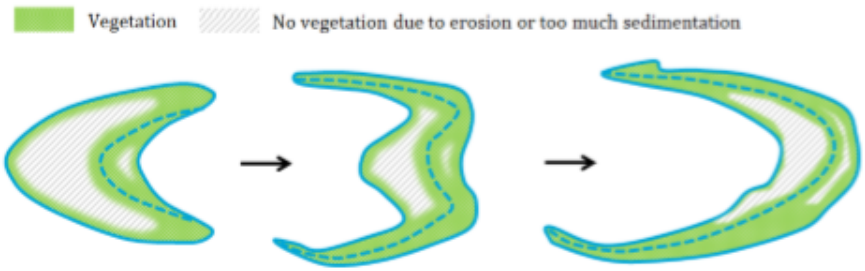

Figure 2.9: Development of a parabolic dune from a barchan dune due to vegetation stabilization van Westen (2018)

Durán and Herrmann (2006) introduced the fixation index $\Theta[-]$ in order to quantify the stabilization process of a parabolic dune. This dimensionless parameter represents the interaction between aeolian sediment transport and vegetation growth rate:

$$\Theta \equiv \frac{Q_0}{V_{dune}^{1/3} V_{ver}} \tag{2.5}$$

With $Q_0[m^3/m/s]$ is the saturated sediment transport over a flat bed, $V_{dune}[m^3]$ is the volume of the dune and $V_{ver}[m/s]$ is the characteristic vertical vegetation growth.

The length L [m] over which the parabolic dune migrates scales with the fixation index. A larger value of Θ means a smaller influence of the vegetation on the development of the dune and leads to long parabolic dunes. For small values of Θ the influence of the vegetation is large, resulting in a shorter parabolic dune as the movement is quickly deactivated by vegetation.

Values of Θ between 0.15 and 0.3 are likely to result in long parabolic dunes that eventually stabilize. Smaller values result in a very quickly stabilized dune, while lager values result in a intermediate state where the dune is still barchan-like. For values larger than $\Theta = 0.5$, vegetation fails to complete the inversion of the barchan dune.

2.4. Concluding remarks

In order to simulate blowout formation in coastal dunes all processes relevant for dune development are to be combined in a numerical model. The evolution of a blowout is divided in three phases: initiation, development and closure. Each phase is governed by a different combination of the relevant processes. As the natural initiation of a blowout feature is the result of an extreme event which is largely unknown, this study focusses on simulations of artificially initiated blowout features. Two academic cases are introduced that consider more simple landforms and can be used to correctly apply and combine the processes in blowout formation.

3

Methodology

The first step of this study is to ensure that the relevant processes from the literature review are included in the numerical model and that the combination of these processes can be used to perform simulations of blowout formation. The first section of this chapter presents a brief description of the model and a basic model set-up for all simulations. Towards performing numerical simulations of blowout formation, the two more simple dune development cases from the literature review are first used to validate the applicability of the processes relevant for these academic cases. Then, a third academic case is set up in order to validate model capabilities regarding the combination of all processes in blowout formation. The academic cases are illustrated in figure 3.1. Sections 3.2 to 3.4 elaborate on improvements made in this study to the key processes of these academic cases and give the model configurations for the simulations. Finally, all processes are combined in a practical field case which is used to compare numerical model results to field data on the development of multiple artificially initiated blowout features in the Dutch coast at Meijendel. Background information and the model set-up of this field case are given in the last section of this chapter.

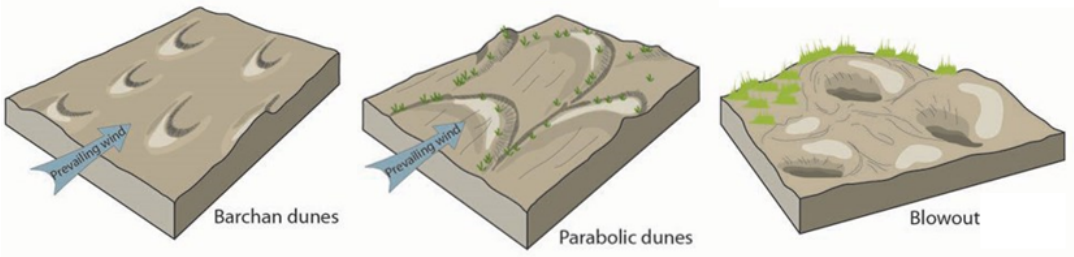

Figure 3.1: Academic landforms: barchan dunes, parabolic dunes and blowout formation in a dune system by Thomberry-Ehrlich (2012).

3.1. Model description

In order to simulate blowout formation in coastal dunes, all discussed dune development processes from the literature study are to be combined in the numerical model AeoLiS. A new conceptual scheme as showed in figure 3.2 is therefore used in this study. Each block represents a different module in the model that includes the estimation of parameters for the relevant processes. The yellow block refers to the module in which the wind shear stress close to the bed is calculated per grid cell. The blue blocks include processes that determine the spatial varying velocity threshold of the grid cells. The orange blocks refer to the processes where aeolian sediment transport is calculated via saltation and where the morphology is updated for the next time step. The two green blocks include the vegetation processes where the block vegetation shear refers to the influence of a present vegetation cover on the total wind shear stress and where the block vegetation growth includes the feedback between net growth of the vegetation cover dependent on erosion and sedimentation rates. An elaborated description of the separate modules and the model in its current state is presented in appendix A.

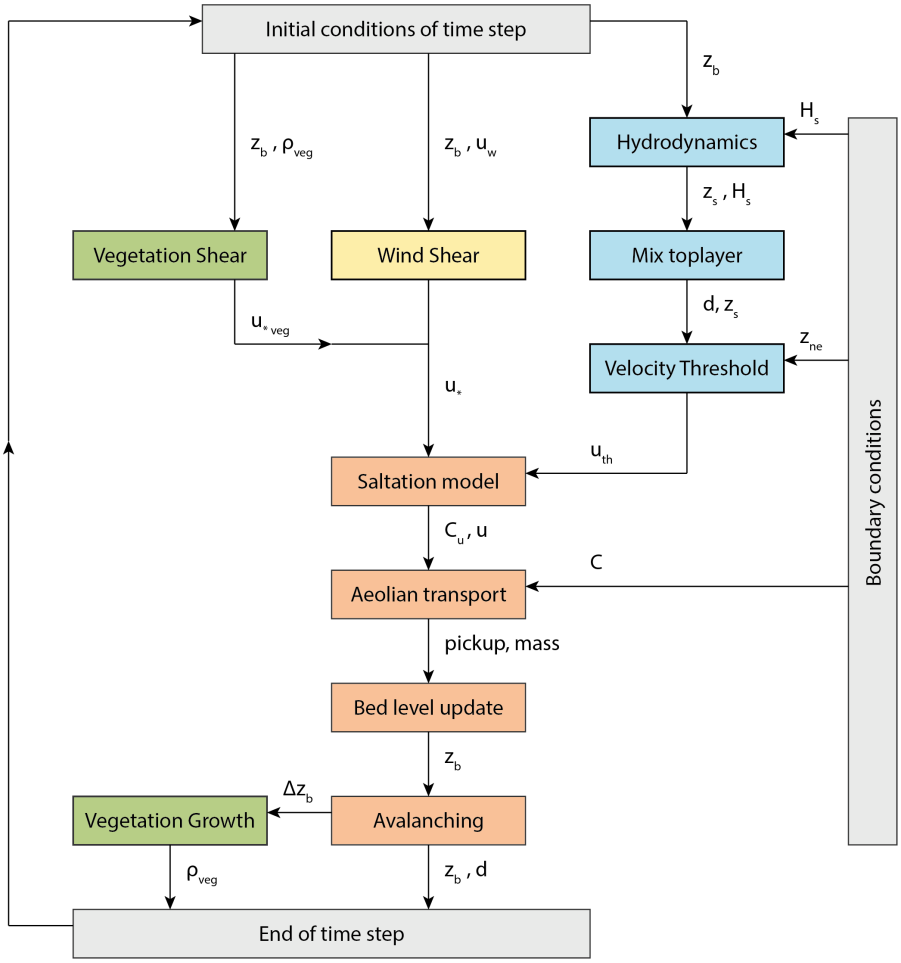

Figure 3.2: New conceptual scheme of numerical model AeoLiS

The key process in simulating dune development is the estimation of the amount of aeolian sediment transport over the grid cells in the domain. This transport governs the erosion and depositional trends, and thus the development of the bed level. Assumptions and decisions regarding the implementation of aeolian sediment transport and the saltation model are relevant for all simulations and are therefore discussed below.

Saltation model

In all simulations of this study, the equilibrium sediment concentration c_u, or saturated sediment concentration, is computed using the definition by Bagnold (1937).

Up to now, the implementation of saltation in AeoLiS was based on a linear relation between the saltation velocity u [m/s] and the wind velocity. As the interaction between the wind field with the morphology and vegetation is highly important in development of the dune landforms, this assumption is now changed to a definition of u that depends on the (morphology induced) shear stress, following literature on the mean horizontal velocity of the grains of section 2.1.2. The saltation velocity u, by Sauermann et al. (2001) is implemented as:

$$\vec{u} = \left(v_{eff} - \frac{u_f}{\sqrt{2\alpha} A} \right) \vec{e}_\tau - \frac{\sqrt{2\alpha} u_f}{A} \vec{\nabla} z_b \tag{3.1}$$

Where $u_f[m/s]$ is the settling velocity of the grains, $\alpha[-]$ represents an effective restitution coefficient and $z_b[m]$ is the bed level. $A = \left| \vec{e}_\tau + 2\alpha \vec{\nabla} z_b \right|$ and $v_{eff}[m/s]$ is the effective wind velocity determined by:

$$v_{eff} = \frac{u_{th}}{\kappa}\left(ln\frac{z_1}{z_0} + \frac{z_1}{z_m}\left(\frac{u_*}{u_{th}} - 1\right)\right) \tag{3.2}$$

in which $u_{th}[m/s]$ refers to the shear velocity threshold, $u_*[m/s]$ to the shear velocity. $\kappa[-]$ is the Von Kármán constant, $z_1[m]$ a reference height in the saltation layer, $z_m[m]$ the characteristic height of this layer and $z_0[m]$ its bed roughness. For realistic applications, the bed roughness of the saltation layer should be in the order of $z_0 = d/30$, where d refers to the grain size. However, a (non-realistic) larger value for z_0 is considered in the academic cases to increase the wind shear velocity and speed up model simulations in terms of the amount of sediment transport. This value is implemented as a constant: $k = 1mm$.

Aeolian sediment transport

The aeolian sediment transport is estimated in the model by solving a 2D advection equation for the instantaneous sediment mass per unit area c [kg/m^2]:

$$\frac{\delta c}{\delta t} + u_x\frac{\delta c}{\delta x} + u_y\frac{\delta c}{\delta y} = E - D \tag{3.3}$$

Where t [s] denotes time, x [m] denotes the cross-shore distance and y [m] denotes the alongshore distance from a zero boundary. u [m/s] is the saltation velocity, denoted in both x- and y-direction. E and D [kg/m^2/s] represent the erosion and deposition terms and hence combined the net entrainment of sediment.

The net entrainment is determined based on a balance between the equilibrium or saturated sediment concentration c_u $[kg/m^2]$, which follows from the saltation model, and the instantaneous sediment transport concentration c. The net entrainment is maximized by the available sediment in the bed m_a [kg/m^2] according to:

$$E - D = min\left(\frac{\delta m_a}{\delta t}, \frac{c_u - c}{T}\right) \tag{3.4}$$

T [s] represents an adaption time scale that is assumed to be equal for both erosion and deposition. A time scale of 1 second is commonly used. Details on the numerical implementation of this advection equation are presented in appendix B.

New is a second option in the model to estimate the instantaneous sediment concentration via a steady state solution for the advection equation: $\delta c/\delta t \approx 0$. This solution type is based on the assumption that the change in sediment concentration over the time steps is relatively small compared to the change in space. It is assumed that this strategy is applicable for dune development processes as there are several orders of magnitude between the time scale of saltation (approximately 2 seconds) and the time scale of the surface evolution of a dune (days to weeks). Also, the use of time steps in the order of hours for the simulation of dune development contributes to the applicability of a steady state solution when fluctuating wind fields are considered. For the steady state solution the advection equation changes to:

$$u_x\frac{\delta c}{\delta x} + u_y\frac{\delta c}{\delta y} = E - D \tag{3.5}$$

First test results of applying the steady state solution to calculate the instantaneous sediment concentration per time step show similar results as simulations that use the full solution. However, the original numerical implementation of the model (steady state and full solution) seems to have problems with the preservation of volume for applications with a rather large initial dune volume. Therefore, all numerical simulations described in this report are performed by using a different implementation of the same advection equation [1], which is much more stable regarding the volume balance. Ideally, the option to use a steady state solution is also added to this implementation. However, due to more complex coding this extra option has not yet been included and all simulation results are performed with the full solution of the advection equation.

[1] carried out by Prof. dr. ir. Pieter Rauwoens from KU Leuven

Basic model set-up

The input of each model simulation includes spatial grid characteristics of the domain and time series for the external forcing:

- x- and y-coordinates of the grid cells in the domain
- bed level per grid cell
- vegetation cover per grid cell (optional)
- level of non-erodible layer per grid cell (optional)
- time series of wind regime
- time series of still water level (optional)
- time series of significant wave height (optional)

Also, for each of the numerical model simulations a standard set of model parameters is implemented, following table C.1.

3.2. Barchan dune simulations

Barchan dunes are the result of aeolian sediment transport processes only, see section 2.3.1. Simulating this dune shape is therefore an ideal case to evaluate the capabilities of the numerical model regarding these processes, without any influence of vegetation and hydrodynamics. The included modules are: wind shear (including perturbation and flow separation), velocity threshold based on the grain size only, saltation, morphological update and avalanching. Especially the wind shear module is updated in this study to allow for simulations with directionally varying wind fields, following the description below.

Wind shear

The wind induced shear stress τ $[N/m^2]$ at the surface is calculated as the sum of shear stresses induced by the wind only (τ_0) and shear stresses induced by the interaction of morphology and the wind field ($\delta\tau$) following:

$$\vec{\tau}(x,y) = \overrightarrow{\tau_0} + \delta\vec{\tau}(x,y) \tag{3.6}$$

The shear stress induced by the wind only is equal to the shear stress on a flat bed and is based on the shear velocity $u_*[m/s]$ that is determined by using the Prandtl-Von Kárman's law of the wall (see section 2.1.1).
The shear stress perturbation $\delta\tau$ is estimated following the analytical description of the influence of a low and smooth hill in the wind profile by Weng et al. (1991). The perturbation is given by the Fourier-transformed components of the shear stress perturbation in the unperturbed wind direction which are the functions $\delta\tau_x$ and $\delta\tau_y$. The x direction is defined by the direction of the wind velocity v_0 on a flat bed, while the y direction is the transverse. The perturbation theory can only estimate the shear stress induced by the morphology-wind interaction in parallel direction of the wind. Therefore, model simulations were, up to now, limited to input wind directions parallel to the cross-shore axis of the grid.

To allow for modelling with directional winds, an overlaying computational grid is introduced, which rotates with the changing wind direction per time step. By doing this, the shear stresses are always estimated in the positive x-direction of the computational grid. The improved implementation of this computational grid (see section A.1) ensures that the model can take into account directionally varying wind fields.

The typical C shape of a barchan dune is the result of flow separation of the wind over the sharp edge dune crest and the development of a eddy at the downwind side of the dune. This is represented in the model by the introduction of a so called separation bubble, following the example of Sauermann et al. (2001). Beneath the surface of the separation bubble the shear stresses are set to zero. The definition of the surface is optimal for the typical formation of a barchan dune under uni-directional

wind conditions, see section 2.3.1. It is expected that the value for the height of the separation bubble (z_{brink}) has no abrupt changes in the y-direction as the brink line lowers regularly from the midpoint of the dune towards the horns and the bed level behind the barchan dune is flat. In other words, there are no abrupt changes of the separation surface between the bubbles in y-direction. However, as the application of flow separation goes further in this study then only for the formation of typical barchan dunes, it is expected that the height of the bubble per slice in y-direction is more irregular as a consequence of variations in both the brink height and level of reattachment point. To avoid abrupt changes in the separation surface, a filter is applied that smooths the surface between bubbles. Also, the previous definition for the minimal level of the separation surface at $z_b = 0$, is adjusted to allow for applications where the bed level may become lower than the reference level.

Model set-up

Four Gaussian shaped sand piles with a different height, width and volume are used as initial topography for the barchan dune simulations, see figure 3.3. The initial topography is one of the variables for different simulations. Other variables are the forcing by wind and boundary conditions regarding sediment fluxes. An overview of the model parameters is given in table C.2.

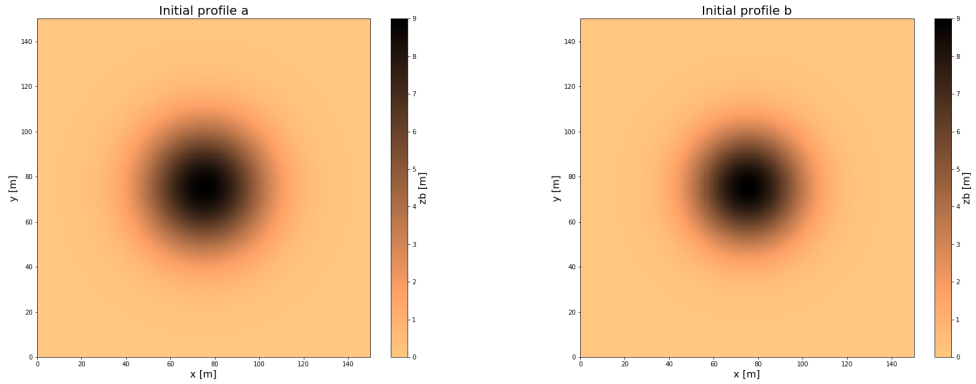

(a) $V = 22614m^3$ (b) $V = 18321m^3$

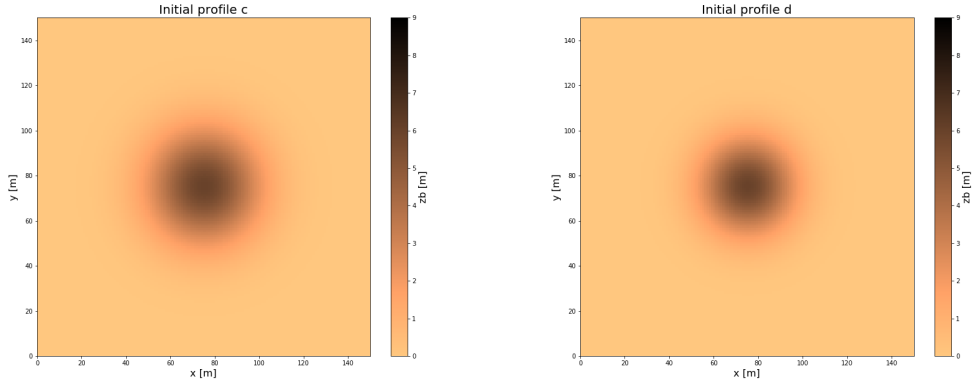

(c) $V = 12214m^3$ (d) $V = 8482m^3$

Figure 3.3: Variation in initial topography and dune volume for barchan simulations

3.3. Parabolic dune simulations

Parabolic dunes form due to the interaction between aeolian sediment transport and stabilization by vegetation, see section 2.3.2. Different numerical simulations of the transformation of barchan dunes into parabolic dunes are performed to test the capabilities of the numerical model regarding the influence of vegetation on the sediment transport and regarding the feedback between morphology and

vegetation growth. The modules that are considered are all previous ones mentioned for barchan dunes plus vegetation shear and vegetation growth. The influence of vegetation on the wind induced shear stress at the surface is calculated following the approach by Raupach et al. (1993), see section A.2. The feedback between morphological changes and the vegetation growth is described below.

Vegetation growth

The vegetation cover per grid cell, which is not subject to erosion, is calculated by $\rho_{veg} = \left(\frac{h_{veg}}{H_{veg}}\right)^2$. Where h_{veg} [m] is the vegetation height and $H_{veg}[m]$ a constant representing the maximum vegetation height. Model implementations regarding vegetation establishment and lateral propagation are given in section A.6 of the model description.

Local growth of the vegetation cover is thus influenced by the the change in vegetation height of that particular cell. The vegetation height depends on one hand by the growth rate of the vegetation and on the other hand by the sediment burial rate Δz_b [m/year]. A constant vegetation cover in time means that there are no morphological changes or that the vegetation grows at the same rate as that the cell is buried with sediment. The optimal growth rate of some vegetation dune species depend on the sediment burial. A shift of the peak for optimal growth is therefore added. This interaction leads to the relation for the change in vegetation height, adopted from Durán and Herrmann (2006):

$$\frac{\Delta h_{veg}}{\Delta t} = V_{ver}\left(1 - \frac{h_{veg}}{H_{veg}}\right) - \gamma\left|\frac{\Delta z_b}{\Delta t} - \Delta z_{b,opt}\right| \tag{3.7}$$

Where the sediment burial factor γ [-] represents the influence of sediment burial on vegetation growth and $\Delta z_{b,opt}$ [m/year] is the sediment burial for optimal growth.

The vertical vegetation growth rate V_{ver} is given in m/year, while the sediment burial rate (Δz_b) is determined as the bed level change per time step. By simply converting this value to a bed level change per year multiple errors are induced, as the time scale over which the bed level change actually occurs is much shorter than this one year. To compare the bed level change per time step with the vegetation growth rate per year, an average bed level change is estimated over a specified time of one day. This averaged value is than converted to a rate per year and used in equation 3.7. This method ensures that sudden changes in the bed level change over one time step are not used as an estimate of the total bed level change in one year, which would be far too high.

Model set-up

The initial profile is that of a barchan dune with a brink height of 6 meters, see figure 3.4. The model parameters remain the same, while the offshore boundary (=upwind) changes to a no-flux condition. The parabolic simulations are performed with a single wind field with only one direction and a constant velocity of 10 m/s.

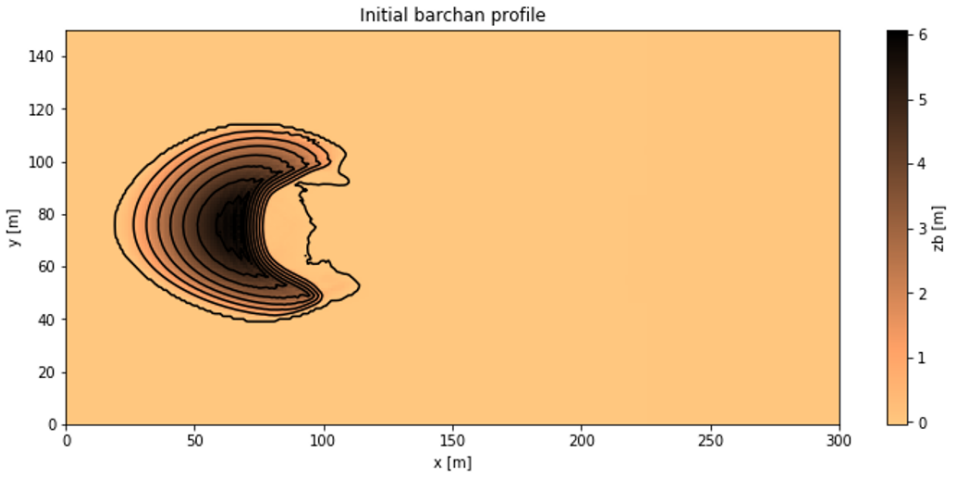

Figure 3.4: Initial barchan topography for parabolic dune simulations.

The vertical vegetation growth is based on obtaining a realistic value for the fixation index Θ, see section 2.3.2. This index is estimated as:

$$\Theta \equiv \frac{Q_0}{V_{dune}^{1/3} V_{ver}} \tag{3.8}$$

A wind velocity of 10 m/s and a dune volume of 10500 m^3 result in a vertical vegetation growth between 2.5 and 8.5 m/year for a value of the index between 0.17 and 0.5 as illustrated in table 3.1.

Table 3.1: Vegetation index θ and resulting vertical vegetation growth rate $V_{ver}[m/y]$

	a.	b.	c.	d.	θ_c
θ	0.17	0.22	0.27	0.38	0.5
V_{ver} $[m/y]$	8.5	7.0	5.5	4.0	2.5

An overview of the model parameters for parabolic dune simulations is given in table C.3.

3.4. Simulations of academic blowout formation

The third academic case is that of simulating blowout formation in a coastal dune. The aim of these simulations it to study the applicability of the numerical model for situations that include the previous studied aeolian sediment transport and vegetation processes plus the influence of a coastal environment. Bed surface properties in a coastal system that influence the sediment supply are discussed in section A.3.

In contrast with the two previous academic cases where the sediment input in the system was manually adjusted, this case with a coastal environment considers hydrodynamics (only still water level) to ensure a more realistic input of sediment at the offshore boundary, see section A.5.

Following literature descriptions on blowout formation, the evolution is divided into three phases depended on the relative importance of environmental and ecological processes, see section 2.2. This study focusses on evolution of artificially initiated blowout features. Therefore, the initiation phase, which is naturally governed by aeolian sediment transport, is the starting point of the simulations. The artificial initiation is introduced as a Gaussian shaped dune profile at which vegetation and the sediment top-layer is removed over a 30 meter wide section. Besides the adapted section, vegetation is assumed to be abundant in the entire dune-domain. A beach profile without vegetation is constructed between the dune and the offshore boundary. Figure 3.5 illustrates the initial topography and vegetation cover.

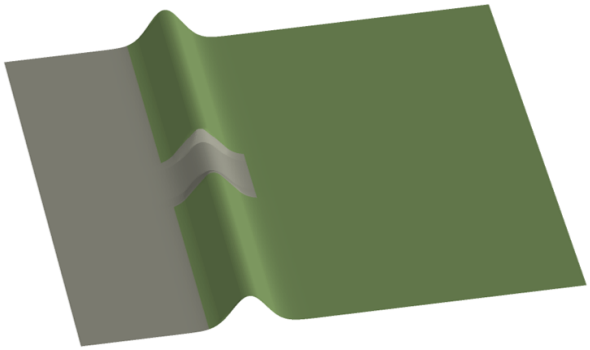

Figure 3.5: Initial topography and vegetation cover for blowout simulations.

A non-erodible layer is used to represent the influence of the ground water table on the amount of sediment available for transport. The bed level at the beach cannot erode further than this layer, as the moisture content of the sediment is too high for the wind to pick up the sediment. This method of using such a non-erodible layer does not represent the influence in reality , but it does prevent an unrealistic erosion pit at the beach. The non-erodible layer is set to be 5 cm below the initial beach profile. Starting from the dune foot further into the dune domain the non-erodible layer is implemented as a constant value, as the ground water table at this location will not be located directly under the bed level.

The second phase, or the development of a blowout feature is governed by the competition between aeolian sediment transport and vegetation stabilization. The sediment transport is forced by a constant wind field with a velocity of 8 m/s from a direction of 270 degrees. Furthermore, the vegetation characteristics are based on the same values for the stabilization index as in the parabolic dune simulations, following table 3.2.

Table 3.2: Vegetation index θ and resulting vertical vegetation growth rate $V_{ver}[m/y]$

	a.	b.	c.	d.
θ	0.17	0.22	0.27	0.38
V_{ver} $[m/y]$	1.3	0.9	0.7	0.5

The third phase of blowout evolution is the closure phase, which is governed by vegetation colonization. In other words, the stabilization by vegetation has become dominant over the sediment transport and results in a shrinking blowout feature. If the blowout feature actually reaches the closure phase depends on the vegetation characteristics and the altered morphology of the blowout, which determines the amount of sediment transport via perturbation.

An overview of the included model parameters in blowout simulations are presented in table C.4.

3.5. Field case with blowout features at Meijendel

Finally, all included processes are used for numerical simulations of the field case at Meijendel. The aim of performing simulations for a real case is to get a better understanding of the model capabilities and limitations on performing results that are quantitatively comparable to field data. The field data was provided by Dunea Duin en Water, who is managing of this dune area.

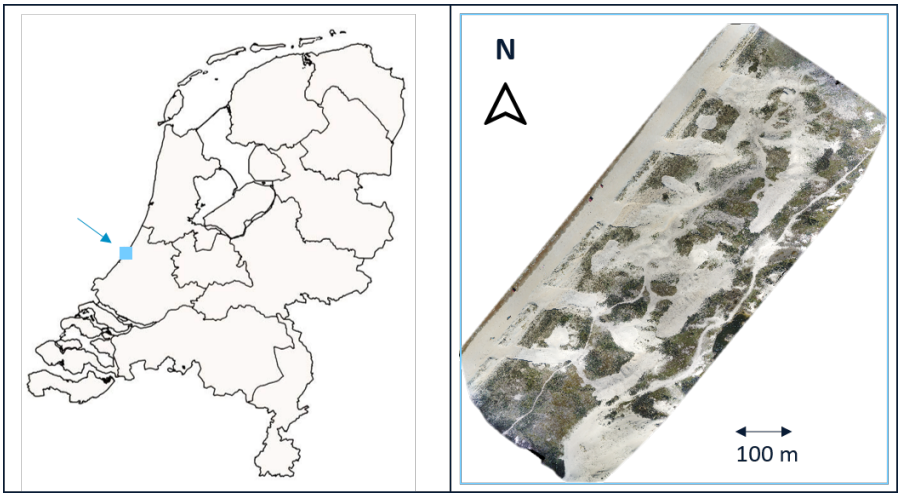

Figure 3.6: Project location in the Netherlands

The project at Meijendel (van der Hagen et al., 2017) is already mentioned shortly in the introduction. It includes artificial initiation of five blowout features in the coastal stretch between Scheveningen and Wassenaar of the Dutch coast, see figure 3.6. This project is used as study location for dynamic dune processes with a particular interest in the evolution of blowouts.

In 2015, the formation of blowouts was initiated at five segments of 50 to 70 meters wide over a total stretch of 750 meters. The artificially initiation was executed by removing the vegetation cover of the segments together with excavating a maximum of 1.5 meters of the top bed layer. The activities were extended from the dune towards the beach and thus included also the excavation of recently formed foredunes. Between excavation number 3 and 4, an old blowout feature (3a) with no direct link to the beach was reactivated, see figure 3.7. Directly after execution of the project in 2015, a high resolution altitude model of the coastal system was made with the use of high resolution drone pictures (orthophotos). In 2017 and 2019 data was again gathered by new drone flights to estimate bed level changes in the system.

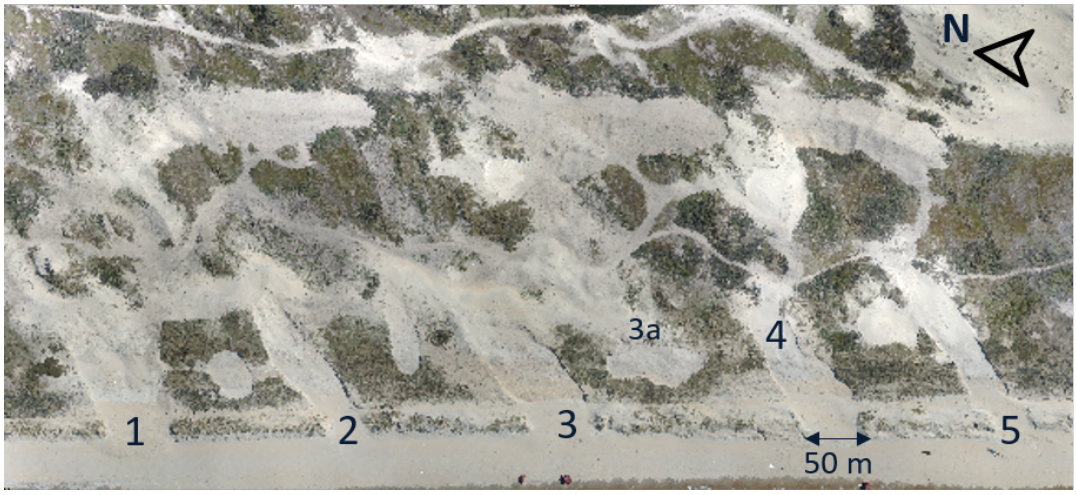

Figure 3.7: Coastal stretch of Meijendel with artificially initiation of five blowout features

The data from the high resolution model of 2015 is used to set up the initial grid for the numerical model. The total area of the domain with 5 blowout features is around 900 x 400 square meters. To perform multiple simulations of this area would take a lot of computational time. Therefore, a small section of the total area is chosen as input grid. It includes blowout feature 3a and 4 to see if the model results make the distinction between a beach connected blowout feature and one that develops in the dune. The grid is rotated over 39 degrees anticlockwise to align the alongshore distance with the y-axis of the model.

The elevation height is determined by interpolation of the measured data over the numerical grid. The beach between x = 0 and 50 meters is manually added as the elevation data domain from the measurements was limited to the foredunes. The width and slope of the beach were estimated from the original orthophoto. The beach slope slightly varies over the domain of the grid to ensure a smooth connection with the elevation data starting at the foredunes (at x = 50). The vegetation cover of the initial profile is estimated with the green values of the original orthophoto. A more realistic method to determine the vegetation density per grid cell would be to calculate the NDVI (normalized difference vegetation index), but unfortunately the required Near-Infrared colour band was not included in the provided data. Figure 3.8 illustrates the cut-out section from the orthophoto and the estimated initial elevation plus vegetation cover for the numerical simulations.

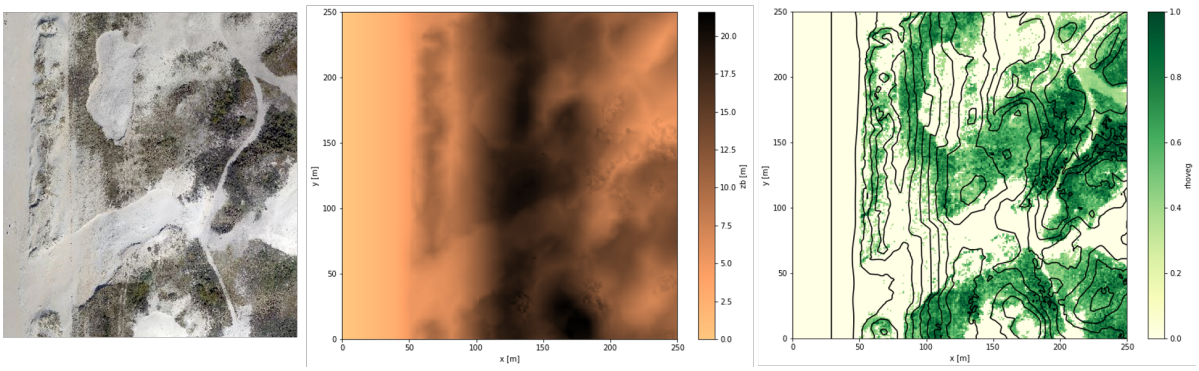

Figure 3.8: Orthophoto (left), numerical grid with elevation in m+NAP (middle) and estimated vegetation cover (right)

To compare numerical model results with field measurement data, the simulation period is to run over the same time with realistic forcing by the wind and hydrodynamics. The simulation period is from April 2015 - April 2019, covering 208 weeks.

The hourly averaged wind velocity input data for this simulation period originates from a measurement station at Hoek van Holland and is obtained from KNMI (Koninklijk Nederlands Meteorologisch Instituut). Wave and tide data are obtained from RWS (Rijkswaterstaat).

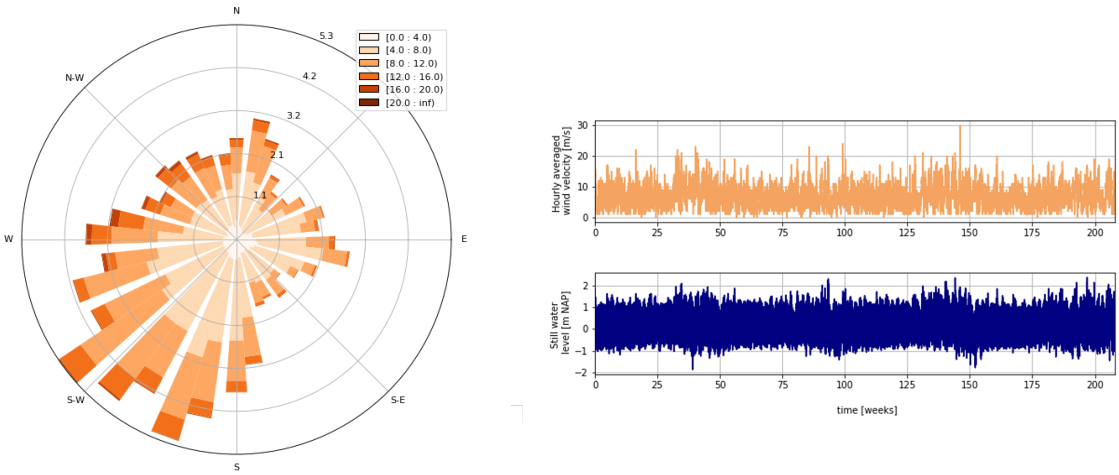

Figure 3.9: Wind rose (left), wind and hydrodynamic input time series from 2015 to 2019 (right)

Only one sediment fraction will be used for the simulations based on three things: (i) there is no data available on the grain size distribution for this project and literature on this topic is limited plus hard to translate to this specific case, (ii) the use of multiple sediment fractions increases the simulation time significantly and (iii) with the assumption that sediment in the dune system consists of aeolian transported sediment only , the amount of larger grains is limited. The bed roughness factor k is estimated following $z_0 \approx d/30$.

An overview of the included model parameters is given in table C.5.

4

Results

Results of simulations performed with the numerical model for three different academic cases and the field case are presented in this chapter. The type of simulations are based on the variables discussed in the previous chapter and are linked to expected behaviour of the academic landforms based on literature.

4.1. Barchan dunes

Numerical simulation results of the typical evolution of a sand pile into a barchan dune under unidirectional wind conditions is illustrated in figure 4.1. Characteristics of this evolution such as development time and (stable) dune dimensions depend on initial model configuration and external conditions.

Variations of these conditions in the numerical simulations lead to different resulting dune shapes. The results are tested for four typical aspects which relate to expected behaviour of this academic landform: sediment supply, morphologic relations, migration velocity and unimodal wind regime.

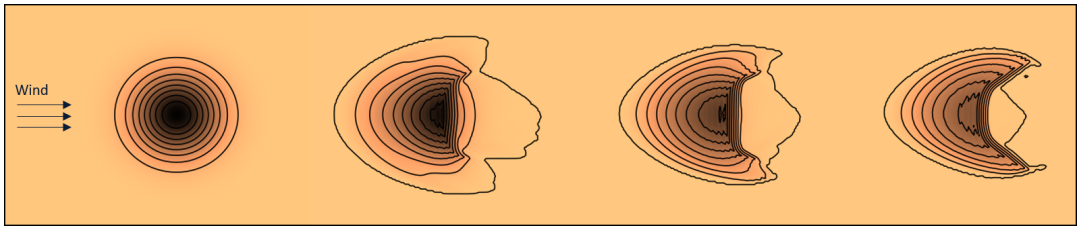

Figure 4.1: Formation of a barchan dune from an initial sand pile

4.1.1. Sediment supply

First, the stability of the simulated barchan dune shapes is tested. The shape of is influenced by the sediment supply that reaches the windward side of the dune, which is in this case the sediment flux that is manually added to the domain at the offshore boundary.

The volume balance of equation 4.1 describes the change in volume ΔV $[m^3]$ of the barchan dune.

$$\Delta V = Q_{in} - Q_{out} = wQ\left(\frac{q_{in}}{Q} - \frac{q_{out}}{Q}\right) \tag{4.1}$$

Where q_{in} and q_{out} are the dune influx and outflux per unit length.

The volume of a barchan dune is constant when the sediment flux that is transported into the dune equals the flux that is transported out of the dune. This outflux is concentrated at the horns of the dune due to the presence of a separation bubble.

Figure 4.2 shows a diagram with the normalized sand flux (q/Q_0) over a numerical simulated dune with initial topography b and a constant wind velocity of 8 m/s. Q_0 is the saturated sediment flux over a flat bed. The diagram indicates that the sediment out-flux is indeed concentrated at the horns of the dune in the numerical simulation.

Durán et al. (2010) states that the ratio between the width of the of horns and the total width of the dune is approximately 0.18, which indicates that the volume of dune remains the same when the sediment influx of the dune is equal to $0.18Q_0$. Following this statement, numerical simulations with an upwind boundary condition for the sediment flux lower than $0.18Q_0$ are expected to result in barchan dune volumes that decrease in time, while a boundary condition for the sediment flux larger than $0.18Q_0$ results in growing barchan dunes.

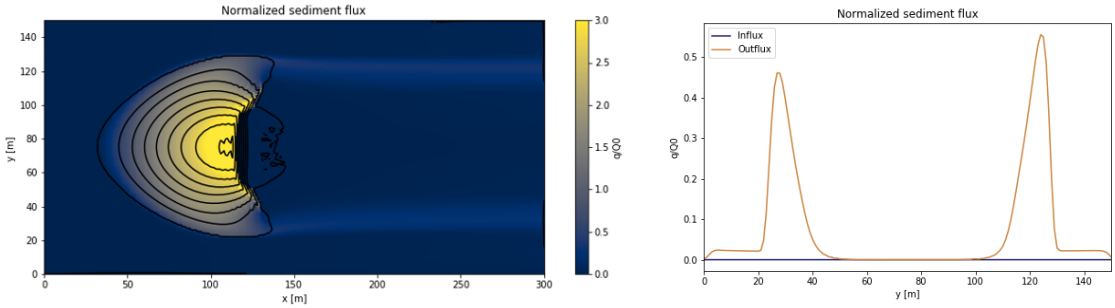

Figure 4.2: Left: Normalized sediment flux over a simulated barchan dune. Right: Sediment in- and out-flux as function of the transversal coordinate y.

The simulation results in figure 4.2 are based on a no-flux upwind boundary ($q_{in} = 0$), which indicates that no sediment reaches the dune in the wind direction. Still, due to the interaction of the wind field and the bed profile of the dune an out-flux is concentrated at the horns. The amount of sediment in this out-flux changes with the evolution of the dune shape. This simulation with a no influx loses around 5% of the dune volume over a period of 2 years.

The same simulation as showed above, but now with a sediment influx of $q_{in} = 0.1Q_0$ still results in a barchan dune that loses volume over time, around 2.5 % in a period of 2 years. A third simulation with $q_{in} = 0.2Q_0$ has a volume loss of 0.4 % while the fourth simulation with $q_{in} = 0.3Q_0$ shows a barchan dune that grows with 2.5 % in volume.

With respect to the suggested equilibrium relation between q_{in} and Q_0, the numerical model results show that the implementations related to aeolian sediment transport are reasonably able to reproduce the volume balance over a barchan dune. The small difference in the factor that actually results in a stable modelled dune compared to the suggested factor, is caused by an asymmetric development of the dune shape, which is visible in figure 4.2 with two slightly uneven peaks in the right panel.

4.1.2. Morphologic relations

Secondly, the resulting shapes of different barchan simulations are compared to field measurements of barchan dunes in Southern Morocco by Sauermann et al. (2000) in combination with proposed linear regressions between the height and width or length by Durán (2007), which are based on numerical simulation results. The field measurements in Southern Morocco consist of the dimensions for eight barchan dunes.

The shape of a barchan mainly depends on the volume of its initial topography. Therefore, four sand piles with a different volume are used as starting point. Two wind fields are used as external forcing to form a barchan dune from the initial sand piles. The morphologic characteristics of a total of 8 simulations, with a variation in the equilibrium brink height are analysed. This height is measured as the maximum height of the dune at the brink line, which is not necessarily the maximum height of the total dune. Furthermore, the equilibrium total length is measured as the difference between the maximum and minimum y-coordinate where the dune crosses the zero bed level line. The equilibrium width is measured similarly but then in x-direction.

The equilibrium dune height of each simulated dune is plotted against the width and total length in figure 4.3 together with the field measurements from Sauermann et al. (2000) and the proposed linear regression by Durán (2007).

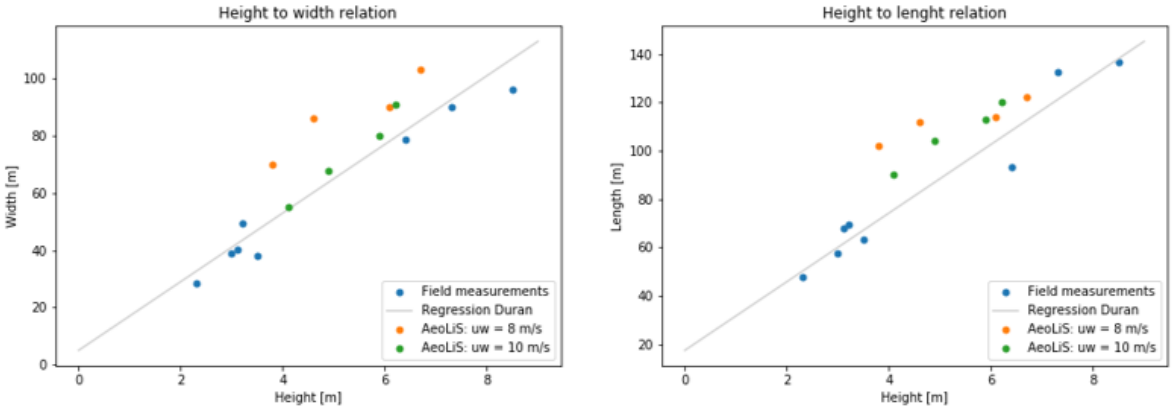

Figure 4.3: Linear relation of dune height to width and length

Compared to the field measurements in Morocco and the linear regression of Durán, numerical simulations results show that both width and length of the dunes are larger than expected in relation to the equilibrium height. This deviation might be related to a lack of wind direction variability in the model simulations compared to situations in the field. This relation is studied in section 4.1.4 where simulation results are considered with variations in the wind directions. Also, the updated implementation of the separation bubble, which ensures a smooth transition between the dune brink and the separation surface, might play a role as the maximum height of the dune is restricted to some extend. This is shown in the equilibrium height of the resulting dune shapes which are somewhat lower than expected when the dune volumes are compared with the field measurements and simulations by Durán.

4.1.3. Migration velocity

The third test of typical behaviour of barchan dunes relates to the migration velocity of the landform. Barchan dunes are highly mobile as there is no interaction with vegetation that can stabilize the dune.

The migration velocity of a stable barchan dune is measured by estimating the travelled horizontal distance of the brink point over a certain time period, see figure 4.4. In this example (simulation number 5) the black arrow shows the travelled distance of the brink in 26 weeks, resulting in a migration velocity of 46.1 m/year.

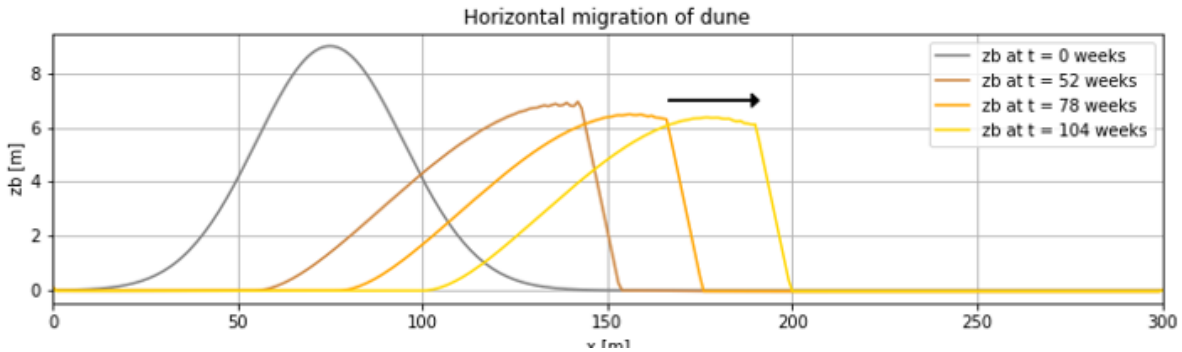

Figure 4.4: Travelled distance of the (stable) dune brink over a period of one year

Durán et al. (2010) found that the migration velocity of barchan dunes scales with the inverse of the width of the dune (W) following:

$$u_b = \alpha \frac{Q_0}{W} \tag{4.2}$$

Where Q_0 refers again to the saturated transport flux over a flat bed and the constant $\alpha = 50$.

Table 4.1 presents the measured migration velocity (v) for each dune following from numerical simulation results and the migration velocity estimated by the scaling from equation 4.2.

Table 4.1: Estimated migration velocity u_b dependent on the dune width W and wind velocity u_w, versus measured migration velocity v of simulated barchan dunes for the eight simulations with different initial profiles.

No.	Profile	u_w [m/s]	W [m]	u_b [m/y]	v [m/y]
1	a	8	103	4.2	18.8
2	b	8	90	4.7	19.6
3	c	8	86	4.9	20.0
4	d	8	70	6.1	21.5
5	a	10	91	18.1	46.1
6	b	10	80	20.5	49.9
7	c	10	68	24.2	53.6
8	d	10	55	29.9	59.3

There is a significant difference between measured migration velocities of the simulated dunes compared to estimated velocity by scaling. The main cause for this difference lies with the chosen saltation method to calculate the saturated sediment flux over a flat bed (Q_0). The scaling of Durán was derived for barchan dunes that are modelled with a different saltation model, see the mass flux relation of Kok et al. (2012) in table 2.1. This saltation model has much higher values for the saturated flux (in order of 10 times bigger) for the same bed roughness, see figure 2.2. Using this saltation method, a wind velocity of 6 m/s results for a barchan dune of 80 meters wide in a migration velocity of 45 m/year. Numerical model results show a comparable migration velocity under a constant wind velocity of 10 m/s. However, these measured values are then again not in the same order as the estimated ones using the scaling with the width of a dune.

One can say that the use of bagnold as saltation model, which has much lower values for the saturated sediment flux than the one used for derivation of the scaling law, makes the prediction of the migration velocity of a barchan dune following this scaling law unreliable.

4.1.4. Unimodal wind regime

Last, numerical results are tested with respect to a more realistic wind field. Barchan dunes typically occur under unidirectional wind conditions. The C shaped dunes, with horns pointing downwind, migrate in the prevailing wind direction. The simulations performed so far and the evaluated typical behaviour of barchan dunes are related to wind forcing from only one direction.

However, in the field barchan shaped dunes are subject to a (small) variation in the wind field. Therefore, several simulations with a more realistic wind field are performed with the numerical model.

The varying wind field of the simulations is filled with random values for the wind direction based on a normal distribution with a standard deviation σ_w between 0 and 40 degrees. The wind velocities are generated with the distribution included in AeoLiS (Hoonhout, 2015), with a mean value of 8 m/s.

Figure 4.5 shows resulting dune shapes of numerical modelling over a time period of 2 years, with respect to variability in wind orientation.

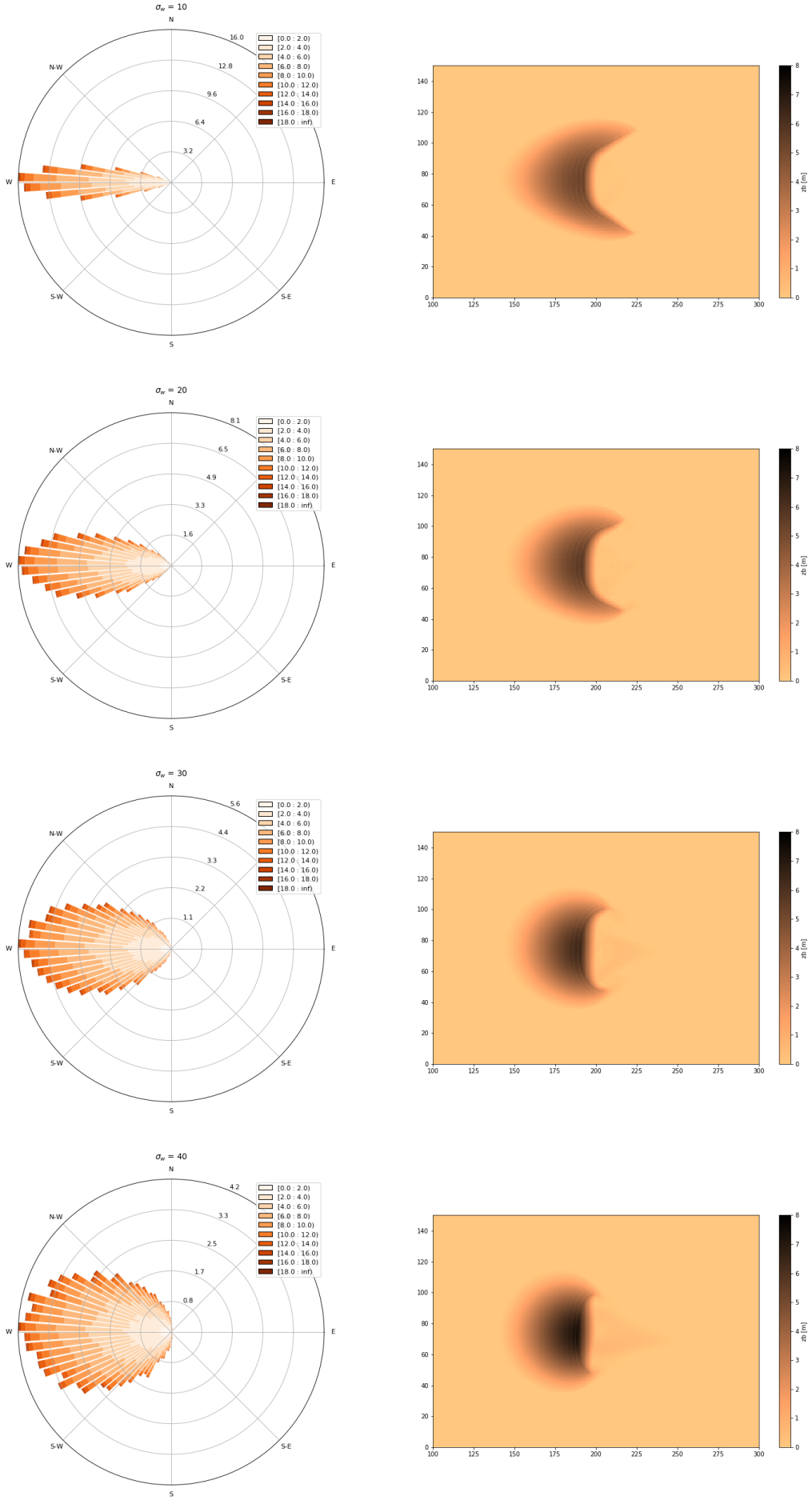

Figure 4.5: Equilibrium dune shape with respect to the variability in wind orientation (standard deviation σ_w)

The results show that the typical barchan shape dune still occurs under conditions with a limited variation in the wind direction. However, the C shape of the dune becomes wider and less elongated. The shape of the barchan dune in the top panel of figure 4.5 indicates that the linear relation between dune height and length as proposed by Durán (2007) and discussed above, is better approached here than in simulations under a uni-directional wind regime. For simulations with a standard deviation larger than the 10 degrees in this panel, the linear relation no longer holds. Also, the migration velocity of the dunes is affected. A larger variation in wind direction induces a more dome shaped dune with very small horns that only migrates at a very slow pace in the mean wind direction.

The resulting dune shapes for the different wind regimes are in good agreement with the results of the study by Gao et al. (2018), where the relationship between wind regimes and dome dune properties in different terrestrial dune systems are analysed by using satellite imagery for the dune shapes and global atmospheric reanalysis data for the surface winds.

The modelling part (based on cellular automaton) of this particular study on barchan and dome dune shapes under unimodal wind regimes, is not used for a qualitative comparison with AeoLiS model results as the two approaches of the modelling do not match.

Overall, the behaviour of the dunes from the numerical simulations show that the implemented processes on aeolian sediment transport produce results that are qualitatively comparable with expectations that are based on literature and other numerical model results. An exact reason for slightly different quantitative results concerning sediment supply, morphological relations and an estimated migration velocity is hard to express, as this model uses a different approach for both the saltation model and advection equation to solve the instantaneous sediment concentration.

4.2. Parabolic dunes

Barchan dunes develop into parabolic dunes when the mobility of the dune is restricted by the invasion of vegetation. The horns of the C shaped dune are stabilized by a growing vegetation cover, while the centre of the dune keeps migrating in downwind direction.

Figure 4.6 shows the result of a numerical model simulation in which a barchan dune is transformed into a not completely stabilized parabolic dune in a time period of 4 years (top left towards bottom right figure). The simulation starts without any vegetation present in the domain (top left), after which the vegetation cover start to increase at grid cells where there is a small net deposition rate. The stabilization by vegetation result in marginal ridges that are left behind at the horns.

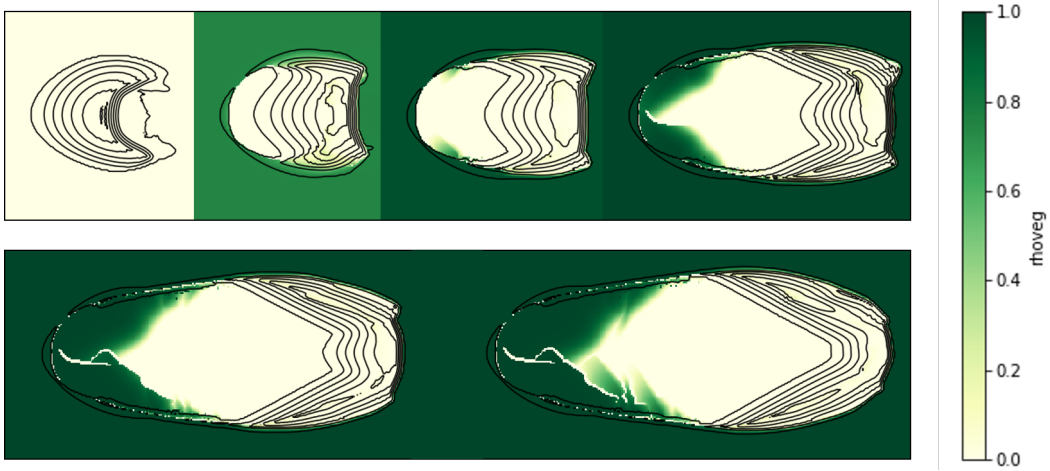

Figure 4.6: Transformation of a barchan dune into a (not completely stabilized) parabolic dune

4.2.1. Vegetation growth

The length over which the barchan dune transforms into a stabilized parabolic dune is related to the fixation index Θ introduced by Durán (2007). This index represents the competition between sediment transport and stabilization by vegetation. Durán found that an index of $\Theta \approx 0.5$ is the critical value beyond which the vegetation is not able to stabilize the initial barchan dune and it thus remains mobile. In order to test the performance of the numerical model with respect to the competition between sediment transport and vegetation growth, various simulations are performed with input parameters such that the stabilization index is comparable with simulation in Durán (2007). Large vegetation growth rates and thus a small value for the stabilization index are expected to result in quick deactivation of the barchan dune, while smaller vegetation growth rates are expected to show a longer time and spatial scale before the dune stabilizes.

Figure 4.7 shows the bed level and vegetation cover including contour lines of the resulting dunes shape per simulation after a simulation time of 3 years, with Θ as variable. The result show that the parabolic dune indeed stabilizes quickly for a small fixation index (top figure). The other three simulations are not at the stabilization point yet, but there is a clear difference between the development length of the transformations. So, the qualitative description of the conceptual ideas that form the parabolic dune, perform results as expected and in agreement with literature on the development of a parabolic dune. However, quantification of model parameters, spatial dimensions and transformation time of this dune development is not in order.

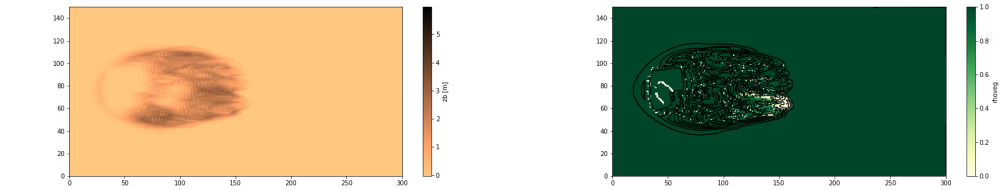

(a) Bed level and vegetation cover for $\Theta = 0.17$ (b)

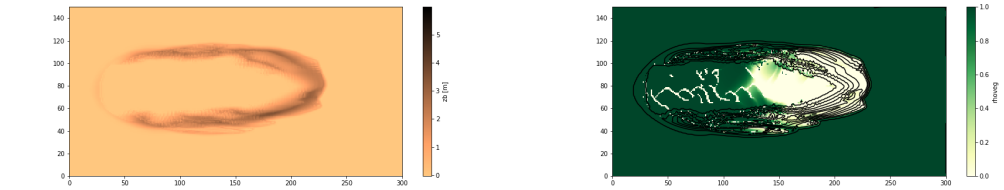

(c) Bed level and vegetation cover for $\Theta = 0.22$ (d)

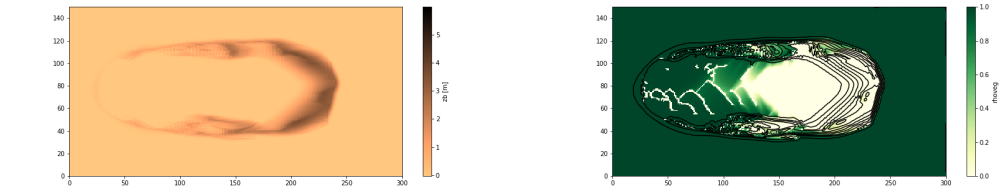

(e) Bed level and vegetation cover for $\Theta = 0.27$ (f)

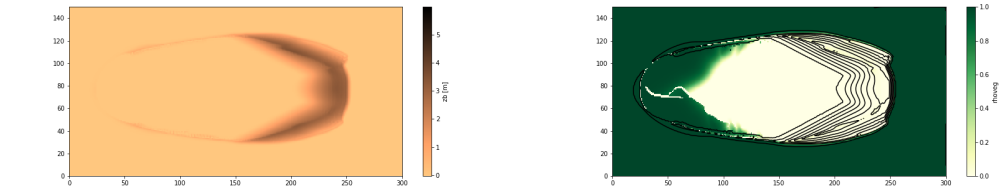

(g) Bed level and vegetation cover for $\Theta = 0.38$ (h)

Figure 4.7: Numerical model result of parabolic dunes shapes for different fixation indexes Θ

4.2.2. Optimization

Although the competition between sediment transport and vegetation growth in the model is as expected, the resulting parabolic shape itself seems also to depend on flow separation and vegetation characteristics influencing the shear stress. To test the influence of these processes and to optimize parabolic dune development, various numerical simulations are performed with variable input parameters related to the flow separation and vegetation characteristics. The third simulation from 4.7 with vegetation index $\Theta = 0.27$ is used as basis for the simulations described below.

Flow separation

Flow separation at the brink line of a barchan dune is one of the key processes to give the dune the typical C shape. However, the process of flow separation and the occurrence of a separation bubble seems to delay the transformation of a barchan dune into a parabolic dune, as the core of the barchan dune takes longer to flip from a C shape to a parabolic dune pointing in downwind direction. This is illustrated by the results of two numerical simulations after the same simulation period, where the first one includes flow separation for angles steeper than 30 degrees at the brink, while the second one does not include the process of flow separation, see figure 4.8. The second simulation without flow separation and a separation bubble allows for sediment transport at the lee side of the dune. This induces migration of the entire cross-section of the dune core in downwind direction, while in the simulation with a flow separation only the upwind slope of the dune migrates in downwind direction as sediment is deposited in the separation bubble.

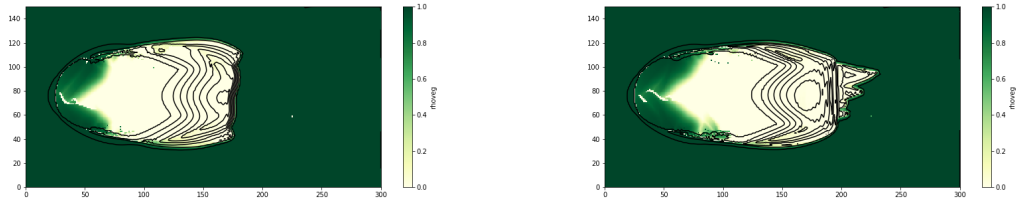

(a) Including flow separation

(b) Without flow separation processes

Figure 4.8: Difference between numerical model result of parabolic dunes with and without flow separation processes

Vegetation characteristics

To avoid abrupt changes in the calculation of the vegetation factor that reduces the shear stress, a filter is applied that takes the vegetation cover of the surrounding grid cells into account. This filter follows a Gaussian distribution and has a standard deviation $\sigma_{veg}[m]$, which determines the (isotropic) distance over which the surrounding values are taken into account. Figure 4.9 presents the resulting vegetation factor after one year of simulations with different values for the standard deviation. The results show that a value of 1.0 for the standard deviation seems too large as the area of stabilization is further towards the core of the dune, while a value of 0.6 and 0.4 for the standard deviation seem too small as the interaction between vegetation growth and morphology becomes unstable during the numerical simulations.

Next to the influence of this filter on the estimated vegetation factor, also the influence of variations in the roughness factor Γ itself are estimated. Previous simulations were performed with a defaults setting of $\Gamma = 16$. Figure 4.10 shows simulation results over a period of 3 years, with values for the roughness factor both smaller and larger than the default setting.

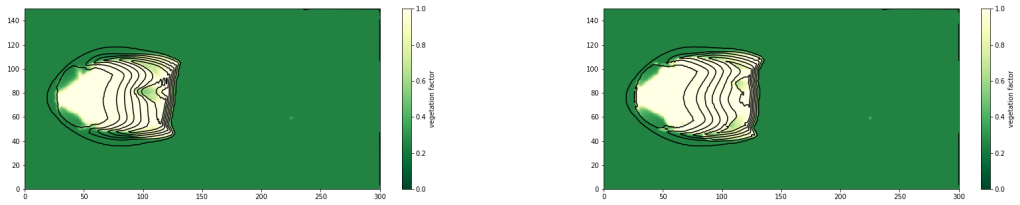

(a) $\sigma_{veg} = 1.0$

(b) $\sigma_{veg} = 0.8$

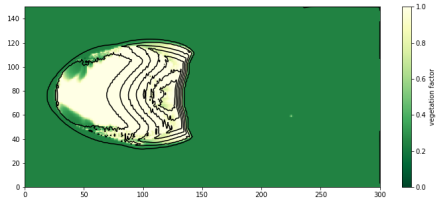

(c) $\sigma_{veg} = 0.6$

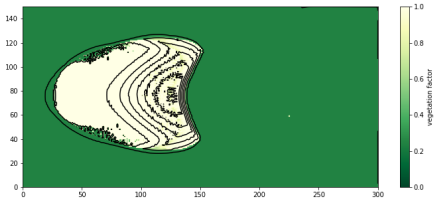

(d) $\sigma_{veg} = 0.4$

Figure 4.9: Vegetation factor of numerical model result with various standard deviations σ_{veg}

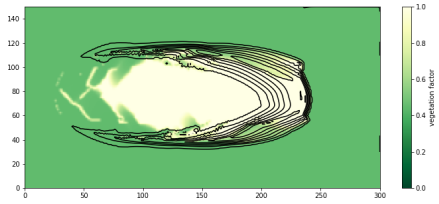

(a) $\Gamma = 4$

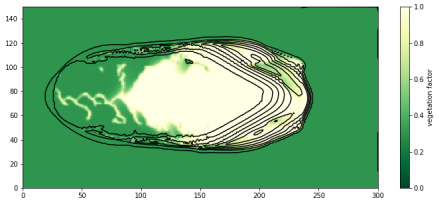

(b) $\Gamma = 10$

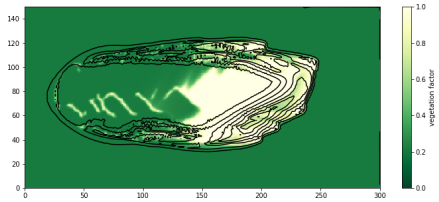

(c) $\Gamma = 22$

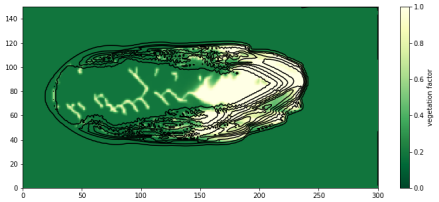

(d) $\Gamma = 28$

Figure 4.10: Vegetation factor of numerical model result for a variable roughness factor Γ

The model results clearly indicate that a lower value for the roughness factor leads to less stabilization by vegetation at the edges of the dune, while a higher value for the roughness factor leads to more sediment trapped at the trailing arms of the parabolic dune. Again, the qualitative description of the conceptual ideas that influence the competition between sediment transport and stabilization by vegetation perform properly. A link between the model results and the quantitative reality of this competition and especially of the influence of vegetation as a roughness element can not be made yet as the model simulations are performed as an academic case.

4.3. Academic blowout formation

The formation of a blowout in coastal dunes is directly related to processes included in development of parabolic dunes. Instead of an isolated barchan dune as initial topography, a small depression in a vegetated dune row is now considered as the starting point. Due to hydrodynamic processes and a regular input of sediment to the system, sediment from the beach and the exposed dune is transported by wind further into the dune system, forming a blowout.

For both cases the core of the feature migrates in the prevailing wind direction. Where vegetation growth and stabilization dominates the competition with aeolian sediment transport at the edges of the parabolic dune, the opposite situation occurs at the start of blowout formation. Due to high aeolian sediment transport rates in the blowout, the walls start to erode and become too steep. The walls collapse and retreat due to avalanching, resulting in dying of vegetation. As a consequence, the blowout width increases to a point where the deflation basin reaches a certain maximum depth and the walls are no longer undermined.

Meanwhile, the core of the blowout feature migrates in the wind direction and starts to form a parabolic dune that develops until the point where the competition with aeolian sediment transport becomes dominated by vegetation stabilization.

When the deflation basin is eroded up to the groundwater level (or other non-erodible layer), it cannot erode further. The bed level change at the entrance of the blowout will therefore reduce and if vegetation growth is sufficient the entrance might even close. An illustration of this blowout development is shown in figure 4.11.

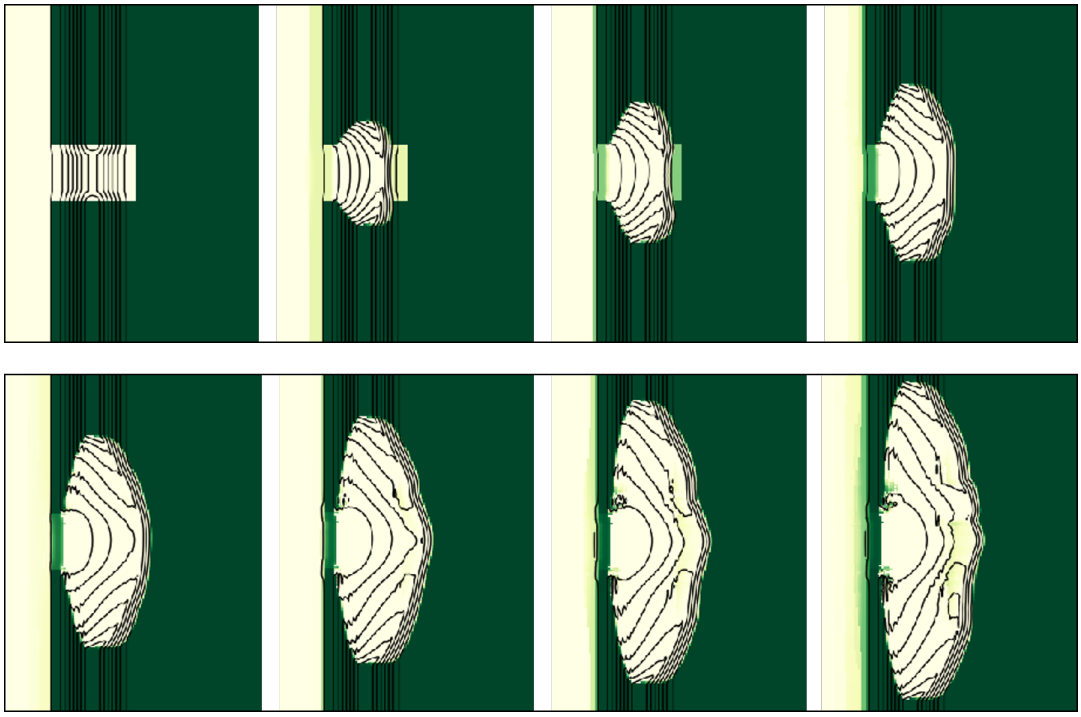

Figure 4.11: Development of blowout, illustrated by the vegetation cover that shrinks over time

4.3.1. Stability of the walls

The width of the blowout depends thus in the first place on the stability of the walls. The maximum steepness of the walls is determined by the static angle of repose which is implemented in the model as a constant value. The default setting of 34 degrees, which is based on dry sand, results in a very wide blowout feature where almost the entire dune row of the simulations gets mobilized within one year and vegetation does not play a roll. This development is not very interesting to study the interaction between sediment transport and stabilization by vegetation as aeolian sediment transport is dominant and the situation changes more into the development of a dessert dune without vegetation. To avoid the mobilization of the entire dune row and to estimate for which steepness of the walls a more elongated

blowout forms, different simulations are performed with increased values for the static angle of repose Θ_{stat}. Figure 4.12 shows the erosion and deposition rates over half a year in this simulations for different values of Θ_{stat}. It is very clear that the erosive walls of the early stage blowout have steeper slopes for an increased static angle of repose, resulting in a smaller width of the blowout for the same erosion rate of the deflation basin.

An increased steepness of the walls is likely to occur in reality for features in coastal areas as the presence of vegetation (including the roots) or an increased moisture content can result in a larger angle of repose. The chosen values only serve with the purpose to estimate the competition between aeolian sediment transport into the back dunes and the vegetation stabilization in this academic case.

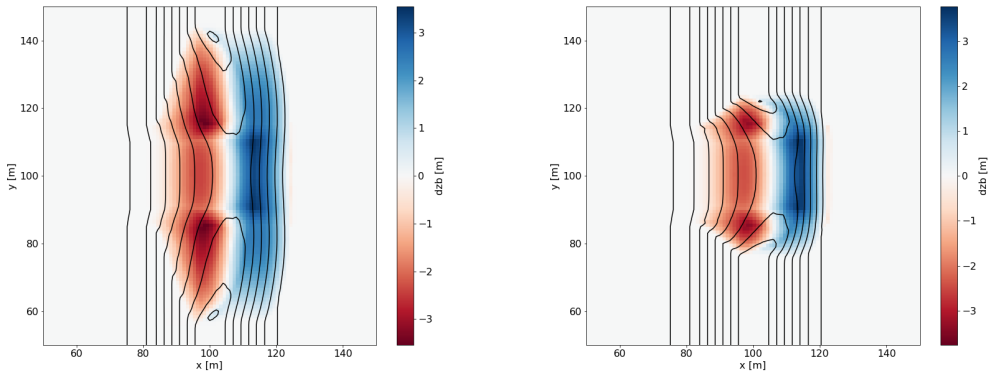

(a) $\Theta_{stat} = 34\ deg$

(b) $\Theta_{stat} = 40\ deg$

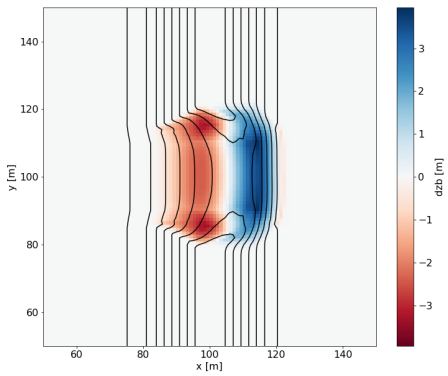

(c) $\Theta_{stat} = 46\ deg$

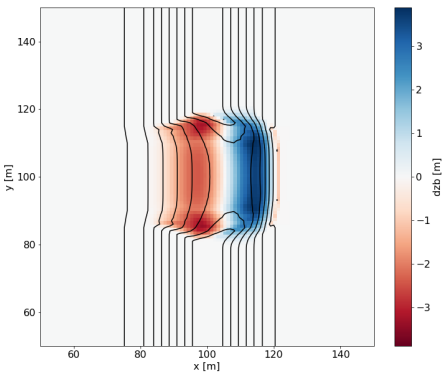

(d) $\Theta_{stat} = 52\ deg$

Figure 4.12: Bed level change in simulations with different values for the angle of repose

4.3.2. Vegetation characteristics

The next simulations are performed with an even larger static angle of repose: $\Theta_{stat} = 60\ deg$ to ensure a more elongated blowout feature that might develop into a parabolic dune. A reference case is performed without vegetation growth, results concerning bed level change and vegetation cover are presented in figure 4.13. It is noticeable that width of the blowout feature is indeed restricted due to the stabilization of the walls by a higher angel of repose. The migration in the wind direction is larger compared to the blowout feature from figure 4.11.

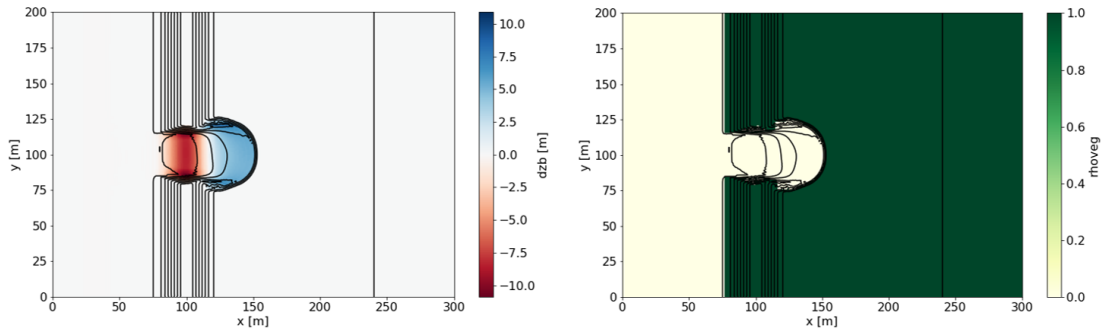

(a) Bed level change (b) Vegetation cover

Figure 4.13: Results after five years for blowout reference simulation without vegetation growth.

The vertical vegetation growth per simulation is based on values for the fixation index Θ that are comparable with the parabolic dune simulations. Figure 4.12 shows per simulations the resulting vegetation cover after 5 years. Again, a low value of the fixation index causes a faster stabilizing feature, while a higher value of the fixation index leaves much of the feature mobile. For each of the simulations the entrance of the blowout feature is closed (to some degree) by vegetation growth. This growth is stimulated at this location as the bed level change is restricted when the deflation basin level approaches the ground water table. The bed becomes non-erodible.

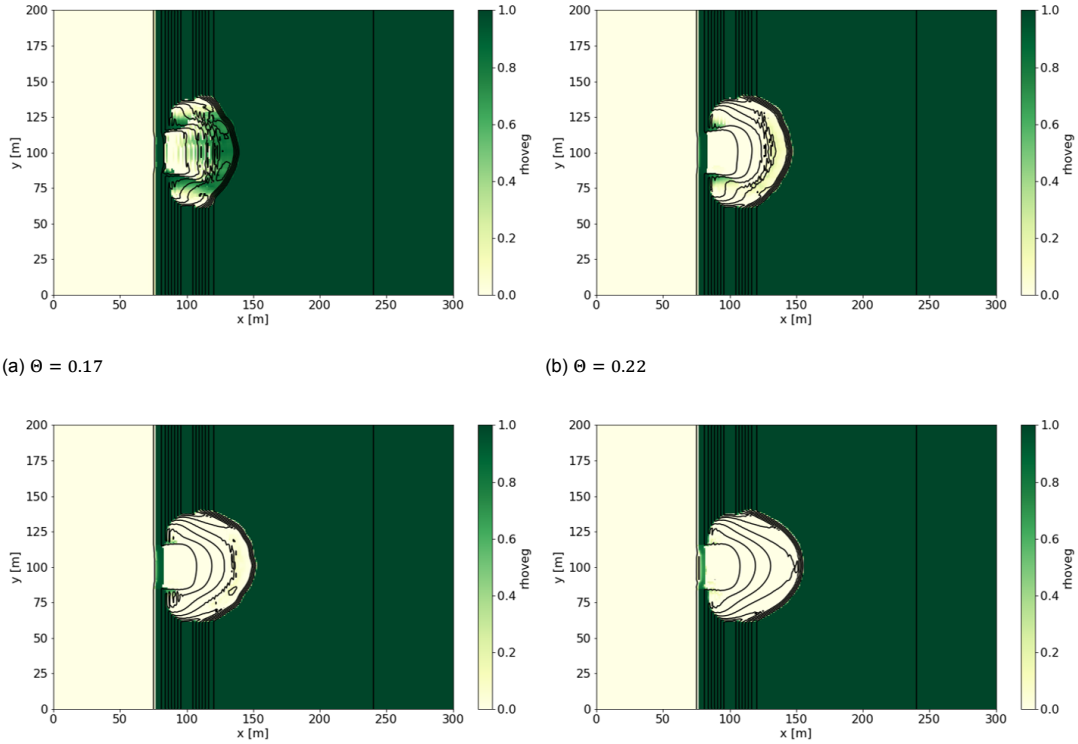

(a) $\Theta = 0.17$ (b) $\Theta = 0.22$

(c) $\Theta = 0.27$ (d) $\Theta = 0.38$

Figure 4.14: Resulting vegetation cover of blowout simulations based on different values for the fixation index Θ

4.4. Blowout features at Meijendel

To compare the model result with the field data, the bed level change between the measured elevation data of 2015 and 2017 is interpolated over the same grid as used for the numerical simulations, indicated with the blue square in figure 4.15. The manually added beach between x = 0 and 50 meters for the numerical simulations is not included here. The results of the bed level change in 2 years are presented in the right figure. Red areas indicate erosion of the bed level and blue areas refer to sedimentation. Blowout features 3a and 4 can be clearly indicated by the erosion patterns. The dark blue area in the middle of the domain represent a depositional lobe behind (the beach connected) blowout 4, while the reactivated blowout feature 3a does not clearly show such a pattern.

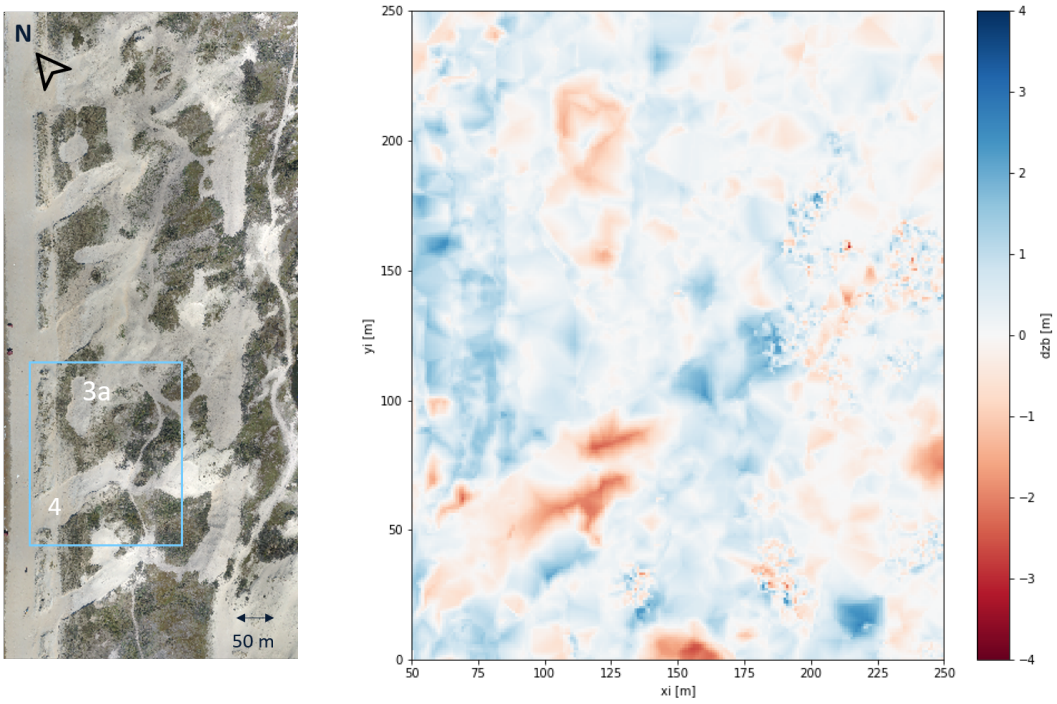

Figure 4.15: Domain of simulations with blowout 3a and 4 (right) and bed level change at this domain between field measurements of 2015 and 2017

4.4.1. Erosion patterns

The simulation takes the still water level, waves and a directionally varying wind field into account, while all processes from the conceptual model scheme are executed. The model remains stable and is able to calculate the bed level changes over the first two years.

First, a reference case, without vegetation growth and with the default setting of the model regarding avalanching, is performed to study the erosion patterns caused by the interaction between wind, morphology and already present vegetation. The bed level change over a simulation period of 2 years is shown in the right panel of figure 4.16.

The general erosion patterns of this simulation are in reasonable agreement with the measurements when it comes to the blowout features. The erosion and deposition rates at the foredunes are to be neglected as the input elevation levels at this location and at the beach were manually created.

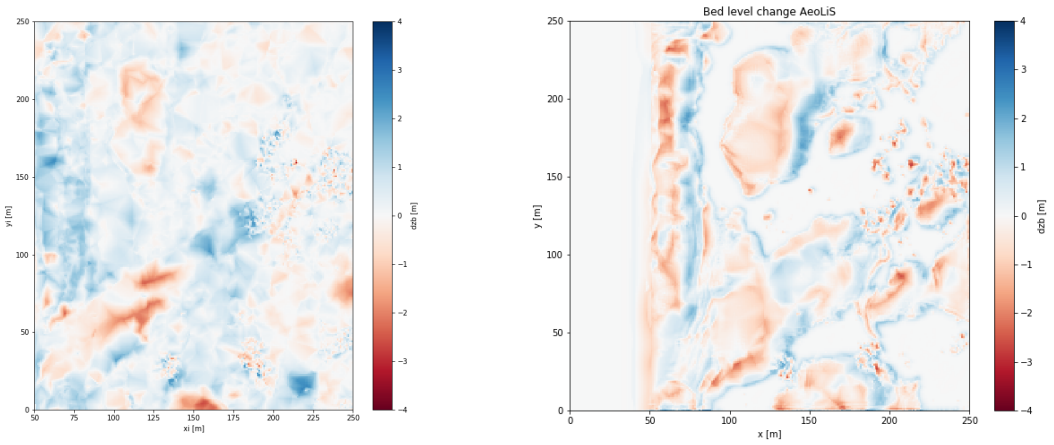

Figure 4.16: Bed level change between 2015 and 2017 of field data (left) and of reference case (right)

The transition between erosion and deposition of both blowout features is clearly visible as the red erosional areas are followed by a blue depositional area. However, the deposition of sediment seems to influence the overall pattern of bed level changes as de deposition takes place over only a short distance behind the plots subject to erosion (in the main wind direction). The measurements show a deposition pattern that is distributed over larger distances.

The model results are hard to compare with the measurements in terms of quantification as the erosion and deposition patterns differ at multiple locations. Despite that, the bed level change at the erosional part of the blowout features are quantitatively comparable to the measurements as the erosion rates are in the same order of magnitude.

Based on the academic blowout simulations, avalanching processes and the angle of repose seem to have a significant influence on the development of the blowout morphology. Therefore, the same simulation for the field case as described above is performed again with larger values for the (constant) static angle of repose. The presented results in figure 4.17 show that the erosion patterns are similar, while volume changes over the simulation period are affected by using larger values for Θ_{stat}. The influence of a larger value for the angle of repose is noticeable at the walls and edges of the blowout features. Also, it seems to have a significant role in erosion and deposition rates in the foredunes. As the erosion patterns of the numerical simulations are only to some extend qualitatively comparable with the field data, it is hard to quantify the effect of a higher angle of the repose and how this relates to simulations that can better approach the field data.

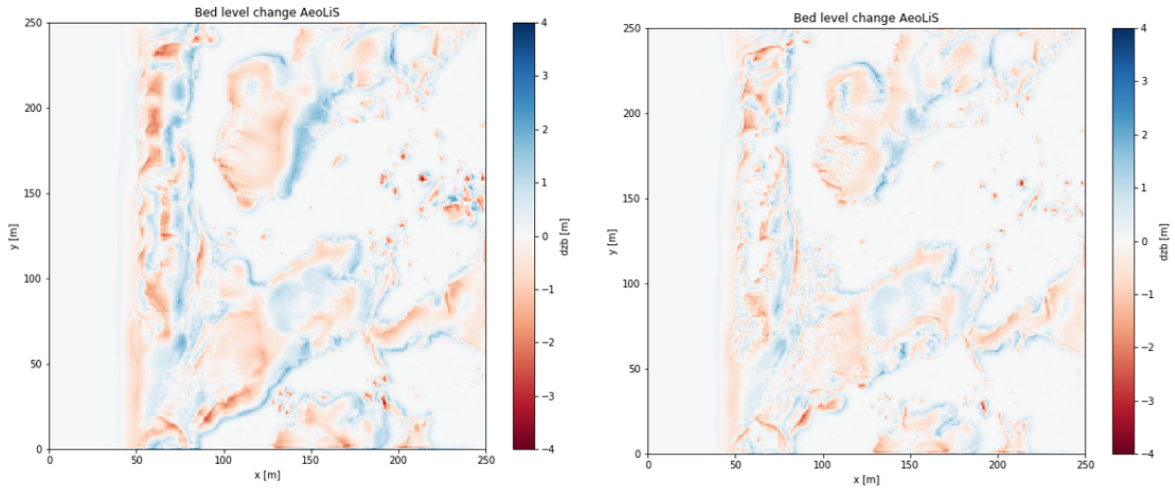

(a) $\Theta_{stat} = 40$ (b) $\Theta_{stat} = 46$

Figure 4.17: Bed level change of simulation results with different values for the static angle of repose Θ_{stat}.

4.4.2. Vegetation feedback

The vegetation cover of the domain at the measurement in 2017 is visible via the orthophoto of figure 4.18. Noticeable is that the vegetation cover around the blowout features mostly decayed and that the topography of blowout 4 migrates towards blowout 3a. Unfortunately, this merging of the features is not represented well in model simulations, see the right figure for resulting vegetation cover of the reference case. This is again most likely caused by the transition between erosion and abrupt sedimentation.

The increased vegetation cover at the foredunes and the triangle shape close to the foredune in between the two blowout features, is not represented in this simulations as vegetation growth was ignored.

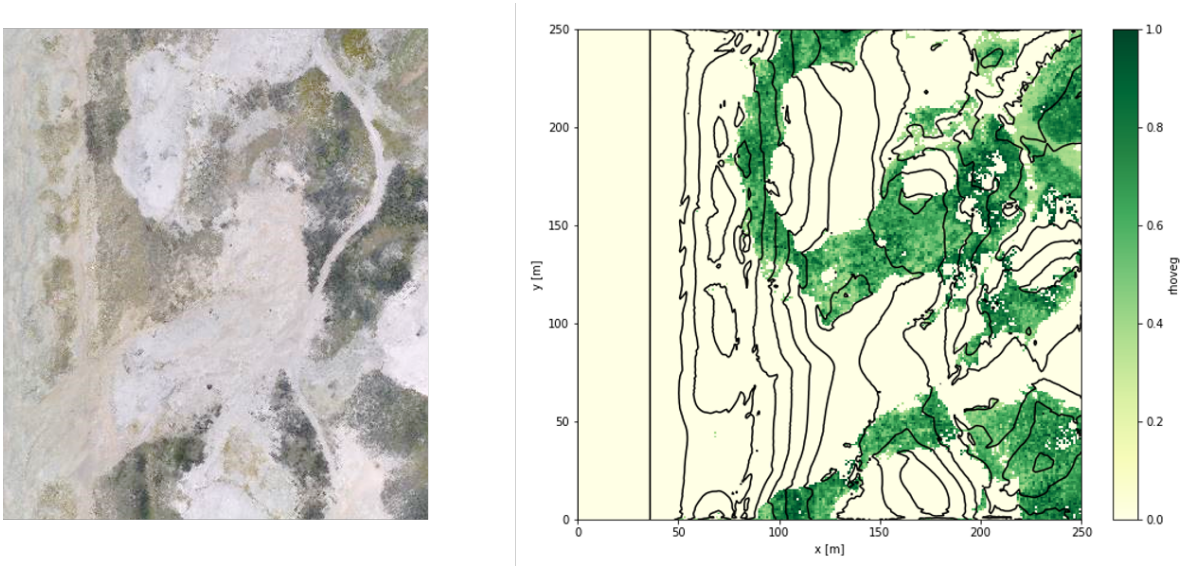

Figure 4.18: Left: vegetation cover via orthophoto 2017. Right: remaining vegetation cover after 2 years of reference simulation.

New simulations are performed with different values for the vegetation growth rate to estimate if the vegetation cover increases at the same locations as seen at the measurement. The reference case without vegetation growth is used to determine the order of magnitude of the vertical vegetation growth (V_{ver}) per year. In the reference simulation the vegetation cover will only be able to remain stable or to reduce in time. Vegetation growth is required at locations where a stable vegetation cover is expected after 2 years but where the reference simulation actually shows a reduction of the cover. The erosion that takes place at these locations should be counteracted by vegetation growth. A range of V_{ver} between 0.5 and 1.5 m/year is applied.

The vertical vegetation growth rates are not linked to the fixation index as used in the academic cases for two reasons. One: the total dune volume per meter varies significantly in the alongshore direction and two: the saturated sediment transport over a flat bed (Q_0) varies in time with the wind regime. For this approach, the fixation index and resulting vegetation growth are thus ideally calculated per time step and vary with the y-axis of the domain, but this is not (yet) possible with the current model implementations.

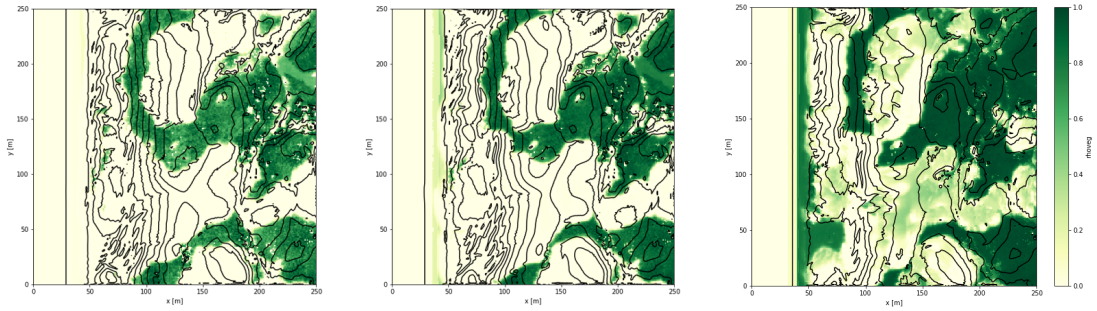

(a) $V_{ver} = 0.5\ m/y$ (b) $V_{ver} = 1.0\ m/y$ (c) $V_{ver} = 1.5\ m/y$

Figure 4.19: Resulting vegetation cover of blowout simulations based on different values for the veritical vegetation growth V_{ver}

The left panel of figure 4.19 indicates that a vertical vegetation growth rate of $0.5\ m/y$ is generally not sufficient to overcome the erosion by aeolian sediment transport. A rate of $1.0\ m/y$ results in some new vegetation plots in the foredunes, but is again not sufficient to overcome erosion at the locations where vegetation is expected following the field measurement. The right panel indicates that a growth rate of $1.5\ m/y$ is probably too large as vegetation is allowed to grow inside the blowout features, which are in reality still mobile after 2 years.

Noticeable is the growing vegetation line at the interaction between the beach and dunes, which is almost constant in the alongshore direction. The orthophoto of the measurement shows that this vegetation line in front of the foredunes is in reality not allowed to grow, most likely because of extreme events. The introduction of an artificial beach solved the problem of a significant erosion pit at the offshore boundary, but has now led to an in reality non-existing growth of vegetation in front of the foredunes.

5 Discussion

The model development part of this study has led to some significant contributions to the applicability of the numerical model for dynamic coastal development:

- The ability to calculate shear stresses as a result of the interaction between a directionally varying wind field and morphology, including flow separation processes.
- Ability to simulate multi-fraction sediment transport in combination with morphology induced shear stresses and spatial varying saltation velocity.
- A more realistic competition between aeolian sediment transport and stabilization by vegetation.
- An overall increased stability of the numerical model, which allows for bigger time steps in the simulations.
- Extra option to perform model simulation based on a steady state solution .

And although, the model validation through numerical model results show that these contributions have positively influenced the applicability for process-based modelling of (academic) dynamic coastal development, there are still multiple points for discussion.

This chapter elaborates on the simulation results of the three academic dune development cases, including limitations of the implemented processes and shortcomings in the validation, and relates the field case results to future engineering purposes.

5.1. Barchan dunes

Overall, the behaviour of the barchan dunes from the numerical simulations show that the implemented processes on aeolian sediment transport produce results that are quantitatively comparable with expectations based on literature.

The asymmetric development that showed up in the analyses of the sediment supply is most likely caused by the definition of the positive y-direction in the numerical scheme in combination with the imposed lateral boundaries. Similar simulations but then performed with the Crank-Nicolson scheme in the model should rule out if this is problem, or that it might be caused by the numerical implementation in general.

An exact reason for the deviation in the results concerning morphological relations and the estimated migration velocity is hard to express, as this model uses a different approach for both the saltation model and advection equation to solve the instantaneous sediment concentration.

One aspect that is likely to improve the model results is related to the adjustment of the advection equation 3.3.

Due to the implementation of a spatial varying saltation velocity, the variability of sediment concentration in space can no longer be ignored in the advection equation used to solve the instantaneous sediment concentration (as is now the case). The saltation velocity u is to be incorporated in the advection term for both x- and y- direction, following:

$$\frac{\delta c}{\delta t} + \frac{\delta c u_x}{\delta x} + \frac{\delta c u_y}{\delta y} = min\left(\frac{\delta m_a}{\delta t}, \frac{c_u - c}{T}\right) \tag{5.1}$$

The proposed adjustments were made to the original solve function in the model. However, the numerical implementation to solve the linear system had significant issues with the volume balance. A different approach was further used in this study. The coding of this new numerical implementation is rather complex. Therefore, this proposed adjustment of the advection equation is not yet implemented and the spatial variation of the saltation velocity has not been taken into account when the advection equation is solved for the instantaneous sediment concentration.

The application of a varying wind field in the barchan dune simulations shows that the model is capable of calculating shear stresses on the rotated computational grid, which is different for each time step. The formation of a more dome shaped dune confirms the expected behaviour of the model regarding the used wind fields. However, this behaviour is not validated and had a more theoretical basis.

To allow for directionally varying winds in the simulations, a second computational grid was implemented, for which the perturbation shear stresses are estimated. The use of this second grid induces a restriction to the range of possible input grids, as an equidistant input grid is required to cope with implemented interpolations. This restriction does not limit the model application in this study, but might be important for future applications.

5.2. Parabolic dunes

The numerical simulation results on the evolution from barchan dunes towards parabolic dunes show that the implementation and interaction of aeolian sediment transport and vegetation processes, perform as expected. The influence on parabolic dune development of vegetation characteristic such as the growth rate and roughness factor, qualitatively compare to results from Durán (2007). However, the combination of a constant wind field, assumptions for flow separation, use of a constant (non-realistic) bed roughness, and made-up values for the vegetation characteristics, proves that the applicability still only concerns academic forms.

In the performed simulations the vegetation growth rate was determined as an optimal range, linked to the undisturbed sediment transport flux Q_0. As this flux was artificially increased to speed up simulations results by increasing the bed roughness, the vegetation growth rates are ideal values that have nothing to do with realistic vegetation growth. Quantitative validation on vegetation growth rates is required to estimate realistic development of the parabolic dunes, where the bed roughness and wind field also refer to existing conditions. Besides this quantification, a more process-based implementation of different vegetation characteristics as elaborated below, is expected to increase the applicability of the model regarding vegetation processes.

Vegetation characteristics

Different vegetation characteristics are implemented with great simplifications, starting with the assumption of only one vegetation type in the domain. The maximum height, vertical growth rate and density of this type are implemented as constant values. In reality it is more likely that not only more vegetation types are present in the domain, but that the characteristics of each type vary over space and time as well.

Vegetation establishment and lateral growth are estimated by a probabilistic approach and are therefore included randomly. The probabilistic value is assumed to be spatially uniform, which limits the predictability of simulations as the value for both establishment and lateral propagation may change over the domain in reality.

Vegetation establishment by the distribution and germination of seeds is likely to depend on the wind direction, as the seeds are transported with the wind from an already vegetated plot. Also, the probability of vegetation establishment at cells that were germinated before is higher due to the remaining dead vegetation that enhance sedimentation and feed the soil with nutrients.

The probability of lateral propagation via rhizomes depends on the characteristics of the existing vegetation plot it propagates from. It is likely that the value increases for fully grown plants compared to the value for newly established ones.

The vertical growth of vegetation is implemented to be spatially varying as it depends on the sediment burial. However, influence of changing soil conditions and variation in growth rate for different vegetation species is missing.

The implementation of a more realistic moisture content module, including a groundwater table and influence of meteorology, would benefit a more process based approach concerning vegetation growth as it depends on the supply of fresh water. The water table is not necessarily uniform along the domain, causing spatial variations in the influence on vegetation. Also, the emergence of a freshwater lens in the dunes can drive vegetation growth. Meteorology influences vegetation growth directly, for instance through temperature, sunshine and precipitation, and indirect by altering the moisture content.

The introduction of a filter for the vegetation factor is at this point of the study a numerical trick to produce better results. However, the conceptual idea that a vegetation cover influences the sediment transport over an area that is somewhat larger than the plot itself seems applicable. Also, it could be applied to account for a (small) sheltering area behind the vegetation where the sediment transport is influenced. The distance and direction over which the filter applies is in this case dependent on the wind field. Quantification of this sheltering effect is required to say something on the applicability of this vegetation filter in process-based modelling.

5.3. Blowout formation

Simulation results on the academic blowout formation show that the numerical model is capable of combining the processes that are governing for blowout formation. The initiation phase of the blowout formation is included in the model set-up of this academic case. The conceptual ideas of blowout development and closure are represented well by the simulations.

The first step of blowout migration, where aeolian sediment transport is dominant over stabilization by vegetation, evolves as expected. The vegetation cover dies at plots that are buried by sedimentation and at plots subject to erosion as a consequence of unstable walls. The further development of the blowout feature into the back dunes is a result of the interaction between aeolian transport, where sediment from both the beach and the deflation basin is transported, and the vegetation stabilization. Vegetation growth rates that are related to the fixation index, which is used in the parabolic dune simulations, turn out to be applicable in the blowout simulations as well. A low value of the fixation index result in fast stabilization of the feature, while higher values indicate a larger development time and distance of the feature into the back dunes. However, this showed applicability only refers to the conceptual idea of this competition as the aeolian sediment transport is based on a constant wind regime and a higher bed roughness than is assumed to be applicable in reality. Also, a critical value for the fixation index, that determines for which vegetation growth rate the feature will not stabilize at all, has not been estimated yet.

The closure phase of a blowout feature is governed by growing vegetation plots at locations where the bed level change due to sedimentation and erosion has been limited. This is the case at the entrance of the blowout for the simulations that include vegetation growth. This closing of the feature is again a conceptual idea that is only represented partly in the simulations. In reality the closure of blowouts also relates to the sedimentation and erosion of the foredunes, which is amongst others influenced by storm induced erosion. Where a closed blowout feature in the model will result in a infinite growing foredune with vegetation, this will be different in reality as the foredunes are mobilized from time to time by storm events.

The academic results are useful to study the interaction between different implemented processes, but do not contribute yet to a better quantitative understanding of blowout behaviour in the field. The earlier mentioned lack of validation regarding the vegetation characteristics play an important role. Furthermore, factors as variability in wind direction, wind regime and topographic position are to be considered as well in determination of the morphological evolution of a blowout.

Two processes that turn out to be important for simulations in coastal systems (and that were not mentioned in the two previous academic cases) are avalanching and the velocity threshold, which is determined by various factors.

Avalanching

The constant value for the angle of repose determines under which slope steepness avalanching of sediment occurs. So far, this angle of repose is implemented in the model as a constant value based on dry sand. However, the maximum steepness of features in a coastal system can in reality be higher due to the presence of vegetation or an increased moisture content. To stabilize the erosional walls of the blowout, the constant value for the angel of repose was increased in the simulations based on the assumption that present vegetation (and their roots) positively effect the stability. The results show that this works as expected at the side walls of the blowout, where the slope steepness increases for larger values of the angle of repose. However, this altered angle does not seem valid for all situations. For example, the angle is expected to be lower at the depositional lobe of the blowout, where sediment at the top will be dry since it arrived here by aeolian transport.

So, to improve the applicability of the numerical model for features in coastal systems it is desired to determine a spatially varying angle of repose (both static and dynamic) that depends on some sort of factor for vegetation stabilization and a factor related to the moisture content, instead of imposing a constant value for the angle of repose for the entire domain.

Velocity threshold

The velocity threshold depends among others on the moisture content. Dry sediment is easier to transport than wet set. For now, the moisture content is estimated based on the volumetric water content, which is calculated based only on the still water level due to hydrodynamic processes. However, the moisture content is also dependent on the groundwater table and meteorological processes. A process-based implementation of both these factors is missing.

Meteorological processes can both positively and negatively influence the sediment transport by respectively drying of sediment in the top-layer, and by increasing the moisture content due to rainfall. The representation of a groundwater table effects the moisture content through precipitation and evaporation at the beach. This (direct) influence will be smaller in the dune system as the groundwater table is there located further from the bed surface. However, it is important for the maximum erosion in the blowout as the deflation basin often erodes until it reaches the groundwater table.

The moisture content is estimated every time step. If the water level is higher than the bed level at a certain point where this is not the case for the next time step, the computed moisture content in the second time step will be much lower. However, in reality the bed requires a certain time to dry, which might be larger than the time step used in simulations. By ignoring this drying time, the sediment transport might be overestimated as is assumes dry sand where it in reality is still (partially) wet. A dry function is implemented in the model to account for this phenomenon, but the application has not been tested thoroughly.

5.4. Blowout features at Meijendel

Despite the mentioned shortcomings in the academic simulations, all processes related to blowout formation in coastal dunes were included in a field case study. The combination of a varying wind field, vegetation characteristics, supply limited sediment transport and both a morphologic and vegetation feedback is unique.

Model results are only compared to field measurements of the first two years of the project (2015 to 2017). The field measurements of the second two years (2017-2019) can be included in the study when numerical simulations perform adequate results regarding both aeolian sediment transport and vegetation growth.

The combination of bagnold saltation model and a bed roughness that is based on dividing the grain size by a factor 30, seems to deliver bed level changes that are in the right order of magnitude compared with the field measurements. The overall erosion patterns of the simulation results are at some locations qualitatively comparable to the field measurements, while at other locations the results are way off. Especially the bed level changes at lateral boundaries form a point of discussion. One of the positive findings is that the transition between erosion and deposition of both blowout features is clearly visible. However, the deposition of sediment seems to influence the overall pattern of bed level changes as de deposition takes place over only a short distance. This trend of excess deposition right behind the locations where erosion takes place (in the prevailing wind direction) is notable over the entire domain and is most likely linked to the overall movement of too little sediment or to a too large influence of vegetation on the transport rate. The erosion and deposition rates in the foredune are to be neglected as the input elevation levels here and at the beach were created manually.

Another positive finding relates to the dying of vegetation plots which occurs in the model simulations more or less at the same locations as can been seen in the measurements. On the other hand, the growing of new vegetation plots over the simulation period of two years is unfortunately not represented well yet. The vegetation growth in front of the foredunes is caused by an unrealistic representation of foredunes in the system. A possible improvement for the results regarding the vegetation growth lies with a more precise translation of the field measurements to the input vegetation cover in the model. However, especially the lack of quantitative validation on the vegetation characteristics seems to limit the applicability of the vegetation module in AeoLiS regarding this practical case.

Although, the results are in the right direction for this stage of application, the field case study also shows that the model requires further development that includes the earlier mentioned factors, before it can produce quantitatively comparable results for simulations regarding features in a coastal environment.

6

Conclusions and recommendations

This final chapter derives the conclusions of the study, based on the current model development state, numerical model results and the discussion of the previous chapter. The conclusions lead to recommendations for future work on this topic. The recommendations are presented in the second section of this chapter.

6.1. Conclusions

In the process of simulating blowout features in coastal dunes, two parts of this study are distinguished. Where relevant processes were implemented and combined in a numerical model in the first part of the study, its application on three academic dune development cases is validated in the second part via numerical modelling. The modelling part is concluded with a practical application of the model regarding simulations of blowout features at the Dutch Coast of Meijendel.

The main research question of the study is formulated as:

To what extend can the numerical model AeoLiS be used as a tool to predict the development of artificially initiated blowout features in coastal dunes?

The research question is answered via three sub questions, which are elaborated below.

1. What are the relevant processes in the development of blowout features and how could these be described by a numerical model?

Relevant processes for blowout formation in coastal dunes are related to:

- Wind induced shear stresses

  The potential aeolian sediment transport is based on shear stresses on the bed surface induced by the wind field. The shear stresses are updated for interaction with the morphology following the perturbation of Kroy et al. (2002).

- Influence of vegetation on shear stresses

  Vegetation acts as a roughness element and therefore reduces the wind shear velocity on the bed level. A factor is estimated based on the present vegetation cover to determine the influence of vegetation on the shear stress, following an adapted definition by Raupach et al. (1993).

- Supply limiting factors

  Supply limiting factors are of importance in coastal systems as the amount of sediment that is available for aeolian transport varies in space and time. Supply liming factors that are applied in this study are the moisture content, which is based on hydrodynamics only, and non-erodible elements.

- Aeolian sediment transport

  The amount of sediment transport is estimated following the saltation model of Bagnold (1937), where the threshold velocity is based on the sediment grain size and supply limiting factors. A definition for the spatial varying saltation velocity follows from Sauermann et al. (2001).

- Feedback between sediment transport and morphology

  The morphology is updated as a consequence of the erosion or deposition related to the aeolian transport, which is based on the instantaneous sediment concentration. To cope with too steep dune slopes, the process of avalanching is included in the model. Also, the bed level at the offshore boundary is updated when hydrodynamics influence the sediment supply.

- Influence of erosion/sedimentation on vegetation growth

  The net growth of a vegetation plot depends on the amount of erosion or sedimentation in relation with the vegetation growth itself. Different factors that influence the vegetation characteristics, such as vertical growth, establishment and propagation of the vegetation cover are included as a feedback in the model.

The relevant processes are implement in the numerical model as separate modules that interact with each other following the conceptual scheme of AeoLiS as presented in the model description of section 3.1. The numerical model runs this scheme with modules every time step and uses the outcome of the updated morphology and vegetation characteristics as new initial conditions for the next time step. Depending on the application of the model, some modules are not executed.

2. How can the combination of these processes be used to model the development of several academic cases relevant for blowout formation?

The application of combined processes in the numerical model is validated for three different academic cases which each include part, or all the relevant processes of blowout formation.

First, only the interaction between aeolian sediment transport due to wind induced shear stresses and the morphological feedback are combined in simulations for the development of barchan dunes. Results show that the model is reasonably capable of performing the development of this dune type, which is quantitatively related to typical behaviour of barchan dunes. Possible improvements regarding this case are within updating the numerical scheme that includes the spatial varying saltation velocity and

Secondly, the development of a barchan dune into a parabolic dune was performed as academic case. The processes of aeolian sediment transport and influence of vegetation on this transport are combined with both a morphological and vegetation growth feedback.

The vegetation index as proposed by Durán and Herrmann (2006) was used to determine the required vertical vegetation growth rate to stabilize the initial barchan dune. Results show that the model is capable of producing the conceptual idea of the competition between aeolian transport rates and vegetation stabilization patterns, leading to a parabolic dune. The influence of several parameters on the development were studied to optimize the formation of a parabolic dune.

The last academic case consists of the development of an artificially initiated blowout in a coastal dune system and includes all relevant processes that were determined in the first section. Simulation results show that the numerical model is capable of producing initial characteristics of blowout formation where the walls erode and a deflation basin plus depositional lobe grow. The vegetation cover dies at plots that are buried by sedimentation and at plots subject to erosion as a consequence of unstable walls. The further development of the blowout feature into the back dunes is a result of the interaction between aeolian transport, where sediment from both the beach and the deflation basin is transported, and the vegetation stabilization. The closure phase of a blowout, where the stabilization by vegetation becomes dominant over the aeolian sediment transport, is again represented well in the model results.

3. How do numerical model results compare to a field case with artificial initiated blowout formations?

The numerical model is used for simulations of dynamic dune development at Meijendel. This project includes 5 artificially initiated blowout features. Elevation data of the project domain was gathered via orthophotos, which are also used to determine the input grid of the numerical simulations.

All relevant processes for blowout formation are combined to determine the bed level change in the domain over a time period of two years. Results show that the overall erosion patterns and the order of magnitude of the bed level change is in reasonable agreement with the field measurements. However, the pattern of deposition is not quite right yet as model simulations show an excess deposition right after locations that are eroded. Dying of vegetation plots as a consequence of bed level changes is represented well in the model results compared to the field measurement, while the growing of new vegetation plots is not working properly yet.

Concluding, the numerical model AeoLiS can be used to perform simulations that include all the relevant processes for blowout formation in coastal dunes, but is not yet suitable as tool to predict the development of blowouts that can be validated quantitatively.

The combination of processes that confirms the conceptual ideas on the development of different academic land forms in this study, is only validated in a qualitative matter. The practical application of the model on blowout features at Meijendel shows that further development is required regarding the processes that are especially important in coastal areas.

6.2. Recommendations

Based on the discussion points and drawn conclusions, further development of the numerical model is recommended to increase predictability of simulations and to expand the range of applications. The suggested items for this development are described below and are related to the following topics:

- Numerical implementation regarding sediment transport
- Groundwater table and meteorology
- Vegetation characteristics
- Avalanching
- Coupling with hydrodynamic models

Numerical implementation

There are three topics regarding the numerical implementation of the advection equation that are expected to improve numerical results. First, the original solve functions has still problems with the volume balance when large dune volumes are considered. Once the solve function remains stable, the already implemented steady state solution can be applied as well in model simulations. Second, application of an upwind numerical scheme seems to results in (small) asymmetric dune development under unidirectional wind conditions. It should be verified if the use of this scheme is actually the cause by applying a different numerical scheme, for example the Crank-Nicolson scheme that is already included in the model, to perform similar simulations. Third, the application of the newly proposed advection equation, with a spatial varying saltation velocity included in the advection term, has to be validated.

Groundwater table and meteorology

A process-based implementation of the groundwater table and meteorological processes that influence the moisture content is required to improve model applicability for coastal systems.

Meteorological processes can both positively and negatively influence the sediment transport by respectively drying of sediment in the top-layer, and by increasing the moisture content due to rainfall. Also, the effect of sunshine and temperature on vegetation growth might be important. This is to be investigated.

The representation of a groundwater table effects the moisture content through precipitation and evaporation at the beach. The groundwater table will act as a non-erodible layer for bed levels that are eroded up to that level. This (direct) influence will be smaller in the dune system as the groundwater table is there located further from the bed surface. However, it is important for the maximum erosion in a blowout as the deflation basin often erodes until it reaches the groundwater table. Also, the groundwater table influences the vegetation growth. It might be interesting to investigate the interface between salt and fresh water in the domain and how this influences the vegetation.

Vegetation characteristics

To improve the applicability for simulations that include vegetation, four items are suggested that need attention.

First, research on the area at which vegetation (acting as a roughness element) influences the shear velocity is desired. Currently, the model only takes the influence into account at the plots where vegetation is present and uses then a filter to smooth out the results. It is however expected that the influenced area will be bigger, especially behind the vegetation in the prevailing wind direction.

Secondly, extra research on a more process-based description of vegetation establishment and propagation is required. The now spatial uniform probabilistic value, with which the establishment and lateral propagation of vegetation is distributed randomly over the domain, changes to a value that depends on the wind regime, already existing vegetation plots and possibly on various abiotic factors.

Third, the definition of the vertical vegetation growth rate in the model now only depends on sediment burial. Besides this direct link with the morphological feedback, vegetation growth also depends on various abiotic factors. Further research on this dependence regarding for example temperature and salinity concentrations is required. The newly described definition of the moisture content from before, which depends on a groundwater table and meteorology, can likely be used to include some abiotic factors already.

Finally, a quantitative validation regarding typical values for the vegetation characteristic in combination with the morphological feedback is required.

Avalanching

Currently, a constant value for the angle of repose determines under which slope steepness avalanching of sediment occurs. The maximum steepness is in reality variable over the coastal system domain as sediment gets stabilized by vegetation or has a higher angle of repose via wet sediment at some locations. Therefore, a spatially varying angle of repose (both static and dynamic) that depends on some sort of factor for vegetation stabilization and a factor related to the moisture content is desired.

Coupling with hydrodynamics

AeoLiS includes hydrodynamics processes very simplistic and is only suitable for situations with a steady shoreline under calm conditions. In order to improve (practical) simulations that consider an entire coastal system the coupling of AeoLiS with a hydrodynamic numerical model is required. To better present the interaction between aeolian sediment transport and marine processes over the long term, a coupling with Delft3D is recommended. Luijendijk et al. (2019) describes this coupling which is related to research on dune growth at the Sand Engine. For applications regarding the influence of a seasonal varying shoreline and long term processes as sea level rise can be investigated with this coupling. For simulations that consider the influence of extreme events on the dune development, a coupling of AeoLiS with XBeach (Roelvink et al., 2009) is recommended.

Bibliography

B. Arens. Kerven in de zeereep van noordsvaarder, 2010.

S. M. Arens, S. de Vries, L. H. W. T. Geelen, G. Ruessink, and H. G. J. M. van der Hagen. Comment on 'is 're-mobilisation' nature restoration or nature destruction? a commentary' by i. delgado-fernandez, r.g.d. davidson-arnott & p.a. hesp. *Coastal Conservation*, 24(17), 2020. doi: https://doi.org/10.1007/s11852-020-00731-1.

R. A. Bagnold. The transport of sand by wind. *The Geographical Journal*, 89(5):409–438, 1937.

R. A. Bagnold. *The physics of blown sand and desert dunes*. Londen: Methuen, 1941.

T. E. Barchyn and C. H. Hugenholtz. Aeolian dune field geomorphology modulates the stabilization rate imposed by climate. *Journal of Geophysical Research: Earth Surface*, 117, 2012.

B. O. Bauer and R. G. D. Davidson-Arnott. A general framework for modelling sediment supply to coastal dunes including wind angle, beach geometry and fetch effects. *Geomorphology*, 49(1):89–108, 2003.

P. Y. Belly. Sand movement by wind. Technical Report Technical Report 1, U.S. Army Corps of Engineers CERC, 1964.

L. M. Bochev-van der Burgh. *Decadal-scale morphologic variability of foredunes subject to human interventions*. PhD thesis, Universiteit Twente, 2012.

N. Cohn, P. Ruggiero, S. de Vries, and G. M. Kaminsky. New insights on coastal foredune growth: the relative contributions of marine and aeolian processes. *Geophysical Research Letters*, 45(10), 2018.

W. S. Cooper. Coastal sand dunes of california. *Geological Society of America - Memoir 101, 131*, 1967.

S. De Vries. *Physics of blown sand and coastal dunes*. PhD thesis, Delft University of Technology, 2013.

S. de Vries, H. N. Southgate, W. Kanning, and R. Rasasinghe. Dune behaviour and aeolian transport on decadal timescales. *Coastal Engineering*, 2012. doi: https://doi.org/10.1016/j.coastaleng.2012.04.002.

S. De Vries, S. Arens, M. de Schipper, and R. Ranasinghe. Aeolian sediment transport on a beach with a varying sediment supply. *Aeolian Research*, 2014a.

S. De Vries, J. S. M. van Thiel de Vries, L. van Rijn, S. M. Arens, and R. Ranasinghe. Aeolian sediment transport in supply limited situations. *Aeolian Research*, 12:75–85, 2014b.

I. Delgado-Fernandez. A review of the application of the fetch effect to modelling sand supply to coastal foredunes. *Aeolian Research*, 2(2):61 – 70, 2010. ISSN 1875-9637. doi: https://doi.org/10.1016/j.aeolia.2010.04.001.

O. Durán. *Vegetated dunes and barchan dune fields*. PhD thesis, Institut für Computerphysik der Universität Stuttgart, 2007.

O. Durán and H. J. Herrmann. Vegetation against dune mobility. *Physical Review Letters*, 97(18):1 – 4, 2006.

O. Durán and L. J. Moorde. Vegetation controls on the maximum size of coastal dunes. *Proceedings of the National Academy of Sciences*, 110(43):17217 – 17222, 2013.

O. Durán, J. R. Parteli, and H. J. Herrmann. A continuous model for sand dunes: Review, new developments and application to barchan dunes and barcham dune fields. *Earth surface processes and landforms*, 35:1, 2010.

EcoShape. Building with nature guidelines, 2019. URL https://publicwiki.deltares.nl/display/BTG/Guideline.

X. Gao, C. Gadal, O. Rozier, and C. Narteau. Morphodynamics of barchan and dome dunes under variable wind regimes. *Geological Society of America*, 46(9):743–746, September 2018.

E. B. Goldstein, L. J. Moore, and O. D. Vincent. Lateral vegetation growth rates exert control on coastal foredune ”hummockiness”and coalescing time. *Earth Surface Dynamics*, 5(3):417 – 427, 2017.

P. Hersen. On the crescentic shape of barchan dunes. *The European Physical Journal B*, 37:507 – 514, 2004.

P. A. Hesp. Foredunes and blowouts: initiation, geomorphology and dynamics. *Geomorphology*, 48 (1-3):245–268, 2002.

P. A. Hesp and I. J. Walker. Coastal dunes. *Treatise on Geomorphology*, 11:328 – 355, 2013.

B. Hoonhout. *AeoLiS's documentation*, 2015. URL https://aeolis.readthedocs.io/en/latest/index.html.

B. Hoonhout and S. de Vries. Aeolian sediment supply at a mega nourishment. *Coastal Engineering*, 2017.

B. Hoonhout, S. de Vries, F. Baart, J. van Thiel de Vries, L. van der Weerd, and K. Wijnberg. Monitoring of beach surface properties with remote sensing. In *Proceedings Coastal Dynamics 2013: 7th International Conference on Coastal Dynamics, Archon, France, 24-28 June 2013*, pages 821–832, Bordeaux, 2013. Bordeaux University - SHOM.

R. Kawamura. Study of sand movement by wind. Technical Report 5, University of Tokyo, 1951. (Japanese).

J. G. S. Keijsers, A. V. D. Groot, and M. Riksen. Vegetation and sedimentation on coastal foredunes. *Geomorphology*, 228:723 – 734, 2015.

J . F. Kok, E. J. R. Parteli, T. I. Michaels, and D. B. Karam. The physics of wind-blown sand and dust. *Report on Progress in Physics*, 75, 2012.

M. J. Koster and R. Hillen. Combat erosion by law: Coastal defence policy for the netherlands. *Journal of Coastal Research*, 11(4):1221 – 1228, 1995.

K. Kroy, G. Sauermann, and H. J. Herrmann. Minimal model for aeolian sand dunes. 2002.

A. Luijendijk, S. de Vries, T. van het Hooft, and M. de Schipper. Predicting dune growth at the sand engine by coupling the delft3d flexible mesh and aeolis models. *Coastal Sediments 2019*, pages 1319–1326, 2019.

R. L. Martin and J. F. Kok. Wind-invariant saltation heifhts imply linear scaling of aeolian saltation flux with shear stress. *Science Advances*, 3, 2017.

M. A. Maun. Adaptions enhancng survival and establishment of seedlings on coastal dune systems. *Vegetation*, 111(1):59 – 70, 1994.

M. A. Maun. *The biology of coastal sand dunes*. Oxford University Press, 2009.

E. J. R. Parteli, K. Kroy, H. Tsoar, J. S. Andrade, and T. Pöschel. Morphodynamic modeling of aeolian dune: Review and future plans. *The European Physical Journal*, 2014.

R. Ranasinghe, D. Callaghan, and M. J. F. Stive. Estimating coastal recession due to sea level rise: beyond the bruun rule. *Climate Change*, 2012.

M. R. Raupach, D. A. Gillette, and J. F. Leys. The effect of roughness elements on wind erosion threshold. *Journal of Geophysical Reasearch: Atmospheres*, 98, 1993.

D. Roelvink, A. Reniers, A. van Dongeren, J. v. T. de Vries, R. McCall, and J. Lescinski. Modelling storm impacts on beaches, dunes and barrier islands. *Coastal Engineering*, 56(11-12):1133–1152, 2009.

G. Sauermann, P. Rognon, A. Poliakov, and H. J. Herrmann. The shape of barchan dunes of southern morocco. *Geomorphology*, 36:47–62, 2000.

G. Sauermann, K. Kroy, and H. J. Herrmann. *A Continuum Saltation Model for Sand Dunes*, 2001.

C. Schwarz, J. Brinkkemper, and G. Ruessink. Feedback between biotic and abiotic processes governing the development of foredune blowouts: A review. *Journal of Marine Science and Engineering*, 2018.

M. J. Stive, M. A. de Schipper, A. P. Luijendijk, S. G. Aarninkhof, C. van Gelder-Maas, J. S. van Thiel de Vries, S. de Vries, M. Henriquez, S. Marx, and R. Ranasinghe. A new alternative to saving our beaches from sea-level rise: The san engine. *Journal of Coastal Research*, 290:1001–1008, 2013.

T. L. Thomberry-Ehrlich. White sands national monument. *Geological Resources Inventory Report*, October 2012.

J. H. van Boxel, P. D. Jungerius, N. Kieffer, and N. Hampele. Ecological effects of reactivation of artificially stabilized blowouts in coastal dunes. *Coast Conservation*, 3(57 - 62), 1997.

B. van den Hurk, P. Siegmund, and A. K. Tank. Knmi'14: Climate change scenarios for the 21st century - a netherlands perspective. Technical report, KNMI, 2014. URL http://www.climatescenarios.nl/. KNMI scientific report WR 2014-01.

H. van der Hagen, ten Napel G., and B. Arens. Grenzen slechten in meijendel: stuifgaten in de zeereep. *Holland's Duinen*, 70:2–6, 2017. In Dutch.

m.E. van Puijenbroek, C Teichmann, N. Meijdam, I. Oliveras, E. Berendse, and J. Limpens. Does salt stress constrain spatial distribution of dune building grasses ammophila arenaria and elytrichia juncea on the beach? *Ecology and Evolution*, 7(18):7290–7303, 2017.

B. van Westen. Numerical modelling of aeolian coastal landform development. Master's thesis, Delft University of Technology, 2018.

W. S. Weng, J. C. R. Hunt, D. J. Carruthers, A. Warren, G. F. S. Wiggs, I. Livingstone, and I. Castro. Air flow and sand transport over sand-dunes. *Acta Mechanica*, 2:1 – 22, 1991.

A

Model description

AeoLiS is a process-based numerical model that was initially developed to simulate aeolian sediment under supply-limited conditions. A full description of the original model can be found at https://aeolis.readthedocs.io/en/latest/index.html by Hoonhout (2015). To use the model for simulating dune development processes, different modules were added by van Westen (2018). Based on these two versions of the model and with the purpose of including governing processes for blowout formation, a new conceptual scheme as showed in figure 3.2 is used in this study.

A.1. Wind shear

The wind induced shear stress is required to calculate aeolian sediment transport rates. It is calculated per time step as the sum of shear stresses induced by the wind only, and shear stresses induced by the interaction of morphology and the wind field.

Wind directions

The wind input data can have two different wind conventions: Nautical and Cartesian. A Nautical wind convention defines the wind direction with a zero angle from the North and uses a positive clockwise rotation, while a Cartesian wind convention defines the wind direction from a zero angle pointing in the positive x-direction of the domain and uses positive anti-clockwise rotations. The difference is illustrated in figure A.1.

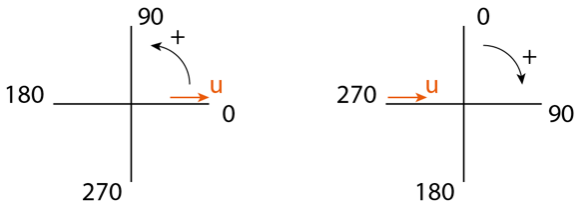

Figure A.1: Cartesian (left) and Nautical (right) wind conventions.

The orange arrow in both figures describe the same wind vector u. For the Cartesian wind convention this vector pointing towards the right has a direction of 0 degrees, while it comes from the left and has a direction of 270 degrees in a Nautical convention. The default setting of AeoliS includes a Nautical wind convention, see figure A.2. This default setting assumes that the used domain is orientated with the positive y-axis following the actual North. If this is not the case, an extra rotation factor α is introduced. Input data with a Cartesian wind convention is rotated in the model with 270 degrees.

By introducing the real world rotation angle α, it is chosen to define the x direction of the (rotated) domain as s and the y direction as n, to avoid confusion with the original domain. The wind vector is divided in two components to determine the magnitude of the wind velocity in the s and n direction, following figure A.3.

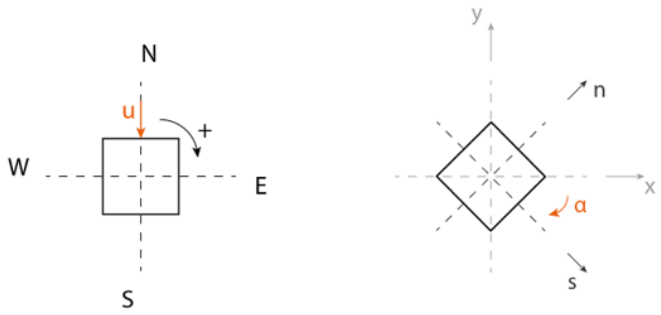

Figure A.2: Default wind convention and real world grid rotation angle α

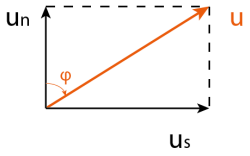

Figure A.3: Wind vector in s and n direction

Where:

$$u_{w,s} = u_w \bullet \sin(\Phi - \alpha) = u_w \bullet \sin(u_{dir} - 180 - \alpha) = -u_w \bullet \sin(u_{dir} - \alpha)$$
$$u_{w,n} = u_w \bullet \cos(\Phi - \alpha) = u_w \bullet \cos(u_{dir} - 180 - \alpha) = -u_w \bullet \cos(u_{dir} - \alpha) \quad \text{(A.1)}$$

With $\phi = u_{dir} - 180$ to account for correct values in positive s and n direction.

Wind induced shear

The shear velocity u_* [m/s] at height z [m] in the saltation layer is determined by using the Prandtl-Von Kárman's law of the wall:

$$u_* = \frac{u_w}{log(\frac{z}{z_0})} * \kappa \quad \text{(A.2)}$$

Where u_w [m/s] is the wind velocity, κ [-] the Von Kárman constant and z_0 [m] is the roughness length of the saltation layer. This length is one of the input variables of the model. For realistic applications, the saltation length should be in the order of $z_0 = d/30$, where d refers to the grainsize. A (non-realistic) larger value for k increases the wind shear velocity and speeds up model simulations in terms of the amount of sediment transport.

From the shear velocity, the shear stress τ [N/m^2] is calculated using:

$$\tau = \rho_a u_*^2 \quad \text{(A.3)}$$

Morphology - wind induced shear

The shear stress as a result of the interaction between morphology and the wind field is calculated by the analytical perturbation theory for turbulent boundary layer flow by Kroy et al. (2002):

$$\tau = \rho(\kappa z)^2 \left(\frac{\delta v}{\delta z}\right)^2 \quad \text{(A.4)}$$

With the vertical velocity profile $\vec{v}(x, y, z)$ leading to the surface shear stress:

$$\vec{\tau}(x, y) = \overrightarrow{\tau_0} + \delta\vec{\tau}(x, y) \quad \text{(A.5)}$$

Where τ_0 is the surface shear stress on a flat bed as calculated in the previous section.

The shear stress perturbation $\delta\tau$ is estimated following the analytical description of the influence of a low and smooth hill in the wind profile by Weng et al. (1991). The perturbation is given by the Fourier-transformed components of the shear stress perturbation in the unperturbed wind direction which are the functions $\delta\tau_x(k)$ and $\delta\tau_y(k)$. The x direction is defined by the direction of the wind velocity v_0 on a flat bed, while the y direction is then the transverse.

As a result, the perturbation theory can only estimate the shear stress induced by the morphology-wind interaction in parallel direction of wind. Therefore, model simulations were, up to now, limited to input wind directions parallel to the cross-shore axis of the grid.

To overcome this limitation and to allow for modelling directional winds, an overlaying computational grid is introduced in AeoLiS, which rotates with the changing wind direction per time step. By doing this, the shear stresses are always estimated in the positive x-direction of the computational grid. The following steps are executed each time step of the simulation:

1. Set computational grid
2. Add and fill buffer around the original grid
3. Populate computation grid by rotating it to the current wind direction and interpolate the original topography on it.
4. Compute the morphology-wind induced shear stress by using the perturbation theory
5. Add the only wind induced wind shear stresses to the computational grid
6. Rotate both the grids and the total shear stress results in opposite direction
7. Interpolate the total shear stress results from the computational grid to the original grid
8. Rotate the wind shear stress results and the original grid back to the original orientation

Note: the extra rotations in the last two steps are necessary as a simplified, but faster in terms of computational time, interpolation method is used.

Separation bubble

The perturbation theory is only applicable for smooth bed profiles. So, at the top of a dune where a sharp edge and steeps slopes may occur, the theory is not valid. The limitation of the theory at sharp bed level changes occurs because the analytical model does not account for non-linear effects like flow separation.

To represent the separation of wind streamlines over the sharp edge dune crest a so called separation bubble is defined for each slice in y direction of the computational grid parallel to the wind direction, following the example of Sauermann et al. (2001). Beneath the surface of the separation bubble the shear stresses are set to zero, following:

$$\tau = \begin{cases} \tau, & \text{if } z_b \geq z_{sep} \\ 0, & \text{if } z_b < z_{sep} \end{cases} \tag{A.6}$$

The adjusted shear stresses on the computational grid are considered in step 5 of the sequence above. Step 6 interpolates the total shear stresses on the domain, including the adjusted shear stresses under the separation bubbles, to the real grid. As an additional step to the sequence, also the separation dimensions are to be interpolated to the real grid in order to view these in the output of the model. If the edge of the dune crest is not sharp enough to induce flow separation, the entire process of defining the bubble and calculating the adjusted shear stresses is skipped.

The surface of the separation bubble is described by a third-order polynomial starting from the brink of the dune and ending at the reattachment point, where the surface of the separation bubble is equal to the bed again. The model determines for each grid cell in x-direction what the slope of the bed is. For an absolute slope larger than 30 degrees and which is negative, a separation bubble will be initiated. The dimensions of the bubble are illustrated in figure A.4.

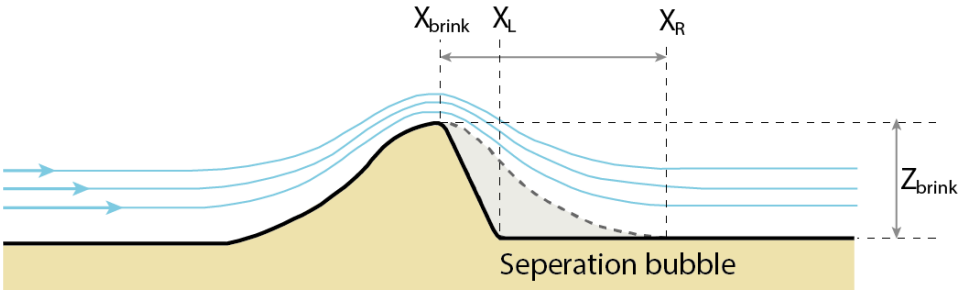

Figure A.4: Dimensions of separation bubble, after Sauermann et al. (2001)

The coefficients of the polynomial are defined by the following conditions:

- Continuity at the brinkline: $z_{sep}(x_{brink}) = z_{brink}$
- Continuity of first derivatives at the brinkline: $z'_{sep}(x_{brink}) = z'_{brink}$
- Smooth conditions at the re-attachment line: $x_r - z_{sep}(x_r) = 0$ and $z'_{sep}(x_r) = 0$.

Assuming a maximum slope c for the separation surface, the reattachment length l_s is obtained by:

$$l_s = \frac{3z_{brink}}{2c}\left(1 + \frac{z_{brink}}{4c} + 2\left(\frac{z_{brink}}{4c}\right)^2\right) \tag{A.7}$$

The surface of the separation bubble z_{sep} is determined with:

$$z_{sep}(x) = a_3(x - x_{brink})^3 + a_2(x - x_{brink})^2 + z'_{brink}(x - x_{brink}) + z_{brink} \tag{A.8}$$

where:

$$a2 = -\frac{3z_{brink} + 2z'_{brink}l_s}{l_s^2} \tag{A.9}$$

$$a3 = \frac{2z_{brink} + z'_{brink}l_s}{l_s^3} \tag{A.10}$$

The implementation so far had regularly problems to determine the slope of the bed near the brink. Small fluctuations in height induce large fluctuations in the derivatives. Even larger ones will be found in the shape of the bubble as the polynomial depends on this local slope near the brink. To tackle this problem, a zero-order separation bubble is calculated first with a zero slope. The resulting shape of the bubble is smoothed by filtering the steep changes and is then used to determine the slope near the brink. This first-order slope is applied in the calculation of the polynomial to determine the surface of the separation bubble.

The definition of this surface is optimal for the typical formation of a barchan dune under uni-directional wind conditions, see section 2.3.1. It is expected that the value for z_{brink} has no abrupt changes in the y-direction as the height of the brink line lowers regularly from the midpoint of the dune towards the horns and the bed level behind the barchan dune is flat. In other words, there are no abrupt changes of the separation surface between the bubbles in y-direction. However, as the application of flow separation goes further in this study then only for the formation of typical barchan dunes, it is expected that te value z_{brink} per slice in y-direction is more irregular as a consequence of variations in both the brink height and level of reattachment point. To avoid abrupt changes in the separation surface, a filter is applied that smooths the surface between bubbles.

Also, the previous definition for the minimal level of the separation surface at $z_b = 0$, is adjusted to allow for applications where the bed level may become lower than the reference level.

A.2. Vegetation shear

The wind shear stress acting on the sediment layer is reduced under the influence of vegetation since it acts as a roughness element. The remaining wind shear velocity is estimated by multiplying the calculated shear velocity with a so called vegetation factor (vegfac). The vegetation factor is calculated following an adapted definition by Raupach et al. (1993):

$$vegfac = \frac{1}{\sqrt{1 + \Gamma \rho_{veg}}} \tag{A.11}$$

Where ρ_{veg} is the vegetation cover and $\Gamma[-]$ a roughness factor describing the effectiveness of shear stress reduction by vegetation. It is one of the variable vegetation characteristics in the model. Calculated from values of plant form drag and geometry for coastal areas, a default value of $\Gamma = 16$ is implemented.

To increase stability of simulations regarding the competition between sediment transport and stabilization by vegetation, a new filter is applied that takes the vegetation cover of the surrounding grid cells into account. This filter follows a Gaussian distribution and has a variable standard deviation.

A.3. Velocity threshold

The critical shear velocity describes a dynamic threshold. If the wind velocity exceeds this threshold, initial movement of sand grains on the surface occurs and the process of sand transport down-wind will continue due to new flying grains. The wind velocity threshold is based on different bed surface properties. The initial value is computed based on the threshold for grain size of all fractions and is potentially altered by including other processes.

Grain size

For sandy beds, individual grains start to move when the shear stress exceeds a certain threshold value. The velocity threshold u_{th} *[m/s]* is described following Bagnold (1937) as:

$$u_{th} = A \sqrt{\frac{\rho_s - \rho_a}{\rho_a} g d_n} \tag{A.12}$$

where:

A	[-]	Empirical coefficient (A≈0.1)
ρ_s	$[kg/m^3]$	Density of sediment
ρ_a	$[kg/m^3]$	Density of air
g	$[m/s^2]$	Gravitational acceleration
d_n	$[m]$	Nominal grain size of sediment fraction

For model application with multiple sediment fractions, the velocity threshold is thus calculated for each fraction separately.

Moisture content

The shear velocity threshold increases for grid cells with wet sediment. The factor $f_{uth}[-]$ with which the threshold value is multiplied depends on 'how wet' the sediment is. This is estimated by means of calculating the moisture content of the grid cell based on the geotechnical mass content $p_g[-]$, following Belly (1964):

$$f_{uth} = 1.8 + 0.6 \bullet log(p_g) \tag{A.13}$$

The geotechnical mass content relates to the volumetric water content $p_V[-]$ and is calculated as:

$$p_g = \frac{p_V \rho_w}{\rho_g (1 - n)} \tag{A.14}$$

Where $\rho_w[kg/m^3]$ and $\rho_g[kg/m^3]$ are respectively the water and grain density, and n [-] is the porosity.

The threshold velocity is updated following:

$$u_{th} = \begin{cases} u_{th} & \text{for } p_g < 0.005 \\ f_{uth} u_{th} & \text{for } 0.005 < p_g < 0.064 \\ \infty & \text{for } p_g > 0.064 \end{cases} \tag{A.15}$$

Non-erodible layer

The presence of non-erodible elements induces a infinite threshold velocity as no value for the wind shear velocity is capable of inducing aeolian sediment transport. Non-erodible elements are implemented in AeoLiS as a user-defined layer. The height of the layer determines at which point the bed level is no longer erodible. When the bed level is lower than the non-erodible layer, the velocity threshold is set to be infinity large:

$$u_{th} = \begin{cases} u_{th}, & \text{if } z_b > z_{ne} \\ \infty, & \text{if } z_b \leq z_{ne} \end{cases} \tag{A.16}$$

A.4. Aeolian sediment transport

To describe the sediment transport a 2D advection equation is adopted in AeoLiS De Vries et al. (2014b), in which c [kg/m^2] is the instantaneous sediment mass per unit area in transport:

$$\frac{\delta c}{\delta t} + u_x \frac{\delta c}{\delta x} + u_y \frac{\delta c}{\delta y} = E - D \tag{A.17}$$

Where t [s] denotes time, x [m] denotes the cross-shore distance and y [m] denotes the alongshore distance from a zero boundary. u [m/s] is the mean horizontal particle speed at the surface, or short the saltation velocity, denoted in both x- and y-direction. E and D [kg/m^2/s] represent the erosion and deposition terms and hence combined the net entrainment of sediment.

The net entrainment is determined based on a balance between the equilibrium or saturated sediment concentration c_u $[kg/m^2]$ and the instantaneous sediment transport concentration c and is maximized by the available sediment in the bed m_a [kg/m^2] according to:

$$E - D = min\left(\frac{\delta m_a}{\delta t}, \frac{c_u - c}{T}\right) \tag{A.18}$$

T [s] represents an adaption time scale that is assumed to be equal for both erosion and deposition. A time scale of 1 second is commonly used. The equilibrium sediment concentration c_u, or saturated sediment concentration is computed using an empirical sediment transport formulation, see the next section on saltation.

To account for the coexistence of multiple sediment fractions in the bed, a weighting factor $\hat{w}_k$ is added to the advection equation in which k represents the sediment fraction index. Despite that this study does not include simulations with multiple sediment fractions, all (new) model implementations are compatible with this option.

Saltation

Multiple empirical transport formula are implemented in AeoLiS, based on the saltation models described in the literature review. The default setting of the model uses the formulation by Bagnold. The equilibrium transport c_u $[kg/m^2]$ is determined by:

$$c_u = \alpha C_b \frac{\rho_a}{g}\left(\frac{(u_* - u_{th})^3}{u}\right) \tag{A.19}$$

Where C_b is an empirical coefficient related to the grain size distribution. This coefficient varies with the chosen method for the definition of the equilibrium sediment concentration, see section 2.1.1. The shear velocity u_* [m/s] and the velocity threshold u_{th} [m/s] in this and other empirical transport formulations are based on the sections as described above.

Up to now, the implementation of saltation in AeoLiS was based on a linear relation between the saltation velocity u [m/s], of both this formula and the advection equation, and the wind velocity. Following literature on the mean horizontal velocity of the grains, this assumption is now changed to (i) a common converged value for the entire grid or (ii) a more complex definition of u depended on the (morphology induced) shear stress, see section 2.1.2. The first option, which enhances the computational time of the model as it is much simpler, is recommended for application with a relative small morphology - shear stress interaction. The second option is recommended for applications where the change in shear stress as result of the morphology and vegetation is significant

As this study focusses on simulations of different land forms in a coastal dune system, the interaction between the wind field with the morphology and vegetation is highly important. Therefore, the second definition for the saltation velocity is used. The saltation velocity u, by Sauermann et al. (2001) is implemented as:

$$\vec{u} = \left(v_{eff} - \frac{u_f}{\sqrt{2\alpha}A}\right)\vec{e}_\tau - \frac{\sqrt{2\alpha}u_f}{A}\vec{\nabla}z_b \tag{A.20}$$

Where $u_f[m/s]$ is the settling velocity of the grains, $\alpha[-]$ represents an effective restitution coefficient and $z_b[m]$ is the bed level. $A = \left|\vec{e}_\tau + 2\alpha\vec{\nabla}z_b\right|$ and $v_{eff}[m/s]$ is the effective wind velocity determined by:

$$v_{eff} = \frac{u_{th}}{\kappa}\left(ln\frac{z_1}{z_0} + \frac{z_1}{z_m}\left(\frac{u_*}{u_{th}} - 1\right)\right) \tag{A.21}$$

in which $u_{th}[m/s]$ refers to the shear velocity threshold, $u_*[m/s]$ to the shear velocity. $\kappa[-]$ is the Von Kármán constant, $z_1[m]$ a reference height in the saltation layer, $z_m[m]$ the characteristic height of this layer and $z_0[m]$ its bed roughness.

A.5. Morphology

As a result of the aeolian sediment transport each grid cell is subject to erosion or deposition. The net entrainment (erosion minus deposition) is estimated from the value for the instantaneous sediment transport, which is solved with the advection equation. The net entrainment, or pickup in AeoliS, is a concentration and is calculated per sediment fraction.

Bed update

The bed module includes an update of the bed composition by moving sediment fractions between bed layers. This moving of sediment is based on a mass balance in each layer. Mass of the sediment that is removed from the top layer as a consequence of aeolian transport is replaced with sediment from the second layer. In the case of excess sediment in the top layer due to net deposition, the additional mass of sediment is moved to underlying layers. An infinite sediment source is present below the lowest defined layer. The source follows the grain size distribution that is defined in the model configurations. The bed level itself is updated following:

$$\Delta z_b = \frac{\Delta m}{\rho_s(1-n)} \tag{A.22}$$

Where Δz_b [m] is the change of bed level height, $\Delta m[kg/m^2]$ is the estimated cumulative pickup of all the sediment fractions, ρ_s $[kg/m^3]$ the sediment density and *n* [-] the porosity of the bed layer.

Hydrodynamics

The last step of the bed update includes the influence of hydrodynamics on the morphology. Hydrodynamics smooth out the beach profile towards the initial profile, assuming that the affected area is dominated by marine processes. Sediment that is transported from the area by wind is compensated by marine accretion. This process is implemented as:

$$\Delta z_b = \frac{z_{b0} - z_b}{T_{swash}}\Delta t \tag{A.23}$$

Where $T_{swash}[s]$ is a adaption time scale for the hydrodynamics to relax the bed level towards the initial profile (z_{b0}). The affected area at which this process takes place is the swash zone, defined as the area where still water level z_s plus the run-up R is larger than the bed level z_b. The run-up is calculated from the input data on significant wave height $H_s[m]$ following:

$$R = \xi H_s \left(1 - min\left(1; \frac{\gamma h}{H_s}\right)\right) \tag{A.24}$$

where h [m] is the water depth ($z_s - z_b$) and with default settings for $\xi = 0.3[-]$ as the Iribarren number and $\gamma = 0.5[-]$ as breaker parameter.

Avalanching

The avalanching module includes the sediment transport due to avalanching following Kroy et al. (2002), where the flux is computed by:

$$Q_{ava} = E(tanh(|\nabla z_b|) - tanh(tanh\theta_{dyn}))\frac{\nabla z_b}{|\nabla z_b|} \tag{A.25}$$

Sediment transport occurs when the dune slope is steeper than the static angle of repose θ_{stat}, until the slope settles down on the dynamic angle of repose θ_{dyn}. It should be noted that both the dynamic and static angle of repose implemented in the model are based on dry sand. However, in reality the values can be spatial varying due to influence of moisture content and due to the presence vegetation.

It is assumed that the avalanching process occurs instantaneously when the dune slope has become too steep as a result of the morphological feedback between the bed level and aeolian sediment transport. The avalanching process is thus initiated in the same time step as the bed update occurs. The model transports sediment of one grid cell, that exceeds the critical slope, to the next one downslope, until the dune slope of the first grid cell becomes stable. This transport of sediment from one cell to another happens in one iteration and the model continues with performing iterations until all grid cells have a stable dune slope. The maximum number of iterations per time step for avalanching can be given as an input value in AeoLiS.

The bed level of the domain after avalanching processes have been executed, is the input for the next time step.

A.6. Vegetation characteristics

Once the new bed level is estimated at the end of the time step, the change in vegetation characteristics as a result of the morphological changes is estimated. This module is only called upon in AeoLiS if vegetation processes are relevant. The module describes different processes that influence the vegetation cover of the grid cells which is used to calculate the vegetation shear in the next time step as described above.

Establishment

The establishment of vegetation is expressed by a probabilistic value $p_{establisch}$ Keijsers et al. (2015), which is set equal for all cells in the domain. Once vegetation is established at a certain grid cell, it is able to start growing locally in the vertical and as lateral growth in the horizontal. If vegetation dies due to flooding, complete sediment burial or erosion (ρ_{veg}), the grid cell has to get germinated once more before vegetation can start growing again.

Vertical growth

The vegetation cover per grid cell is calculated by $\rho_{veg} = \left(\frac{h_{veg}}{H_{veg}}\right)^2$. Where h_{veg} [m] is the vegetation height and $H_{veg}[m]$ a constant representing the maximum vegetation height.

The change of the vegetation cover per grid cell is thus related to the change in vegetation height of that particular cell. The vegetation height is influenced on one hand by the growth rate of the vegetation and on the other hand by the sediment burial rate Δz_b [m/year]. A constant vegetation cover in time means that there is no sedimentation or that the vegetation grows at the same rate as that the cell is buried with sediment. The optimal growth rate of some vegetation dune species depend on the

sediment burial. A shift of the peak for optimal growth is therefore added. This interaction leads to the relation for the change in vegetation height, following Durán and Herrmann (2006):

$$\frac{\Delta h_{veg}}{\Delta t} = V_{ver}\left(1 - \frac{h_{veg}}{H_{veg}}\right) - \gamma\left|\frac{\Delta z_b}{\Delta t} - \Delta z_{b,opt}\right| \tag{A.26}$$

Where the sediment burial factor γ [-] represents the influence of sediment burial on vegetation growth and $\Delta z_{b,opt}$ [m/year] is the sediment burial for optimal growth.

The vertical vegetation growth rate V_{ver} is given in m/year, while the sediment burial rate (Δz_b) is determined as the bed level change per time step. By simply converting this value to a bed level change per year multiple errors are induced, as the time scale over which the bed level change actually occurs is much shorter than this one year. To compare the bed level change per time step with the vegetation growth rate per year, an average bed level change is estimated over a specified time (default is one day). This averaged value is than converted to a rate per year and used in equation A.26. This method ensures that sudden changes in the bed level change over one time step are not used as an estimate of the total bed level change in one year, which would be far too high.

Lateral growth

Lateral propagation is again expressed by a probabilistic value $p_{lateral}$ which is equal for all cells adjacent to vegetated cells Keijsers et al. (2015). Once the lateral propagation has occurred, the change in vertical vegetation growth has to be positive, or the vegetation dies immediately and lateral propagation in terms of a probabilistic value has to happen again.

B

Numerical implementation

To include spatiotemporal varying sediment availability in AeoLiS, the bed is discretized in horizontal grid cells and in vertical bed layers (2DV). Moreover, the grain size distribution is discretized into fractions. This allows the grain size distribution to vary both horizontally and vertically. A separate bed composition module is used to compute the sediment availability for each sediment fraction individually. The sediment transport is estimated by solving the advection equation A.17 for the instantaneous sediment concentration c. This equation does not include any vertical components, which is the result of the approach described below.

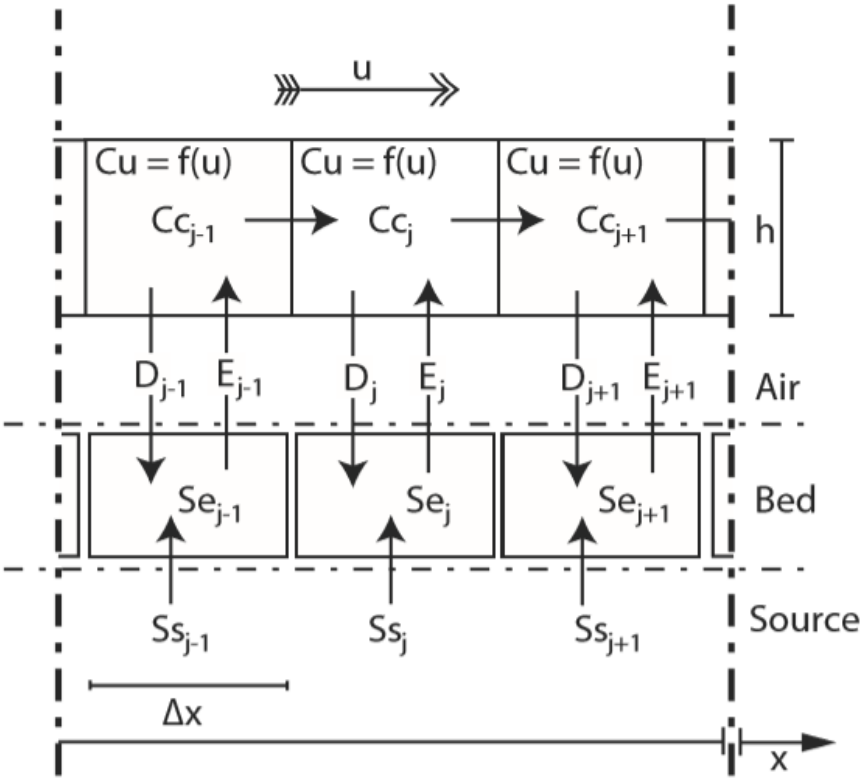

Figure B.1: Arrangement of spatial domain with concentration parameters

Figure B.1 illustrates the arrangement of a 1DV spatial domain with index j as the cell location within the domain, and indicates the concentration parameters per bed layer, where: Cc is the sediment concentration of the air; Cu is the wind driven sediment transport; Se is the available sediment on the

bed; E represents the potential pickup and D the potential deposition; Ss is the supply magnitude which supplies to the available sediment (Se) at the bed. It should be noted that the sediment concentration C_c $[kg/m^3]$ of these parameters differs from the sediment concentration c $[kg/m^2]$ from equation A.17. In this illustration a saltation height h [m] is defined. This saltation height h is not solved in AeoLiS and it is therefore chosen to define the sediment concentration per unit area: $c = hC_c$ $[kg/m^2]$.

B.1. Advection equation

The 2D advection equation A.17 is implemented in the model by a discretization following a first order upwind scheme assuming that the wind velocity u_z is positive in both x- and y-direction:

$$\frac{c_{i,j,k}^{n+1} - c_{i,j,k}^{n}}{\Delta t^n} + u_{z,x}^{n} \frac{c_{i,j,k}^{n} - c_{i-1,j,k}^{n}}{\Delta x} + u_{z,y}^{n} \frac{c_{i,j,k}^{n} - c_{i,j-1,k}^{n}}{\Delta y} = \frac{w_{i,j,k}^{n} c_{u_{i,j,k}}^{n} - c_{i,j,k}^{n}}{T} \tag{B.1}$$

The discretization is generalized for any wind direction by:

$$\begin{aligned} &\frac{c_{i,j,k}^{n+1} - c_{i,j,k}^{n}}{\Delta t^n} + u_{x+}^{n} \frac{c_{i,j,k}^{n} - c_{i-1,j,k}^{n}}{\Delta x} + u_{y+}^{n} \frac{c_{i,j,k}^{n} - c_{i,j-1,k}^{n}}{\Delta y} \\ &+u_{x-}^{n} \frac{c_{i+1,j,k}^{n} - c_{i,j,k}^{n}}{\Delta x} + u_{y-}^{n} \frac{c_{i,j+1,k}^{n} - c_{i,j,k}^{n}}{\Delta y} = \frac{w_{i,j,k}^{n} c_{u_{i,j,k}}^{n} - c_{i,j,k}^{n}}{T} \end{aligned} \tag{B.2}$$

In which:

$$u_{x+}^{n} = max(0, u_{z,x}^{n}) \qquad u_{y+}^{n} = max(0, u_{z,y}^{n})$$
$$u_{x-}^{n} = min(0, u_{z,x}^{n}) \qquad u_{y-}^{n} = min(0, u_{z,y}^{n})$$

Where *n* is the time step, index *i* and *j* are the cross-shore and alongshore spatial grid cell indices and *k* is the grain size fraction index. *w*[-] is the weighting factor used for the weighted addition of the saturated sediment concentrations over all grain size fractions.

A weight factor Γ that ranges from 0 – 1 is introduced to make the implicitness of the scheme variable in AeoLiS, equation B.2 is rewritten to:

$$\begin{aligned} &c_{i,j,k}^{n+1} + \Gamma \Delta t^n \left(u_{x+}^{n+1} \frac{c_{i,j,k}^{n+1} - c_{i-1,j,k}^{n+1}}{\Delta x} + u_{y+}^{n+1} \frac{c_{i,j,k}^{n+1} - c_{i,j-1,k}^{n+1}}{\Delta y} \right. \\ &\left. +u_{x-}^{n+1} \frac{c_{i+1,j,k}^{n+1} - c_{i,j,k}^{n+1}}{\Delta x} + u_{y-}^{n+1} \frac{c_{i,j+1,k}^{n+1} - c_{i,j,k}^{n+1}}{\Delta y} - \frac{w_{i,j,k}^{n+1} c_{u_{i,j,k}}^{n+1} - c_{i,j,k}^{n+1}}{T} \right) \\ &= c_{i,j}^{n} - (1-\Gamma) \Delta t^n \left(u_{x+}^{n} \frac{c_{i,j,k}^{n} - c_{i-1,j,k}^{n}}{\Delta x} + u_{y+}^{n} \frac{c_{i,j,k}^{n} - c_{i,j-1,k}^{n}}{\Delta y} \right. \\ &\left. +u_{x-}^{n} \frac{c_{i+1,j,k}^{n} - c_{i,j,k}^{n}}{\Delta x} + u_{y-}^{n} \frac{c_{i,j+1,k}^{n} - c_{i,j,k}^{n+1}}{\Delta y} - \frac{w_{i,j,k}^{n} c_{u_{i,j,k}}^{n} - c_{i,j,k}^{n}}{T} \right) \end{aligned} \tag{B.3}$$

Rewritten to:

$$\begin{aligned} &c_{i,j,k}^{n+1} \left(1 + \Gamma \Delta t^n \left(\frac{u_{x+}^{n+1}}{\Delta x} + \frac{u_{y+}^{n+1}}{\Delta y} - \frac{u_{x-}^{n+1}}{\Delta x} - \frac{u_{y-}^{n+1}}{\Delta y} + \frac{1}{T} \right) \right) \\ &-\Gamma \Delta t^n \left(\frac{u_{x+}^{n+1}}{\Delta x} c_{i-1,j,k}^{n+1} + \frac{u_{y+}^{n+1}}{\Delta y} c_{i,j-1,k}^{n+1} - \frac{u_{x-}^{n+1}}{\Delta x} c_{i+1,j,k}^{n+1} - \frac{u_{y-}^{n+1}}{\Delta y} c_{i,j+1,k}^{n+1} \right) \\ &= c_{i,j,k}^{n} \left(1 - (1-\Gamma) \Delta t^n \left(\frac{u_{x+}^{n}}{\Delta x} + \frac{u_{y+}^{n}}{\Delta y} - \frac{u_{x-}^{n}}{\Delta x} - \frac{u_{y-}^{n}}{\Delta y} + \frac{1}{T} \right) \right) \\ &+(1-\Gamma) \Delta t^n \left(\frac{u_{x+}^{n}}{\Delta x} c_{i-1,j,k}^{n} + \frac{u_{y+}^{n}}{\Delta y} c_{i,j-1,k}^{n} - \frac{u_{x-}^{n}}{\Delta x} c_{i+1,j,k}^{n} - \frac{u_{y-}^{n}}{\Delta y} c_{i,j+1,k}^{n} \right) \\ &+\Gamma \frac{\Delta t^n}{T} w_{i,j,k}^{n+1} c_{u_{i,j,k}}^{n+1} + (1-\Gamma) \frac{\Delta t^n}{T} w_{i,j,k}^{n} c_{u_{i,j,k}}^{n} \end{aligned} \tag{B.4}$$

Equation B.4 is simplified to:

$$a_{i,j}^{0,0} c_{i,j,k}^{n+1} + a_{i,j}^{1,0} c_{i+1,j,k}^{n+1} + a_{i,j}^{0,1} c_{i,j+1,k}^{n+1} - a_{i,j}^{-1,0} c_{i-1,j,k}^{n+1} - a_{i,j}^{0,-1} c_{i,j-1,k}^{n+1} = y_{i,j,k} \tag{B.5}$$

$$\begin{aligned}
a_{i,j,k}^{0,0} &= 1 + \Gamma \Delta t^n \left(\frac{u_{x+}^{n+1}}{\Delta x} + \frac{u_{y+}^{n+1}}{\Delta y} - \frac{u_{x-}^{n+1}}{\Delta x} - \frac{u_{y-}^{n+1}}{\Delta y} + \frac{1}{T} \right) \\
a_{i,j}^{1,0} &= \Gamma \Delta t^n \frac{u_{x-}^{n+1}}{\Delta x} \\
a_{i,j}^{0,1} &= \Gamma \Delta t^n \frac{u_{y-}^{n+1}}{\Delta y} \\
a_{i,j}^{-1,0} &= \Gamma \Delta t^n \frac{u_{x+}^{n+1}}{\Delta x} \\
a_{i,j}^{0,-1} &= \Gamma \Delta t^n \frac{u_{y+}^{n+1}}{\Delta y}
\end{aligned}$$

With the right-hand side R as:

$$\begin{aligned}
y_{i,j,k} = c_{i,j,k}^n \left(1 - (1-\Gamma) \Delta t^n \left(\frac{u_{x+}^n}{\Delta x} + \frac{u_{y+}^n}{\Delta y} - \frac{u_{x-}^n}{\Delta x} - \frac{u_{y-}^n}{\Delta y} + \frac{1}{T} \right) \right) \\
+ (1-\Gamma) \Delta t^n \left(\frac{u_{x+}^n}{\Delta x} c_{i-1,j,k}^n + \frac{u_{y+}^n}{\Delta y} c_{i,j-1,k}^n - \frac{u_{x-}^n}{\Delta x} c_{i+1,j,k}^n - \frac{u_{y-}^n}{\Delta y} c_{i,j+1,k}^n \right) \\
+ \Gamma \frac{\Delta t^n}{T} w_{i,j,k}^{n+1} c_{u_{i,j,k}}^{n+1} + (1-\Gamma) \frac{\Delta t^n}{T} w_{i,j,k}^n c_{u_{i,j,k}}^n
\end{aligned} \tag{B.6}$$

B.2. Steady state solution

New is the implementation of a steady state solution as second option to solve the advection equation for the instantaneous sediment concentration. This solution type is based on the assumption that the change in sediment concentration over the time steps is relatively small compared to the change in space. The assumption is applicable for dune development processes as there are several orders of magnitude between the time scale of saltation (approximately 2 seconds) and the time scale of the surface evolution of a dune (days to weeks). The advection of equation A.17 changes to:

$$u_x \frac{\delta c}{\delta x} + u_y \frac{\delta c}{\delta y} = \frac{c_u - c}{T} \tag{B.7}$$

The advection equation is discretized into the following:

$$\begin{aligned}
+ u_{x+}^n \frac{c_{i,j,k}^n - c_{i-1,j,k}^n}{\Delta x} + u_{y+}^n \frac{c_{i,j,k}^n - c_{i,j-1,k}^n}{\Delta y} \\
+ u_{x-}^n \frac{c_{i+1,j,k}^n - c_{i,j,k}^n}{\Delta x} + u_{y-}^n \frac{c_{i,j+1,k}^n - c_{i,j,k}^n}{\Delta y} = \frac{w_{i,j,k}^n c_{u_{i,j,k}}^n - c_{i,j,k}^n}{T}
\end{aligned} \tag{B.8}$$

Simplified to:

$$a_{i,j}^{0,0} c_{i,j,k}^n + a_{i,j}^{1,0} c_{i+1,j,k}^n + a_{i,j}^{0,1} c_{i,j+1,k}^n - a_{i,j}^{-1,0} c_{i-1,j,k}^n - a_{i,j}^{0,-1} c_{i,j-1,k}^n = y_{i,j,k} \tag{B.9}$$

$$
\begin{aligned}
a_{i,j,k}^{0,0} &= \left(\frac{u_{x+}^n}{\Delta x} + \frac{u_{y+}^n}{\Delta y} - \frac{u_{x-}^n}{\Delta x} - \frac{u_{y-}^n}{\Delta y} + \frac{1}{T}\right) \\
a_{i,j}^{1,0} &= \frac{u_{x-}^n}{\Delta x} \\
a_{i,j}^{0,1} &= \frac{u_{y-}^n}{\Delta y} \\
a_{i,j}^{-1,0} &= \frac{u_{x+}^n}{\Delta x} \\
a_{i,j}^{0,-1} &= \frac{u_{y+}^n}{\Delta y} \\
y_{i,j,k} &= w_{i,j,k}^n c_{u_{i,j,k}}^n
\end{aligned}
$$

B.3. Boundary conditions

Three boundaries are imposed in the model; an offshore boundary, an onshore boundary and the lateral boundaries. As the model was originally orientated at the Sand Engine in the Netherlands, the offshore boundary is located at the West side of the domain, the onshore boundary at the East side and the lateral boundaries at the North and South sides.

Each boundary has a new defined set of optional conditions to determine the sediment concentration:

- flux
- constant
- gradient
- circular

The first option called flux uses an input factor (f) that relates the boundary concentration to C_{u0} which is the saturated sediment concentration over a flat bed. The factor f varies between 0 and 1, where $f = 0$ refers to a zero sediment concentration at the boundary and where $f = 1$ refers to a saturated sediment concentration. The boundary condition for the sediment concentration can vary over the simulation time for a value of f larger than zero as C_{u0} is based on the wind forcing.

The second option uses a constant sediment concentration as input value. This manually added value for the sediment concentration $[kg/m^2]$ is called upon every time step and remains constant during the simulation time. Note that the default input value for this condition is zero, which makes this option actually the same as a flux boundary condition with $f = 0$.

The third boundary condition option is a so called gradient condition, where the sediment concentration at the boundary is determined from the gradient between the two neighbouring grid cells. The sediment concentration at the boundary is variable during the simulation time.

The last option is a circular boundary condition, which implies that the sediment concentration at the boundary is determined based on the sediment concentration at the opposite boundary. Again, the sediment concentration at the boundary is variable during the simulation time.

The default setting of the model uses a no-flux condition ($f = 0$) at the offshore boundary, a gradient flux at the onshore boundary and circular fluxes at the lateral boundaries.

$$
\begin{aligned}
c_{1,j,k}^{n+1} &= 0 \\
c_{n_x+1,j,k}^{n+1} &= 2c_{n_x,j,k}^{n+1} - c_{n_x-1,j,k}^{n+1} \\
c_{i,1,k}^{n+1} &= c_{i,n_y+1,k}^{n+1} \\
c_{i,n_y+1,k}^{n+1} &= c_{i,1,k}^{n+1}
\end{aligned}
\tag{B.10}
$$

The boundary conditions are combined with the simplified discretization from the full solution (equation B.5) or from the steady state solution (equation B.9) to form a linear system of equations, following:

$$\begin{bmatrix} A_1^0 & A_1^1 & 0 & \cdots & 0 & A_1^{n_y+1} \\ A_2^{-1} & A_2^0 & \ddots & \ddots & & 0 \\ \mathbf{0} & \ddots & \ddots & \ddots & \ddots & \vdots \\ \vdots & \ddots & \ddots & \ddots & \ddots & 0 \\ \mathbf{0} & & \ddots & \ddots & A_{n_y}^0 & A_{n_y}^1 \\ A_{n_y+1}^{-n_y-1} & 0 & \cdots & 0 & A_{n_y+1}^{-1} & A_{n_y+1}^0 \end{bmatrix} \begin{bmatrix} \vec{c}_1 \\ \vec{c}_2 \\ \vdots \\ \vdots \\ \vec{c}_{n_y} \\ \vec{c}_{n_y+1} \end{bmatrix} = \begin{bmatrix} \vec{y}_1 \\ \vec{y}_2 \\ \vdots \\ \vdots \\ \vec{y}_{n_y} \\ \vec{y}_{n_y+1} \end{bmatrix} \tag{B.11}$$

Where each item in the matrix is again a matrix A_j^l and each item in the vectors is again a vector $\vec{c}_j$ and $\vec{y}_j$ respectively. The form of matrix A_j^l depends on the diagonal index l and reads:

$$A_j^0 = \begin{bmatrix} 0 & 0 & 0 & 0 & \cdots & \cdots & 0 \\ a_{2,j}^{0,-1} & a_{2,j}^{0,0} & a_{2,j}^{0,1} & \ddots & & & \vdots \\ 0 & a_{3,j}^{0,-1} & a_{3,j}^{0,0} & a_{3,j}^{0,1} & \ddots & & \vdots \\ \vdots & \ddots & \ddots & \ddots & \ddots & \ddots & \vdots \\ \vdots & & \ddots & a_{n_x-1,j}^{0,-1} & a_{n_x-1,j}^{0,0} & a_{n_x-1,j}^{0,1} & 0 \\ \vdots & & & 0 & a_{n_x,j}^{0,-1} & a_{n_x,j}^{0,0} & a_{n_x,j}^{0,1} \\ 0 & \cdots & \cdots & 0 & 1 & -2 & 1 \end{bmatrix} \tag{B.12}$$

for l = 0 and

$$A_j^l = \begin{bmatrix} 1 & 0 & \cdots & \cdots & \cdots & \cdots & 0 \\ 0 & a_{2,j}^{l,0} & \ddots & & & & \vdots \\ \vdots & \ddots & a_{3,j}^{l,0} & \ddots & & & \vdots \\ \vdots & & \ddots & \ddots & \ddots & & \vdots \\ \vdots & & & \ddots & a_{n_x-1,j}^{l,0} & \ddots & \vdots \\ \vdots & & & & \ddots & a_{n_x,j}^{l,0} & 0 \\ 0 & \cdots & \cdots & \cdots & \cdots & 0 & 1 \end{bmatrix} \tag{B.13}$$

for $l \neq 0$. The vectors $\vec{c}_{j,k}$ and $\vec{y}_{j,k}$ read:

$$\vec{c}_{j,k} = \begin{bmatrix} c_{1,j,k}^{n+1} \\ c_{2,j,k}^{n+1} \\ c_{3,j,k}^{n+1} \\ \vdots \\ c_{n_x-1,j,k}^{n+1} \\ c_{n_x,j,k}^{n+1} \\ c_{n_x+1,j,k}^{n+1} \end{bmatrix} \quad \text{and } \vec{y}_{j,k} = \begin{bmatrix} 0 \\ y_{2,j,k}^{n} \\ y_{3,j,k}^{n} \\ \vdots \\ y_{n_x-1,j,k}^{n} \\ y_{n_x,j,k}^{n} \\ 0 \end{bmatrix} \tag{B.14}$$

For the steady state solution the vector $\vec{c}_{j,k}$ changes to:

$$\vec{c}_{j,k} = \begin{bmatrix} c_{1,j,k}^{n} \\ c_{2,j,k}^{n} \\ c_{3,j,k}^{n} \\ \vdots \\ c_{n_x-1,j,k}^{n} \\ c_{n_x,j,k}^{n} \\ c_{n_x+1,j,k}^{n} \end{bmatrix} \tag{B.15}$$

B.4. Implicit solver

The linear system defined by the full or steady state solution and the boundary conditions, is solved by a sparse matrix solver for each sediment fraction separately in ascending order of grain size. Initially, the weights $w_{i,j,k}^{n+1}$, or $w_{i,j,k}^{n}$ in case of a steady state solution, are chosen according to the grain size distribution in the bed and the air. The sediment availability constraint is checked after each solve:

$$m_a \geq \frac{w_{i,j,k}^{n+1} c_{u_{i,j,k}}^{n+1} - c_{i,j,k}^{n+1}}{T} \Delta t^n \tag{B.16}$$

If the constraint is violated, a new estimate for the weights is calculated following:

$$w_{i,j,k}^{n+1} = \frac{c_{i,j,k}^{n+1} + m_a \frac{T}{\Delta t^n}}{c_{u_{i,j,k}}^{n+1}} \tag{B.17}$$

The linear system is solved again using the new weights. This procedure is repeated until a weight is found that does not violate the sediment availability constraint. If the time step is not too large, the procedure typically converges in only a few iterations. Finally, the weights of the larger grains are increased proportionally as to ensure that the sum of all weights remains unity. If no larger grains are defined, not enough sediment is available for transport and the grid cell is truly availability-limited. This situation should only occur occasionally as the weights in the next time step are computed based on the new bed composition and thus will be skewed towards the large fractions. If the situation occurs regularly, the simulation time step is chosen too large compared to the rate of armouring.

C

Simulation configurations

Basic model parameters

Table C.1: Overview of standard model parameters for landform simulations

symbol	parameter	value	unit
d	Grain size	0.225	mm
$n_{fractions}$	Number of sediment fractions	1	-
n_{layers}	Number of bed layers	3	-
h_{layer}	Thickness of the bed layers	0.01	m
g	Gravitational constant	9.81	m/s^2
v	Air viscosity	1.5 e-5	m^2/s
ρ_a	Density of air	1.225	kg/m^3
ρ_g	Density of grains	2650	kg/m^3
ρ_w	Density of water	1025	kg/m^3
n	Sediment porosity	0.4	-
κ	Von Kármán constant	0.41	-
z	Measurement height of wind velocity	10	m
Θ_{dyn}	Dynamic angle of repose	33	deg
Θ_{stat}	Static angle of repose	34	deg
T	Adaptation time scale for saltation process	1	s

Barchan dune simulations

Table C.2: Overview of model parameters for barchan dunes

	symbol	parameter	value	unit
Model parameters				
	n_x	Number of grid cells in x-direction	300	-
	n_y	Number of grid cells in y-direction	150	-
	Δx	Grid cell size in x-direction	1	m
	Δy	Grid cell size in y-direction	1	m
	Δt	Time step	3600	s
Initial topography				
	h	Height of the Gaussian shaped sand pile	6 - 9	m
	σ_g	Standard deviation of Gaussian shaped sand pile	15 - 20	m
	ne_{layer}	Level of non-erodible layer	0	m
	k	Bed roughness	1	mm
Boundary conditions				
		Offshore boundary (=upwind)	*flux*	
		Onshore boundary (=downwind)	*gradient*	
		Lateral boundaries	*circular*	
	f	Factor for relative offshore sediment flux	0 - 1	-
Wind				
	u_w	Wind velocity	6 - 10	m/s
	u_{dir}	Wind direction	$270 \pm \sigma_w$	deg
	σ_w	Standard deviation of wind direction distribution	0 - 40	deg

Parabolic dune simulations

Table C.3: Overview of model parameters for parabolic dunes

	symbol	parameter	value	unit
Model parameters				
	n_x	Number of grid cells in x-direction	300	-
	n_y	Number of grid cells in y-direction	150	-
	Δx	Grid cell size in x-direction	1	m
	Δy	Grid cell size in y-direction	1	m
	Δt	Time step	3600	s
Initial topography				
	h	Height of barchan dune	6	m
	W	Width of barchan dune	70	m
	V	Volume of barchan dune	10500	m^3
	ne_{layer}	Level of non-erodible layer	0	m
	k	Bed roughness	1	mm
Boundary conditions				
		Offshore boundary (=upwind)	*flux*	
		Onshore boundary (=downwind)	*gradient*	
		Lateral boundaries	*circular*	
	f	Factor for relative offshore sediment flux	0	-
Wind				
	u_w	Wind velocity	10	m/s
	u_{dir}	Wind direction	$270 \pm \sigma_w$	deg
	σ_w	Standard deviation of wind direction distribution	0	deg
Vegetation				
	Γ	Roughness factor for vegetation	16	-
	p_g	Possibility of germination per year	1	$1/year$
	p_l	Possibility of lateral expansion per year	0	$1/year$
	V_{ver}	Vertical growth of vegetation	2.5 - 8.5	$m/year$
	$\delta z_{b,opt}$	Sediment burial for optimal vegetation growth	0 - 0.6	$m/year$
	γ_{veg}	Constant on influence of sediment burial	1	-
	σ_{veg}	Standard deviation in vegetation cover filter	0.4 - 1.0	-

Academic blowout formation

Table C.4: Overview of model parameters for blowout simulations

	symbol	parameter	value	unit
Model parameters				
	n_x	Number of grid cells in x-direction	300	-
	n_y	Number of grid cells in y-direction	200	-
	Δx	Grid cell size in x-direction	1	m
	Δy	Grid cell size in y-direction	1	m
	Δt	Time step	3600	s
	k	Bed roughness	1	mm
Boundary conditions				
		Offshore boundary	*gradient*	
		Onshore boundary	*gradient*	
		Lateral boundaries	*circular*	
Wind				
	u_w	Wind velocity	8	m/s
	u_{dir}	Wind direction	270 $\pm$ σ_w	deg
	σ_w	Standard deviation of wind direction distribution	0	deg
Vegetation				
	Γ	Roughness factor for vegetation	16	-
	p_g	Possibility of germination per year	1	$1/year$
	p_l	Possibility of lateral expansion per year	0	$1/year$
	V_{ver}	Vertical growth of vegetation	0 - 8.5	$m/year$
	$\delta z_{b,opt}$	Sediment burial for optimal vegetation growth	0	$m/year$
	γ_{veg}	Constant on influence of sediment burial	1	-
	σ_{veg}	Standard deviation in vegetation cover filter	0.8	-
Hydrodynamics				
	z_s	Still water level (sine function of the tide)	-1.0 to 1.0	m
	H_s	Significant wave height	0	m

Table C.5: Overview of model parameters for the field case simulations

	symbol	parameter	value	unit
Model parameters				
	α	Real-world grid cell orientation (clockwise)	39	deg
	n_x	Number of grid cells in x-direction	225	-
	n_y	Number of grid cells in y-direction	225	-
	Δx	Grid cell size in x-direction	1	m
	Δy	Grid cell size in y-direction	1	m
	Δt	Time step	3600	s
	k	Bed roughness	0.01	mm
Boundary conditions				
		Offshore boundary	*gradient*	
		Onshore boundary	*gradient*	
		Lateral boundaries	*circular*	
Vegetation				
	Γ	Roughness factor for vegetation	8 - 20	-
	p_g	Possibility of germination per year	1	$1/year$
	p_l	Possibility of lateral expansion per year	0	$1/year$
	V_{ver}	Vertical growth of vegetation	0 - 2	$m/year$
	$\delta z_{b,opt}$	Sediment burial for optimal vegetation growth	0	$m/year$
	γ_{veg}	Constant on influence of sediment burial	1	-
	σ_{veg}	Standard deviation in vegetation cover filter	0.8	-